file MLBP

AFWAL-TR-88-4244
ADA 207288

ELECTRONIC PROPERTIES OF ORDERED LADDER POLYMERS

Dr. Samson A. Jenehke
Honeywell, Inc.
Sensors and Signal Processing Laboratory
10701 Lyndale Avenue South
Bloomington, Minnesota 55420

January 1989

Final Report for Period March 1986 - March 1988

MATERIALS LABORATORY
AIR FORCE WRIGHT AERONAUTICAL LABORATORIES
AIR FORCE SYSTEMS COMMAND
WRIGHT-PATTERSON AIR FORCE BASE, OHIO 45433-6533

NOTICE

When Government drawings, specifications, or other data are used for any purpose other than in connection with a definitely Government-related procurement, the United States Government incurs no responsibility or any obligation whatsoever. The fact that the government may have formulated or in any way supplied the said drawings, specifications, or other data, is not to be regarded by implication, or otherwise in any manner construed, as licensing the holder, or any other person or corporation; or as conveying any rights or permission to manufacture, use, or sell any patented invention that may in any way be related thereto.

This report is releasable to the National Technical Information Service (NTIS). At NTIS, it will be available to the general public, including foreign nations.

This technical report has been reviewed and is approved for publication.

IVAN J. GOLDFARB
Project Scientist
Nonmetallic Materials Division

R. C. EVERS, Acting Chief
Polymer Branch
Nonmetallic Materials Division

FOR THE COMMANDER

MERRILL L. MINGES, Director
Nonmetallic Materials Division

IF YOUR ADDRESS HAS CHANGED, IF YOU WISH TO BE REMOVED FROM OUR MAILING LIST, OR IF THE ADDRESSEE IS NO LONGER EMPLOYED BY YOUR ORGANIZATION PLEASE NOTIFY WRDC/MLBP , WRIGHT-PATTERSON AFB, OH 45433-6523 TO HELP MAINTAIN A CURRENT MAILING LIST.

COPIES OF THIS REPORT SHOULD NOT BE RETURNED UNLESS RETURN IS REQUIRED BY SECURITY CONSIDERATIONS, CONTRACTUAL OBLIGATIONS, OR NOTICE ON A SPECIFIC DOCUMENT.

REPORT DOCUMENTATION PAGE

Form Approved
OMB No. 0704-0188

1a. REPORT SECURITY CLASSIFICATION Unclassified	1b. RESTRICTIVE MARKINGS
2a. SECURITY CLASSIFICATION AUTHORITY	3. DISTRIBUTION/AVAILABILITY OF REPORT Approved for public release; distribution unlimited.
2b. DECLASSIFICATION/DOWNGRADING SCHEDULE	
4. PERFORMING ORGANIZATION REPORT NUMBER(S)	5. MONITORING ORGANIZATION REPORT NUMBER(S) AFWAL-TR-88-4244
6a. NAME OF PERFORMING ORGANIZATION Honeywell, Inc. Sensors and Signal Processing Laboratory 6b. OFFICE SYMBOL (If applicable)	7a. NAME OF MONITORING ORGANIZATION Wright Research and Development Center
6c. ADDRESS (City, State, and ZIP Code) 10701 Lyndale Avenue South Bloomington, Minnesota 55420	7b. ADDRESS (City, State, and ZIP Code) WRDC/MLBP Wright-Patterson AFB, Ohio 45433-6523
8a. NAME OF FUNDING/SPONSORING ORGANIZATION Wright Research and Development Center 8b. OFFICE SYMBOL (If applicable)	9. PROCUREMENT INSTRUMENT IDENTIFICATION NUMBER Contract # F33615-85-C-5091
8c. ADDRESS (City, State, and ZIP Code) Wright-Patterson Air Force Base, Ohio 45433-6523	10. SOURCE OF FUNDING NUMBERS PROGRAM ELEMENT NO. 61101F; PROJECT NO. 0100ML; TASK NO. 1L1R01; WORK UNIT ACCESSION NO. 1L1R0175
11. TITLE (Include Security Classification) Electronic Properties of Ordered Ladder Polymers	
12. PERSONAL AUTHOR(S) Samson A. Jenekhe	
13a. TYPE OF REPORT Final Technical Report 13b. TIME COVERED FROM 3/23/86 TO 3/23/88	14. DATE OF REPORT (Year, Month, Day) Jan 1989 15. PAGE COUNT 85
16. SUPPLEMENTARY NOTATION	

17. COSATI CODES		
FIELD	GROUP	SUB-GROUP
07	04	
11	04	

18. SUBJECT TERMS (Continue on reverse if necessary and identify by block number)
Ordered ladder polymers; Electronic properties; Electrical conductivity; Ion implantation; Mediated solubilization and processing; Electrochemical properties; conducting BBL films;

19. ABSTRACT (Continue on reverse if necessary and identify by block number)

Please see reverse

20. DISTRIBUTION/AVAILABILITY OF ABSTRACT ☐ UNCLASSIFIED/UNLIMITED ☒ SAME AS RPT. ☐ DTIC USERS	21. ABSTRACT SECURITY CLASSIFICATION Unclassified
22a. NAME OF RESPONSIBLE INDIVIDUAL Bruce A. Reinhardt	22b. TELEPHONE (Include Area Code) 513-255-9162 22c. OFFICE SYMBOL WRDC/MLBP

18. Ladder polyquinoxalines

Block 19. ABSTRACT

Experimental studies of the electronic and electrical properties of high-temperature ordered ladder polymers, exemplified by benzimidazobenzophenanthroline-type ladder polymer (BBL) and ladder polyhydroquinoxalines (PHQXL), are reported. In addition, this report presents results of studies on the structural, electrochemical, and mechanical properties of undoped insulating and doped conducting ladder polymers as well as a novel processing approach for the rigid chain and ladder polymers. The two types of ladder polymers investigated, BBL and PHQXL were found to be insulators ($\sigma_{RT} < 10^{-12}$ ohm^{-1}cm^{-1}) in the undoped state. However, upon chemical, electrochemical, or ion implantation doping the room temperature electrical conductivity of films of these ladder polymers was enhanced up to 2-220 ohm^{-1} cm^{-1} depending on the method of doping. Thus, high-temperature ladder polymers constitute a promising new class of highly conducting polymers for potential electronic and aerospace applications.

High molecular weight BBL polymer samples with intrinsic viscosity in methane sulfonic acid (MSA) of 4.78 to 7.91 dL/g were prepared by polymerization in the liquid crystalline phase in polyphosphoric acid (PPA). Moderate molecular weight PHQXL samples with intrinsic viscosity of 0.65 to 0.80 dL/g in MSA were similarly obtained. These polymers were soluble in strong acids but insoluble in organic solvents. A novel mechanism of solubilization of the rigid chain polymers in aprotic organic solvents was discovered in this study. The new solubilization approach involves the reversible formation of soluble complexes of the rigid chain polymers using Lewis acids as the mediating agents. Isotropic and anisotropic (>8% wt) BBL solutions in organic solvents (nitroalkanes and nitrobenzene) were prepared and processed to films and coatings.

The electrochemical properties of BBL were investigated as a function of pH and it was found that the redox potential ($E^{o'}$) of BBL varied linearly between -1.25V (vs. Ag/Ag^+) at neutral pH to -0.39V (vs. Ag/Ag^+) at a pH of -0.24. The pH dependence of redox potential of BBL was suggested to arise from protonation/de-protonation phenomena in acid media. Thin films of BBL on Pt electrode were found to exhibit electrochromism, red $\leftrightarrow$ blue color switching, when cycled between -0.5 to -2.0V (vs. Ag/Ag^+). The feasibility of direct electrochemical synthesis of ladder polymer films was demonstrated by the preparation of uniform, coherent, and electroactive ladder polyquinoxaline films from o-phenylenediamine or 1,2,4,5-tetraaminobenzene.

The mechanical properties of undoped insulating and doped conducting BBL films were characterized by dynamic tensile moduli measurements in the temperature range -150 to 350°C. All the mechanical properties of undoped and potassium-doped BBL films we found to be virtually identical. Thus, the excellent mechanical properties of BBL and related ladder polymer films are retained in the doped highly conducting state.

FORWARD

The research described in this report is an investigation of the electronic and electrical properties of ordered ladder polymers. This final technical report covers work performed under Air Force Wright Aeronautical Laboratories, Materials Laboratory, (AFWAL/MLBP), Contract No. F33615-85-C-5091 by Honeywell Inc., Sensors and Signal Processing Laboratory, Bloomington, Minnesota, in the period of 3 March 1986 to 3 March 1988. The principal investigator, Dr. Samson A. Jenekhe, acknowledges the technical assistance and contributions of Mr. James R. Peterson, Mr. Richard Douglas, Mr. Stanley J. Tibbetts, Mr. Lee Hallgren, and Dr. Robert D. Horning of Honeywell. The principal investigator also expresses his gratitude to Drs. Fred Arnold and Ivan J. Goldfarb of Polymer Branch, (AFWAL/MLBP) for their help and discussion.

TABLE OF CONTENTS

SECTION 1
INTRODUCTION AND SUMMARY

1.1 Background

Electrically conducting polymers have emerged over the past several years as a frontier in electronic and electro-optical materials research. Scientific and theoretical interest in this novel class of polymers are due in part to the new phenomena of semiconducting to metallic conductivity (10^{-4} to 10^{5} $ohm^{-1}cm^{-1}$) achieved in synthetic organic macromolecules. New and basic questions that lack fundamental understanding are raised by the novel polymeric materials regarding the nature of electronic charge transport in quasi one-dimensional solids; the possibility of a rational design, synthesis, and processing of new materials of predicted electronic and electro-optical properties as well as other functional properties; and the nature of the structure/property/processing relationships in the materials.

Technological interest in electroactive polymers stems from (1) the potential of combining such traditional polymer properties as light weight, high strength-to-weight ratio, noncorrosiveness, flexibility, low-temperature solution or melt processing, and low cost, with the additional characteristics of controllable electronic and optical properties; and (2) the numerous application possibilities for the new electronic/electro-optic materials, including such long-term generic applications as molecular electronics and optical signal processing and near-term applications such as batteries, gas sensors, microelectronic devices and interconnection, electromagnetic interference (EMI) shielding, and low-cost large-area devices such as solar cells and optical sensors.

Many conjugated polymers with semiconducting to metallic conductivity (10^{-4} to 10^{5} $ohm^{-1}cm^{-1}$) have been synthesized and widely studied by academic and industrial research groups in the past 10 years. Among the well-known conducting polymers are polyacetylene, polyp-phenylene, polypyrrole, polythiophone, polycarbazoles and their derivatives. Unfortunately, most of these conducting polymers do not combine the traditional polymer properties with the novel electronic properties and, consequently, have not yet found commercial applications. Although polyacetylene system shows the highest conductivity (about 10^{5} $ohm^{-1}cm^{-1}$) to date, it is also the most unstable to ambient conditions; it is intractable and the mechanical properties degrade upon doping. All the other materials mentioned above combine, in various degrees,

environmental instability, intractability, or embrittlement caused by doping. For example, electrochemically prepared and simultaneously doped polypyrrole has conductivities as high as 10-100 $ohm^{-1}cm^{-1}$, remains quite stable in air, but it is intractable; poly p-phenylene sulfide, while having high conductivity (1-10 $ohm^{-1}cm^{-1}$) and solution and melt processibility, is environmentally unstable and has poor mechanical properties. Our own previous work on conducting polymers has been on heteroaromatic polycarbazoles and derivatives and on polythiophenes, polypyrroles, and polyfurans containing aromatic and quinoid segments in the main chain. Our results have shown that heteroaromatic conjugated polymers which have excellent stability are more promising as organic semiconductors or metals. The conjugated polymers that have previously been studied are largely amorphous and disordered systems.

Ladder polymers, as a class, provide a scientifically and technologically promising new direction in research on semiconducting and metallic polymers. The highly ordered conformation imposed by the rigid chain ladder structure can be expected to lead to a high mobility of charge carriers and, hence, potential intrinsic semiconductivity or metallic conductivity. Structurally, double-stranded conjugated ladder polymers provide a bridge between the strictly single-stranded quasi one-dimensional conjugated polymers such as polyacetylene, polythiophenes, polyaniline, and polyp-phenylene and two-dimensional graphite which is a metal with an extremely high in-plane electronic charge mobility. Theoretical interest in the electronic and electrical properties of ladder polymers has also been stimulated by recent theoretical calculations of the electronic structures of ideal ordered ladder polymers, such as polyacene, polyacenacene, polyphenanthrene, polyquinoxaline and polypyrene, which suggest the possibility of achieving intrinsic semiconductors, metals, and high-temperature superconductors in such a class of polymers.

Many heterocyclic ladder polymers, such as benzimidazobenzophenanthroline-type ladder (BBL) and ladder polyquinoxalines (PQXL), have been previously synthesized and widely studied for their excellent thermal stability and mechanical properties. These previously known thermally stable ladder polymers provide ideal starting materials for the investigation of the electronic properties of polymeric solids with ladder structures and the effects of molecular structure and morphology on electronic properties. However, the rigid chain structure of ladder or double-stranded polymers gives rise to the problems of infusibility and insolubility in organic solvents. Consequently, this class of polymers can only be processed into films,

coatings, and fibers with great difficulty. Furthermore, molecular weight and other important molecular and structural properties have not yet been fully characterized because of insolubility in organic solvents.

1.2 Research Project Objectives and Scope

The primary technical objective of this research project was to determine the feasibility of achieving high electrical conductivity in ordered ladder polymers and thereby to establish the role of the molecular order of ladder structures in attaining high electronic conductivity in polymeric solids. Among secondary objectives of the research effort were to explore novel conduction mechanisms which do not require conventional doping procedures; to determine the feasibility of direct electrochemical synthesis of films of ladder polymers; and to investigate novel film processing techniques for ordered ladder polymers and determine effects of processing on ladder polymer film morphology. The basic technical approach encompassed the synthesis, characterization, and detailed study of two types of ladder polymer systems: benzimidazobenzophenanthroline-type ladder polymer (BBL) and ladder polyhydroquinoxaline (PHQXL).

1.3 Summary of Major Results and Accomplishments

A detailed discussion of the technical approaches and results of the research effort is to be found in Section 2 as well as future publications. The following is a brief summary of the major results and accomplishments of the project:

(1) High room temperature dc conductivity (σ_{RT}>220 $ohm^{-1}cm^{-1}$) was achieved in flexible films of high molecular weight BBL by means of ion implantation doping. Electrochemical and chemical doping of BBL films also produced highly conducting (2-5 $ohm^{-1}cm^{-1}$) and air stable materials.

(2) Investigation of novel methods of processing rigid chain and ladder polymers resulted in the discovery of mediated solubilization of BBL and other rigid chain polymers in aprotic organic solvents such as nitroalkanes. Both isotropic and anisotropic (>8%wt) solutions of BBL in organic solvents have been prepared, allowing solution processibility to films, fibers, and coatings from organic solvents for the first time.

(3) Novel highly conducting macroscopic crystals of 5,12-dihydro-5,7,12,14-tetraazapentacence (DHTAP) complexes, a model compound of ladder

polyhydroquinoxalines (PHQXL), were prepared, characterized, and studied in detail.

(4) We have demonstrated the feasibility of direct electrochemical synthesis of ladder polymer films by successful preparation of uniform, coherent, and electroactive ladder polyquinoxaline films from 1,2-phenylenediamine or the tetramine monomer.

(5) The mechanical properties of undoped insulating and doped highly conducting BBL films were measured in the temperature range -150°C to 300°C and found to be virtually identical. This result shows that the generally excellent mechanical properties of pristine ordered ladder polymer films are retained in the doped conducting state unlike most of the other previously known conducting polymers.

(6) Metallic composite films of a metal (Ag) and doped conducting BBL were prepared by electrochemical methods. The composite Ag/BBL films have a room temperature conductivity of 324 $ohm^{-1}cm^{-1}$ and a metallic temperature-dependent conductivity.

(7) Electrochemical studies of the redox properties of BBL and PHQXL films revealed a dependence of the redox and electrochromic properties on pH which is suggested to arise from protonation phenomena. Furthermore, the air stability of n-type doped BBL films is attributed to its favorably low redox potential (<-1.25V vs Ag/Ag^{+}) and highly fused heteroaromatic rings which allow extensive delocalization of the polymeric carbanion ions.

1.4 Conclusions and Recommendations

Some areas of the present research effort were of necessity exploratory in nature and would require further study to fully clarify and develop. The following specific areas are recommended for subsequent research effort:

(1) Undertake a detailed investigation of mediated solubilization and processing of rigid chain and ladder polymers in aprotic organic solvents. This discovery of a novel mechanism of solubilization of BBL and related rigid chain polymers organic solvents is of utmost theoretical and practical importance. Such a study is expected to give rise to new fundamental results on the chemistry of polymer processing as well as immediate improvements in the processing and applications of BBL and related rigid chain polymers. The solubilization of these rigid chain polymers in organic solvents should produce both isotropic and liquid crystalline solutions which are important for future commercial processing of the

materials but also for understanding of the molecular and physical properties of the polymers.

(2) Further studies of ion implantation of high-temperature ladder polymers are needed to answer the question whether room temperature conductivities in the 10^3 to 10^5 $ohm^{-1}cm^{-1}$ can be achieved while retaining the excellent mechanical properties of ordered ladder polymers. If the answer to this question is affirmative, many immediate applications of the thermally stable materials in microelectronics, such as microelectronic interconnection and flexible circuits, are expected. The optical properties of such ion implanted ladder polymers are also of technological interest.

SECTION 2
TECHNICAL APPROACHES AND RESULTS

2.1 Model Compound DHTAP and its Complexes

2.1.1 Introduction

Numerous ladder or double-stranded polymers have been synthesized and widely studied[1-17] since the early 1960s, including major synthetic and thermal stability characterization efforts on aromatic and heterocyclic type of ladder polymers at the Air Force Materials Laboratory[1-6] and in Stille's[7-10] and Marvel's[13-15] research groups. However, the solid-state properties of this class of polymers, especially electronic and optical properties, have largely been neglected until very recently[17-20].

Our current interest in the electronic, linear and nonlinear optical, and electrochemical properties of conjugated ladder polymers[19-20], stems in part from their greater structural order compared to most single-stranded conjugated polymers, and their generally excellent thermal stability, mechanical strength, and resistance to degradation. The rigid rod nature of the backbone of conjugated ladder polymers suggests that anisotropy would be a central feature of their morphology and physical properties. In this regard, it should be noted that π-conjugated ladder polymers provide a structural bridge between the single-stranded quasi one-dimensional conjugated polymers and two-dimensional graphite. Ladder polyquinoxalines have additional attractive features: (1) variations of ladder polyquinoxalines and related ladder polymers containing 1,4-pyrazine ring can be synthesized using a number of synthetic routes[7-13,16]; (2) the highly regular or symmetric chain structure and composition and planar chain conformation of the ladder polyquinoxalines can be expected to favor crystallization, not previously reported in ladder polymers; and (3) although the band structure and electronic properties of the ladder polyquinoxalines have not yet been calculated, their molecular structures are intermediate between polyacene and paracyanogen (i.e., 1,4-pyrazine type ladder) which are predicted to be intrinsic semiconductors with small bandgaps or metals with a zero bandgap[21-26].

The structural and physico-chemical properties of the model compound 5,12-dihydro-5,7,12,14-tetraazapentacene (II or DHTAP) have direct implications for the higher molecular weight ladder polyquinoxalines. Also, the properties of DHTAP are of interest per se; it is desirable to compare the structural and physical properties to the parent fused hydrocarbon, pentacene,

whose crystal structure[27], electronic, and optical properties have been widely studied[27-29]. Although previously synthesized[9,30] and its molecular structure established via synthetic methods by Badger and Pettit[30], very little is known about its properties: for example, even the melting point has not been reported. We have prepared DHTAP according to the scheme suggested by Stille and co-workers[9-10] and carried out the condensation in polyphosphoric acid (PPA) under conditions similar to the synthesis of the corresponding high molecular weight polymer.

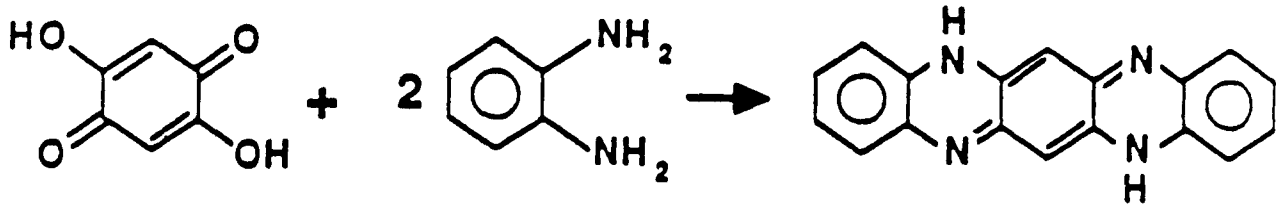

I II

Our studies of DHTAP reported here include crystallization and melting, X-ray diffraction, morphology, spectroscopy, electrochemistry, charge-transfer complex formation, and electrical conductivity. We have discovered that DHTAP forms conductive crystalline charge-transfer complexes and one of these, a 7,14-protonated DHTAP methanesulfonate salt, is studied in detail also.

2.1.2 Experimental Section

Synthesis and Purification of DHTAP

A reaction mixture of 13.007g (71.84 mmol) of *o*-phenylenediamine dihydrochloride and 5.032g (35.92 mmol) of 2,5-dihydroxy-*p*-benzoquinone in 55.282g of 77% poly(phosphoric acid) (PPA) was prepared in a flask. The reaction mixture was heated in nitrogen atmosphere: first, to 110°C overnight (15 hrs.); and finally to 170-175°C for 19 hours. The metallic green solution was cooled and poured into 1000 mL of methanol. A deep blue-purple powder was recovered. DSC revealed low melting impurities (<200°C) in this product. The product was refluxed in 2000 mL water twice for a total of 24 hours, washed with acetone, and dried in vacuum at room temperature (25°C). The resulting deep blue-purple product had a sharp melting point of 545°C as determined by

DSC (heating rate 7.5°C/min). FTIR spectrum: 3440 (vs), 2928 (w), 1630 (vs), 1530 (vs), 1472 (s), 1245 (vs), 1152 (s), 1030 (s), 904 (w), 820 (s), 758 (s), 600 (w), 535 (w), 500 (w) cm^{-1}.

DHTAP Charge-Transfer Complexes

DHTAP samples can be re-crystallized from its acid solutions; for example, when a solution of DHTAP in methanesulfonic acid (MSA) was poured into a large volume of acetone, a crystalline greenish to blue-purple powder was precipitated and recovered. However, when a concentrated solution of DHTAP in MSA was placed on a glass slide or a shallow Petri dish, gold-yellow needle-like crystals began to grow in about 1 day, reaching macroscopic sizes (~1mm to 1 cm in length) after several days. Preliminary measurements showed that these needlelike crystals were highly conductive, unlike authentic blue-purple DHTAP, and also they showed a different melting point compared to the parent compound. These initial observations suggested the formation of a charge-transfer complex between DHTAP and MSA. Samples of such a DHTAP/MSA charge-transfer complex were subsequently produced for a detailed study as follows:

(a) 10-15mL of a 0.24M DHTAP solution in MSA was placed in a 14.5cm diameter Petri dish or a very shallow large (19cm in diameter) beaker and allowed to crystallize at room temperature (23°C) for at least four days. The brilliant gold-yellow crystals were recovered by adding 20-50mL acetone followed by vacuum filtration through #44 Whatman filter paper and a Buchner funnel; the recovered crystals were thoroughly washed with 150-200mL acetone and vacuum dried at 25°C or 100°C for 2 hours. The yield was about 86%. Elemental analysis: calculated for $(C_{18}H_{12}N_4)(CH_3SO_3H)_2$ -- %C = 50.41, %H = 4.23, %N = 11.76, %S = 13.46, and %O = 20.15; found -- %C = 48.78, %H = 4.26, %N = 10.86, %S = 12.77, and %O = 23.51.

(b) Conductive gold-yellow crystals of DHTAP/MSA complex were also prepared by solvent evaporation from liquid films of DHTAP/MSA solutions on various substrates (glass, silicon wafers) heated on a hot plate. Polycrystalline films exhibiting different morphologies were obtained by this technique.

In a preliminary investigation of the feasibility of preparing radical cation complexes of DHTAP, i.e., $DHTAP^{+}\cdot X^{-}$, it was reacted with hot solutions of nitrosyl salts ($NO^{+}X^{-}$). A hot solution of $NOBF_4$ was prepared by adding 0.235 g (~2 mmol) $NOBF_4$ in 25 ml of acetonitrile (CH_3CN) in a 100-ml jar on a hot plate. 0.569 g (~2 mmol) DHTAP was added to the solution while stirring, and then left for 10 hours. A dark blue powder was recovered from the hot solution, pressed into a pellet and shown to be conductive. Similarly, a copper colored $DHTAP^{+}\cdot HSO_4^{-}$ was prepared from $NO^{+}HSO_4^{-}/CH_3CN$ and shown to be conductive.

Solubility

The qualitative solubility of DHTAP powder and DHTAP/MSA crystals in various solvents was determined by placing ~2 mg sample in a test tube and adding the solvent (~5 mL). In cases where ready solubilization did not occur, the solubility test results were recorded after 1-5 weeks. Table 1 shows the solubility and appearance of solutions.

Characterization

A. Differential Scanning Calorimetry (DSC). Thermal analysis, including DSC and thermogravimetric analysis (TGA) was done using a DuPont Model 1090B thermal analyzer equipped with a DSC cell module and a Model 991 TGA module. An indium DSC standard showed a peak melting point of 160.6°C compared to the true melting point of 156.6°C; therefore, all the present DSC data were reduced by 4°C. Samples were sealed in DSC cells and run from 25-600°C at 7.5°C/min. TGA runs were performed in air or nitrogen atmospheres at a heating rate of 7.5°C/min.

B. Infrared Spectra. Fourier transform infrared (FTIR) spectra of thin films cast on sapphire or KCl plates or KBr mulls were obtained using a Digilab model FTS-14 spectrometer. Thin films of DHTAP were cast from a MSA or concentrated sulfuric acid solution. Thin films of the DHTAP/MSA complex were cast from a methanol, N,N-dimethylformamide (DMF), or dimethysulfoxide (DMSO) solution.

C. UV-Visible-Near Infrared Spectra of DHTAP were obtained in concentrated sulfuric acid and methanesulfonic acid solutions using a Perkin-Elmer Model

TABLE 1. SOLUBILITY AND APPEARANCE OF SOLUTIONS OF DHTAP AND DHTAP/MSA CRYSTALS

Solvent	ϵ'	DHTAP Powder		DHTAP/MSA Crystals	
		Solubil.	Appearance	Solubil.	Appearance
Glacial Acetic Acid	6.15	NS	---	VS	blue soln.; red fluorescence
Aniline	6.89	SS	red soln.; resid. solid	SS	reddish/purple soln.; resid. xtls.
N,N-Dimethyl acetamine (DMAc)		SS	lt. red soln.; resid. solid	VS	blue soln.
N,N-Dimethyl formamide (DMF)	36.7	SS	opaque red soln.; resid. solid	VS	blue soln.; red fluorescence
N,N-Dimethyl sulfoxide (DMSO)	49	SS	red soln.; resid. solid	VS	blue soln.
Acetonitrile	36.2			SS	lt. blue soln.; xtls. remain
Acetone	21.2			SS	pink soln.; xtls. remain
N-methyl-2-pyrrolidone (NMP)		SS	opaque red soln.; resid. solid	VS	blue soln.; red fluorescence
Methanol	32.63	NS	---	VS	blue soln.; red fluorescence
Methylethyl ketone (MEK)		NS	---	NS	---
Methylene Chloride	9.08	NS	---	NS	---
Pyridine	12.3	S	red soln.	S	red soln.; resid. xtls.
Tetrahydrofuran (THF)	7.6	NS	---	SS	pink soln.; xtls. remain
Toluene	2.38	NS	---	NS	---
Nitromethane	36	NS	---	SS	lt. blue soln.; xtls. remain
Nitrobenzene	34.82	SS	lt. grn. soln.	NS	---
Methanesulfonic acid (MSA)		VS	blue soln.; red fluoresc.	VS	blue soln.; red fluorescence
Conc. H_2SO_4		VS	blue soln.; red fluoresc.	VS	blue soln.; red fluorescence
Water	78	NS	---	SS	blue soln.

NS = Not Soluble
SS = Slightly Soluble
S = Soluble
VS = Very Soluble

Lambda 9 UV-Vis-NIR spectrophotometer in the wavelength range 185-3200nm. Solutions with concentrations in the 10^{-4} to 10^{-2} mol/liter were studied in 1mm cells. Thin films of DHTAP and DHTAP/MSA complex were cast from MSA and DMSO solutions, respectively, on sapphire substrates. Solution spectra of DHTAP/MSA in methanol and pyridine were obtained using 10^{-4} molar solutions.

D. Fluorescence Emission Spectra. The fluorescence emission spectra of DHTAP and its complex, DHTAP/MSA, were obtained in solutions of varying concentration at room temperature (23°C) using a Perkin-Elmer model MPF-2A fluorescence spectrometer, 5mm cells, and a number of excitation wavelengths. The emission spectra of DHTAP in concentrated sulfuric acid solutions were obtained at several concentrations from ~10^{-6}M to ~10^{-3}M. The emmission spectra of DHTAP/MSA complex in conc. H_2SO_4, DMF, and MeOH solutions were also obtained at several concentrations.

E. X-Ray Diffraction patterns of samples were obtained using a Rigaku powder X-ray diffractometer and computerized diffraction analyzer with a sealed tube CuK_α X-ray radiation at 1.540562Å wavelength. The 2θ scans were from 3-93°, step size of 0.02° and 1-second counting time per step. Powdered samples or crystallites were held on a single crystal silicon wafer with grease. The silicon wafer was detuned 2° to suppress reflections from the Si crystal.

F. SEM and Optical Microscopy. The morphology of as-synthesized and vacuum baked (30°C) crystals of DHTAP/MSA complex was observed with an optical microscope and a JEOL Model JSM 810AII scanning electron microscope (SEM).

G. Electrical Conductivity. The dc conductivity measurements were made on compressed pellets of DHTAP and DHTAP/MSA complex and on films of the complex cast on glass slides using a two-point probe technique. Electrical contacts were made using a conductive silver paste.

H. Electrochemical Experiments and Cyclic Voltammetry. All electrochemical experiments were performed in a three-electrode, single-compartment cell of about 50mL volume using a double junction Ag/Ag^+ ($AgNO_3$) reference electrode. Cyclic voltammograms of polycrystalline films of DHTAP on platinum electrode, prepared by solvent evaporation of MSA solution on a hot plate, were obtained using a platinum flag as the working electrode and a platinum spiral as the counter electrode in 0.1M tetraethylammonium perchlorate (TEAP)/acetonitrile.

Cyclic voltammograms of DHTAP/MSA complex in solution were obtained using 10^{-3}M solutions in 0.1M TEAP/DMSO and a platinum wire and a platinum spiral as working and counter electrodes, respectively. Attempts were made to obtain solution cyclic voltammograms of pristine DHTAP in aqueous H_2SO_4 solutions (10^{-4} and 10^{-2}M), but there were too many redox couples which could not be reproduced. All the electrochemical experiments were performed using a programmable EG&G Princeton Applied Research Model 273 potentiostat/galvanostat and Model RE0091 X-Y recorder.

2.1.3 Results and Discussion

Structure, Charge-Transfer Complexes, and Morphology

The structure of DHTAP has previously been established[9,30] as well as the present synthetic scheme[30]. The IR spectrum of the pristine DHTAP sample was consistent with the structure II. In particular, the bands at 3440, 1630, and 1245 cm^{-1} are assigned to ν N-H, ν C=N, and ν C-N, respectively.

Elemental analysis of DHTAP/MSA crystals showed elemental composition corresponding to $(C_{18}H_{12}N_4)(CH_3SO_3H)_2$. The structure of DHTAP/MSA complex suggested from the infrared spectrum and elemental analysis is the salt:

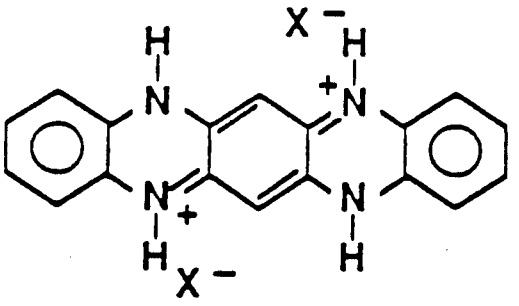

where X^- is the methanesulfonate anion. This structure is also consistent with the high conductivity of the complex and its ready solubility in polar solvents. It is expected that similar 1:2 salts of protonated DHTAP, i.e., $(DHTAPH_2)^{2+}(X^-)_2$ can be prepared from other anions (X^-). In preliminary experiments under similar crystal growth conditions, conductive bisulfate anion salt of $DHTAPH_2^{2+}$ crystallized from concentrated sulfuric acid solutions after several weeks; films cast from the concentrated H_2SO_4 solutions were also conductive. However, salts of X^- = Cl^- did not crystallize from hydrochloric acid solutions in part because of the poor solubility of DHTAP in HCl. Inability of the chloride complexes of DHTAP to crystallize is most likely due to steric factors and the small size of Cl^- compared to DHTAP,

which has an estimated molecular length of ~14-15Å. It is well known in conductive organic charge-transfer crystals that crystallization and high conductivity is usually favored in a donor/acceptor pair of about the same molecular size[31-32], as in the case of tetrathiafulvalene/7,7,8,8-tetracyano-*p*-quinodimethane (TTF/TCNQ)[33]. Thus, other crystalline salts of protonated DHTAP are expected to form with anions of a size comparable to or greater than methanesulfonate or bisulfate, e.g., $CF_3SO_3^-$ and *p*-CH_3-Ph-SO_3^-. Besides the simple salts of the 7,14-protonated DHTAP, i.e., $(DHTAPH_2)^{2+}(X^-)_2$, crystalline complexes of the unprotonated DHTAP with acceptors like TCNQ are expected to form and to be more conductive in view of precedents like phenazine-TCNQ complexes, which are metals with single crystal room temperature conductivities as high as 100 S/cm[34]. Preliminary powdered samples of $DHTAP^+ \cdot X^-$ (X = BF_4, HSO_4) prepared by reaction of DHTAP with hot acetonitrile solutions of the corresponding NO^+ salts were conductive, but not as high as the DHTAP/MSA crystals. The structure of the radical cationic complex was inferred from the reaction DHTAP + NO^+X^- ---> $DHTAP \cdot X^-$ + NO. Electron Spin Resonance (ESR) spectroscopy will be used to confirm the nature of these later complexes in future studies.

Figure 1A shows the X-ray diffraction (XRD) pattern of powdered samples of DHTAP. The d-spacings at 9.81, 4.96, and 3.27Å, which are also the most intense, correspond to (001), (002), and (003) reflections, respectively. Thus, one of the unit cell parameters is ~9.81Å. However, all the d-spacings of Figure 1A are yet to be indexed; so, the unit cell and crystallographic structure of DHTAP remain unknown. An XRD pattern taken from a DHTAP compressed pellet (3600 psi) was found to be virtually identical to Figure 1A, except that an additional peak appeared at 13.56Å and the 9.81Å peak became the most intense. This suggests that more reflection peaks will be found with a much purer and more crystalline sample of DHTAP. In anticipation of how the crystal structure of DHTAP might relate to the corresponding higher molecular weight ladder polymer, the polyacenes provide an interesting example. Although naphthalene and anthracene both have a monoclinic unit cell, the higher oligomers including tetracene, pentacene, and hexacene all have a triclinic unit cell with virtually identical a and b lattice parameters. However, the c parameter was found to increase from 13.53Å in tetracene to 16.01Å in pentacene to 18.4Å in hexacene[27-28]. Thus, it is reasonable to expect that the crystal structure of DHTAP is probably identical to that of the corresponding high molecular weight ladder polymer.

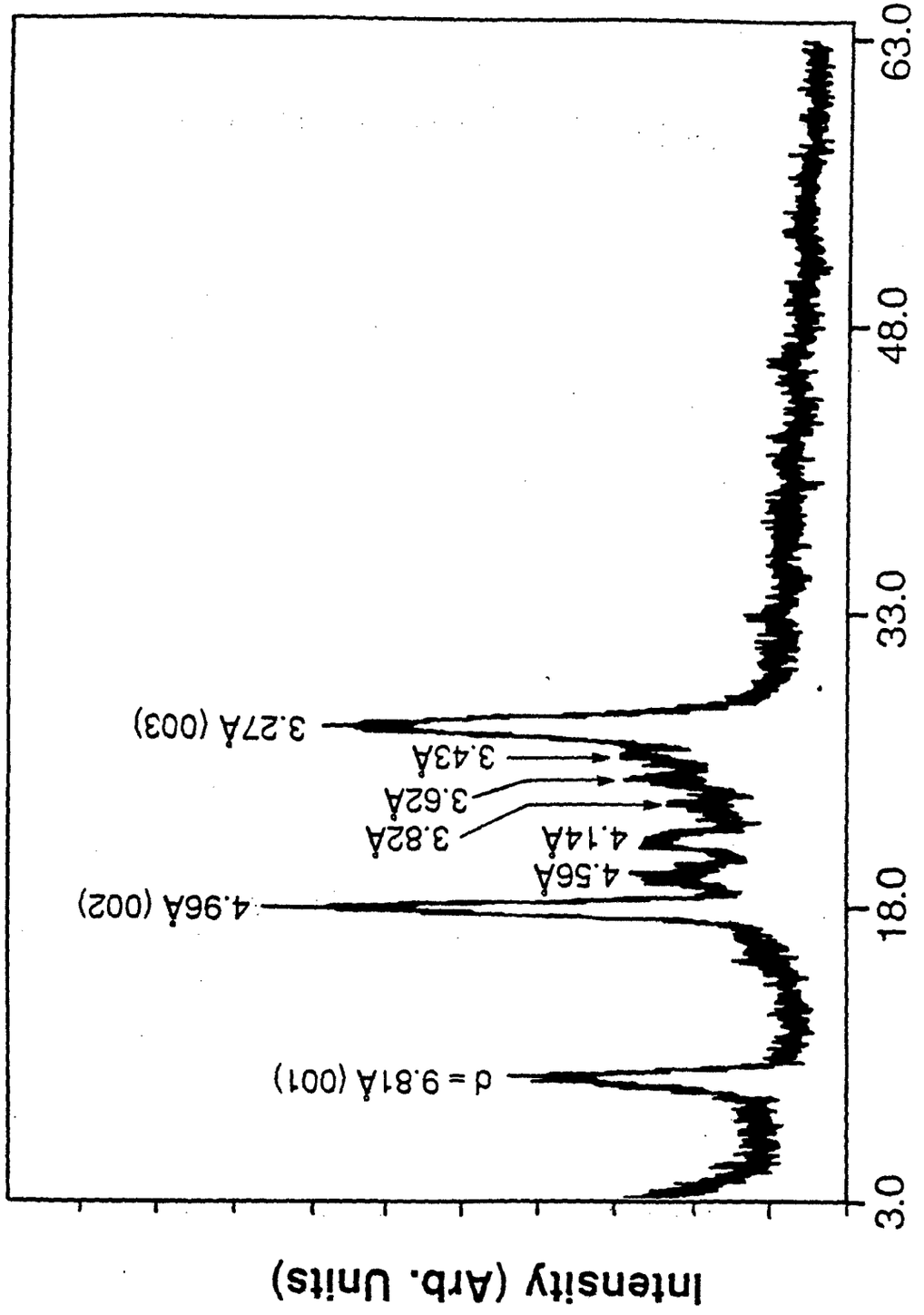

70882

Figure 1A: X-ray diffraction pattern of DHTAP powder.

The XRD pattern of the gold-yellow crystals of DHTAP/MSA complex is shown in Figure 1B. This pattern, when compared to that of DHTAP in Figure 1A, indicates that the methanesulfonate salt of protonated DHTAP has a completely different crystal structure. Also, the very sharp XRD peaks in Figure 1B and their relatively large intensities compared to Figure 1A indicate that the complex is fully crystalline with no amorphous regions or impurities. The XRD pattern of the DHTAP/MSA complex also suggests that the relatively broad and low intensity peaks of the pristine DHTAP powder may be due to amorphous impurities. Attempts to identify the crystal symmetry by a fit to the observed 30 reflections in the powder data of Figure 1B were unsuccessful. However, the crystal structure was narrowed to either monoclinic or triclinic symmetry. Weissenberg photograph gave one of the unit cell parameters to be ~21.5Å. Measured characteristic cleavage angles were 109° and 116°. Determination of the true crystallographic structure of DHTAP and its complexes will require growth of large single crystals.

The macroscopic crystals of conductive DHTAP/MSA complex, as-synthesized from a concentrated MSA solution of DHTAP, are highly anisotropic, as shown in the optical micrographs of Figures 2 and 3. Though the gold-yellow crystals are needlelike in overall appearance, the needles are aggregates of rectangular platelets, as revealed in the optical micrographs and in SEM pictures (Figure 4) of vacuum-baked DHTAP/MSA crystals grown from concentrated MSA solution of DHTAP on a silicon wafer at room temperature. Steps along the needle axis are evident in the crystals. The layered nature of the crystals is revealed by the steps and clearage planes. The large needle-like crystals had lengths of up to 20-80 mm and diameters up to 0.1-0.4 mm. However, some of the constituent platelets were as small as 10μm wide by 30-60μm in length and as thin as 0.4-1.0μm. In contrast to the crystal morphologies shown in Figures 2 through 4, crystals of DHTAP/MSA complex grown on glass or silicon wafer substrates by evaporation of a MSA solution on a hot plate generally exhibited a spherulitic morphology with a fibrous substructure in the radial direction.

Thermal Properties

Figure 5 shows the thermal stability fo DHTAP and its methanesulfonate complex in nitrogen atmosphere as determined by TGA. A slight weight loss of about 2-3% in DHTAP between 300 and 530°C is followed by a very slow weight loss between about 550°C and 800°C where a residue of about 70% is obtained.

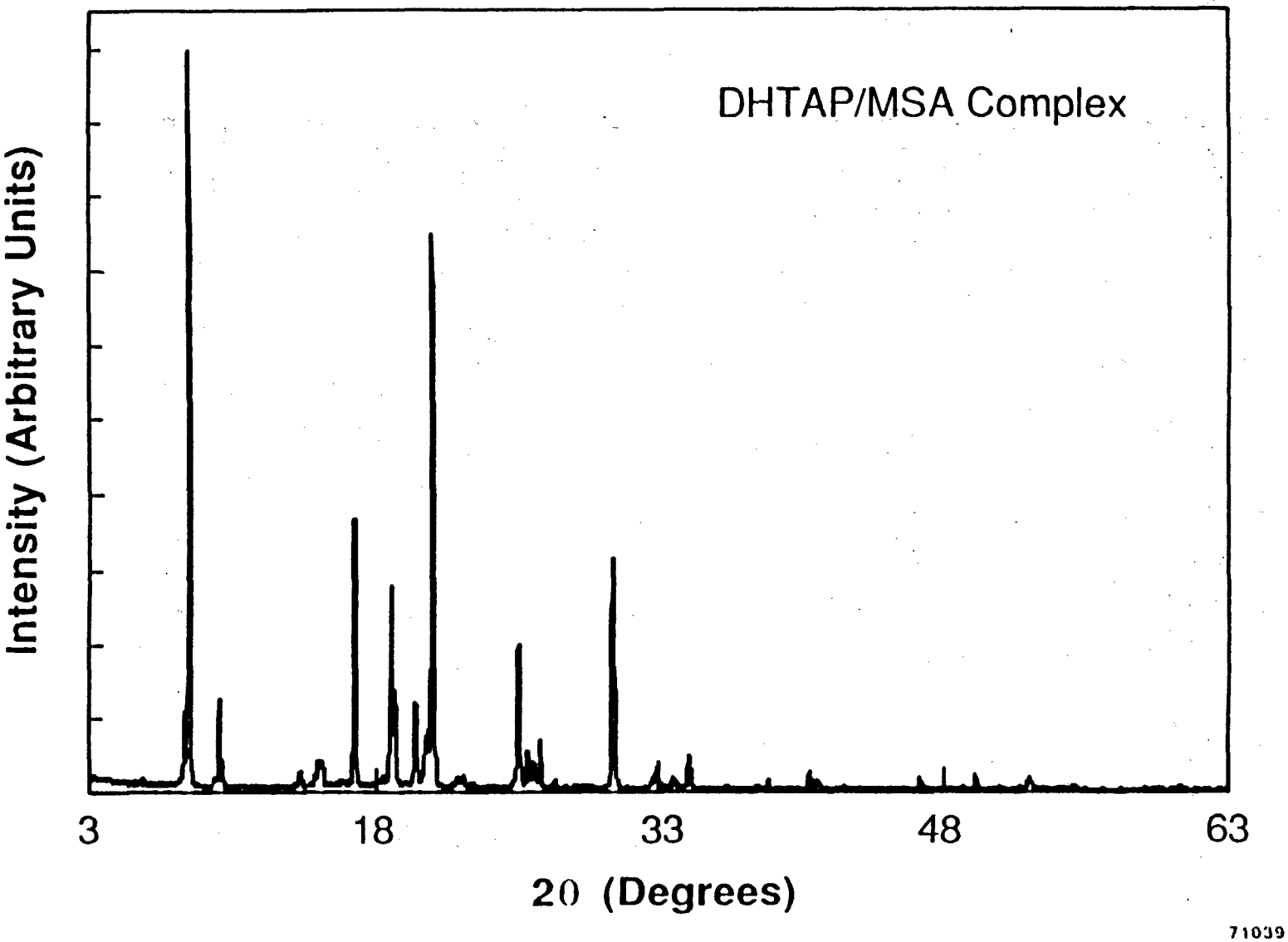

Figure 1B: X-ray diffraction pattern of DHTAP/MSA complex.

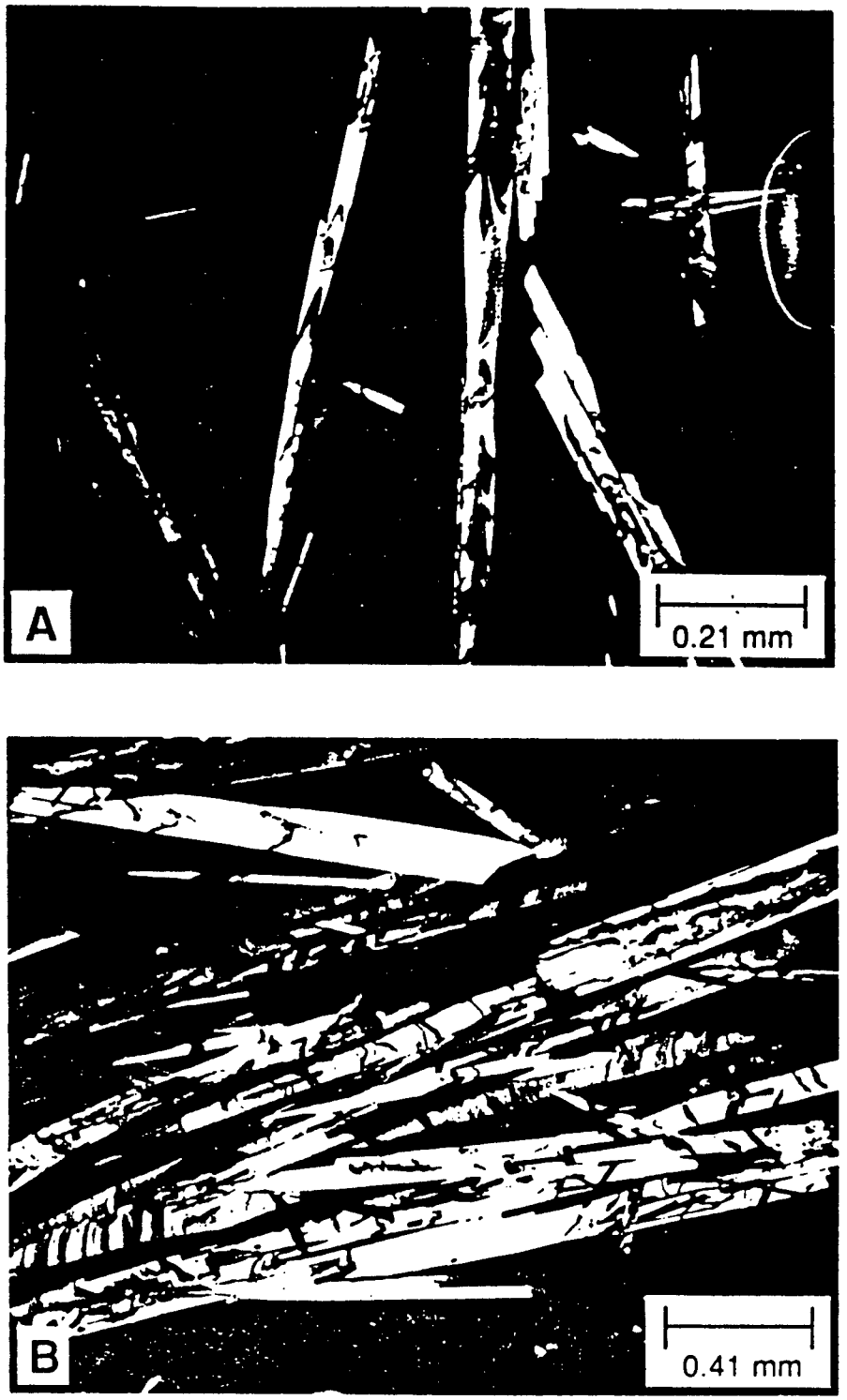

Figure 2: Optical micrographs of DHTAP/MSA crystals.

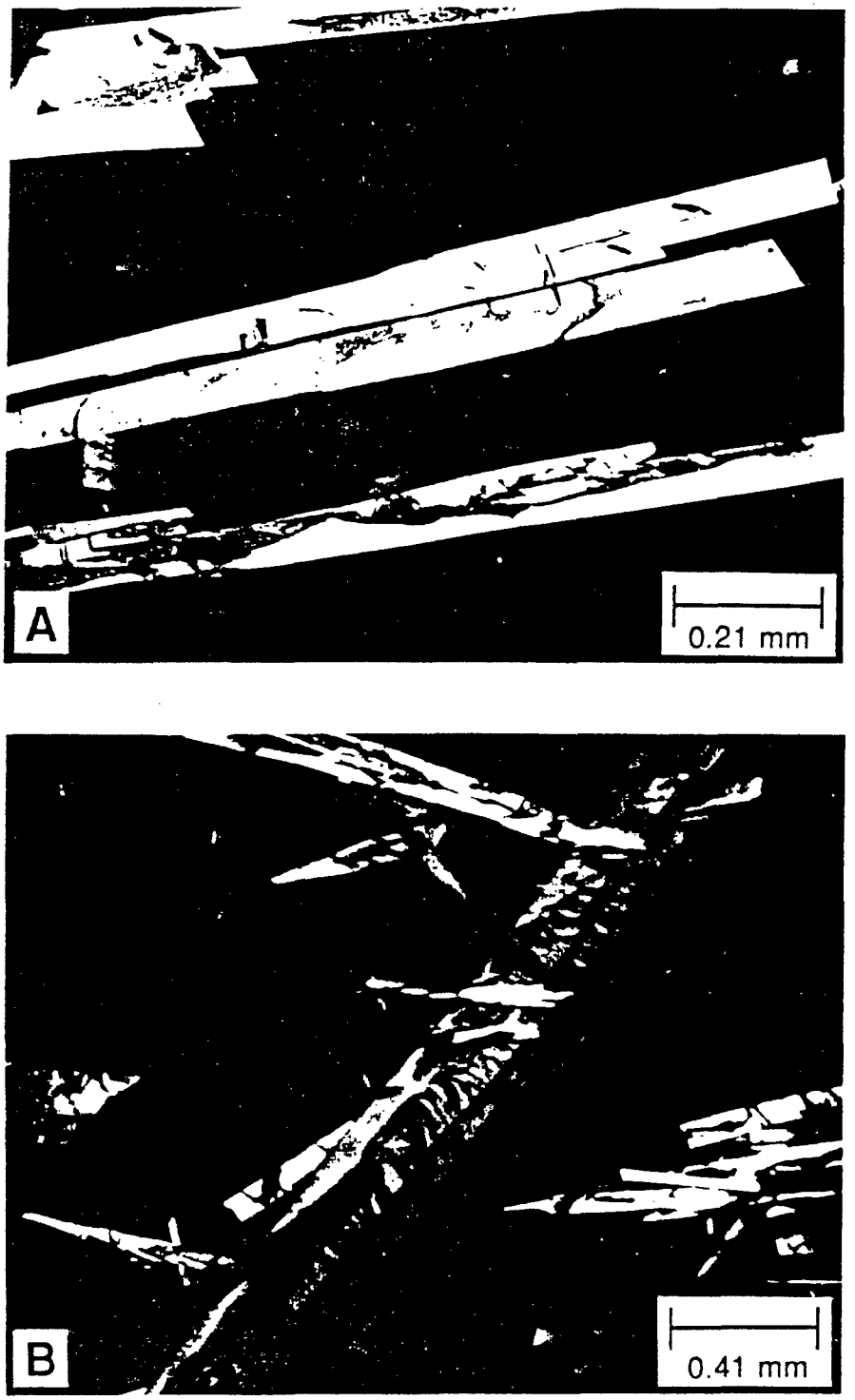

Figure 3: Optical micrographs of DHTAP/MSA crystals.

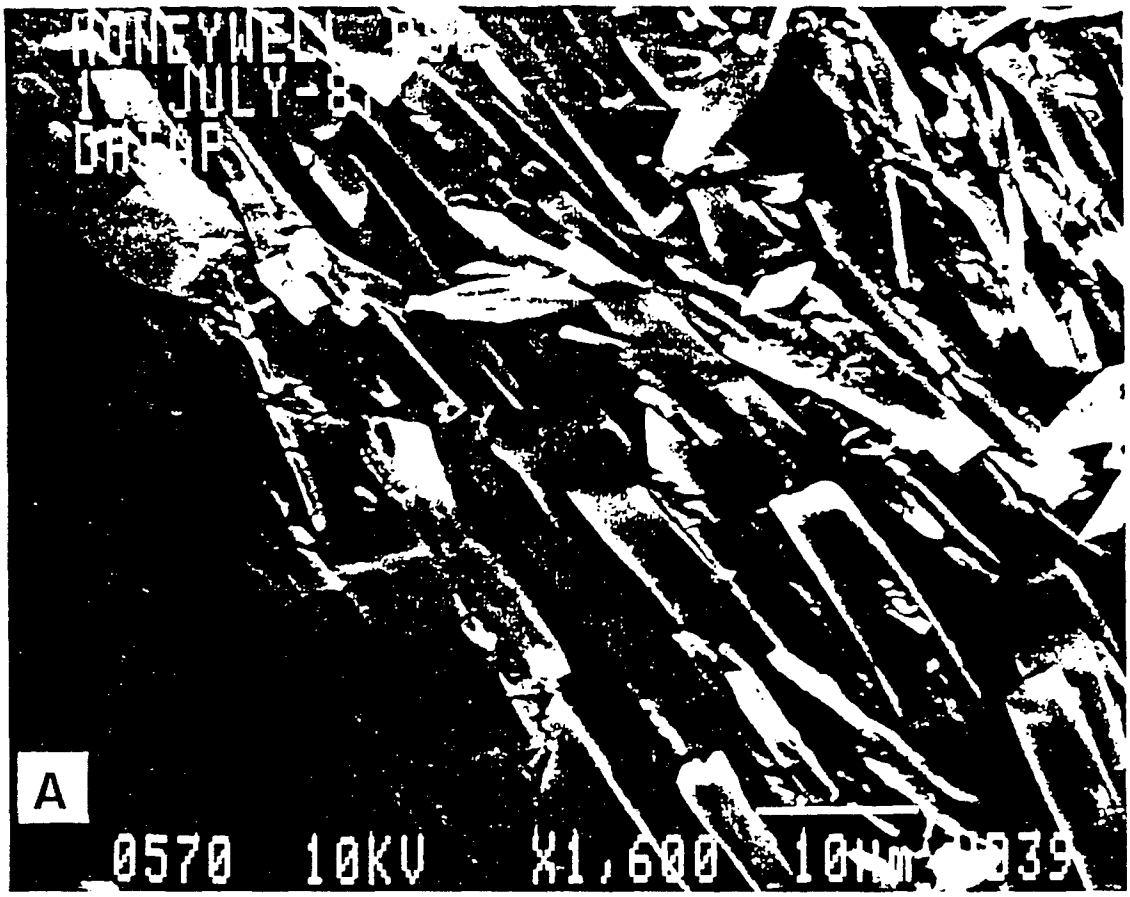

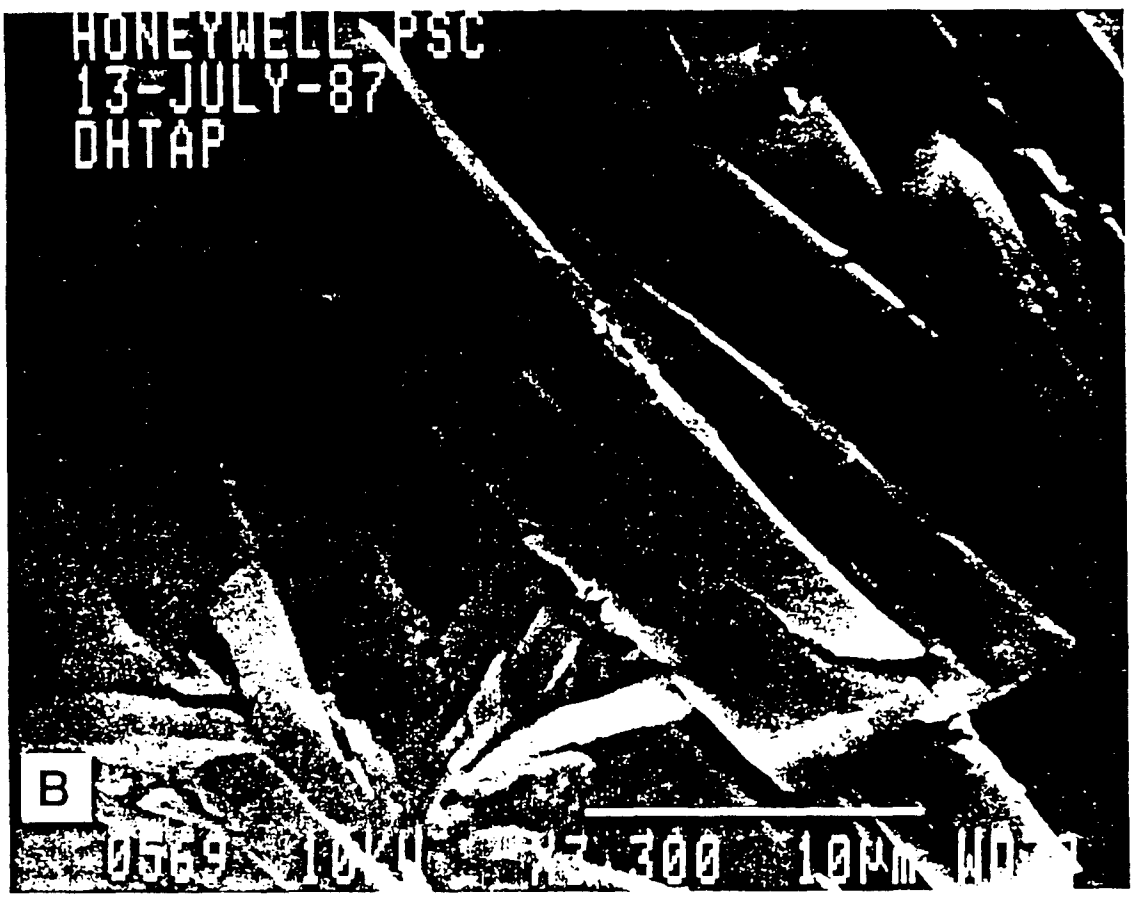

Figure 4: A SEM micrograph of DHTAP/MSA crystallites.

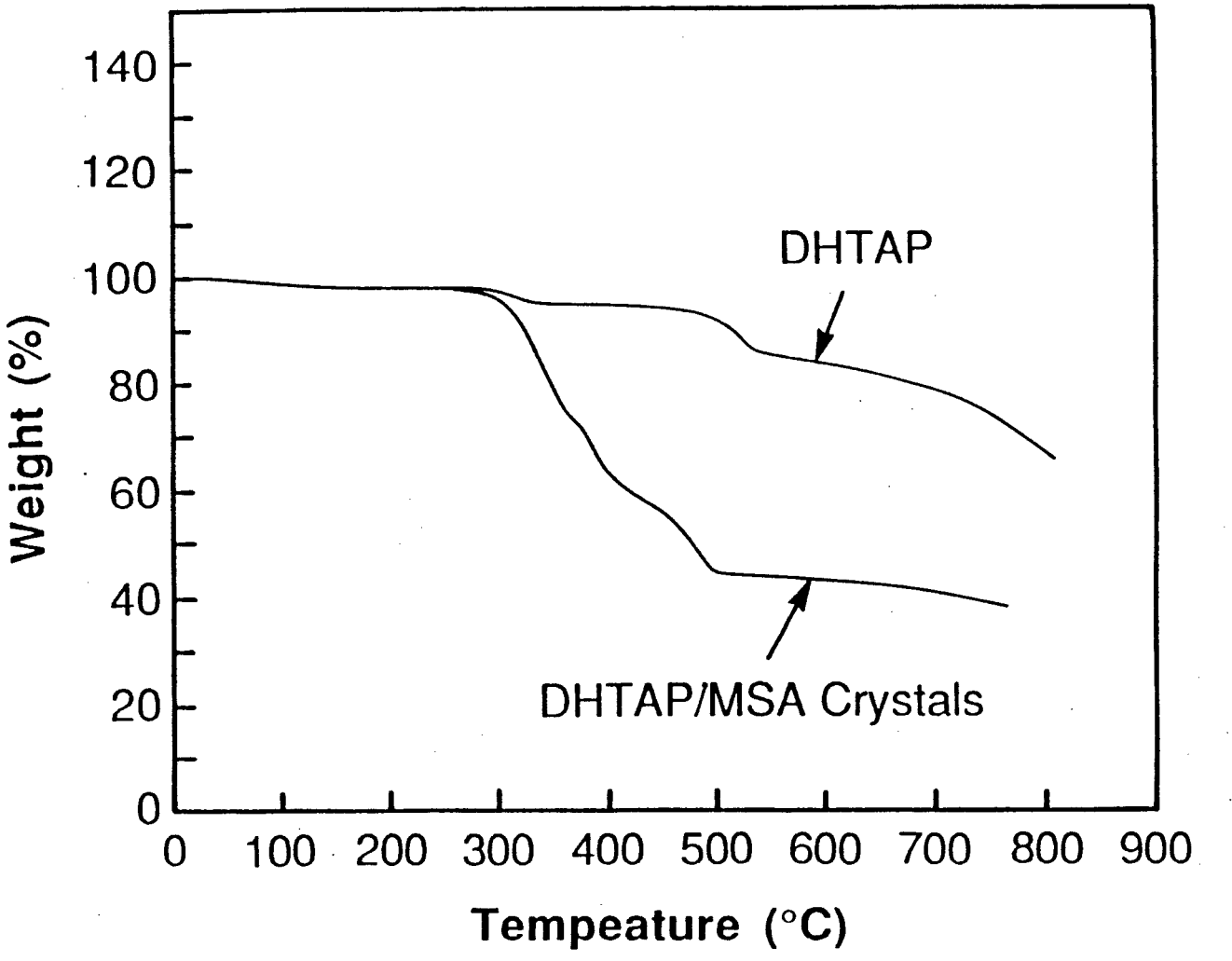

Figure 5: The thermal stability of DHTAP and DHTAP/MSA complex in nitrogen atmosphere; 7°C/min heating rate.

The few percent weight loss at ~300°C is probably due to partial sublimation evidenced by a thin blue coating on the TGA quartz tube wall. It is known that DHTAP sublimes at 280-290°C under moderate vacuum (0.1 torr).[9,30]. Crystals of DHTAP/MSA complex are less stable than the parent compound; onset of significant thermal decomposition is observed at ~300°C. After the initial major weight loss of 55% up to 500°C, very slow weight loss continues and results in about 38% residue at 750°C.

The DSC thermograms of DHTAP and DHTAP/MSA complex are shown in Figures 6 and 7, respectively. The sharp endothermic peak in Figure 6 is interpreted as the melting of DHTAP in the light of the above TGA data which shows its relative stability up to such a high temperature. The peak melting point of DHTAP determined from Figure 6 is 545°C; an estimated heat of fusion obtained by integration of the endothermic peak is 45.5 kJ/mol (10.9 kcal/mol). This high melting point is what might be expected from its molecular structure. Also, it was previously reported that the melting point of DHTAP could not be determined in sealed tubes, apparently up to 400-450°C[9,30]. It is to be noted that the melting point of DHTAP is very close to its decomposition temperature as the TGA data already indicated. Repeated DSC scans of several DHTAP samples also showed partial decomposition prior to the melting point (545°C). However, the sharp melting point was always observed. The peak melting point of DHTAP/MSA complex is 138°C (Figure 7) and the estimated heat of fusion is 84.6 kJ/mol (20.2 kcal/mol).

Electronic Absorption and Emission Spectra

The electronic absorption spectrum of DHTAP in methanesulfonic acid solution is shown in Figure 8. The optical absorption maximum (λ_{max}) is 622 nm (1.97 eV) with a corresponding ϵ value of 10^5 liter $mol^{-1}cm^{-1}$. The other absorption bands and molar absorptivitivies are ($\lambda;\epsilon$): (571 nm; 33,000); (527 nm; 8,800); (293 nm; 51,000); (272 nm; 45,000). A virtually identical electronic absorption spectrum was obtained in sulfuric acid solution: 628 nm (ϵ = 1.13 x 10^5), 576 nm (37,000), 535 nm (10,300), 294 nm (53,000), 271 nm (45,000).

A characteristic feature of the solution electronic spectra of DHTAP is the two relatively narrow and intense absorption bands -- one near 300 nm and the other near 600 nm. Although there are apparently no molecular orbital calcu-lationns or models of the electronic structure and optical properties of DHTAP or closely related molecules that could be used to fully understand the

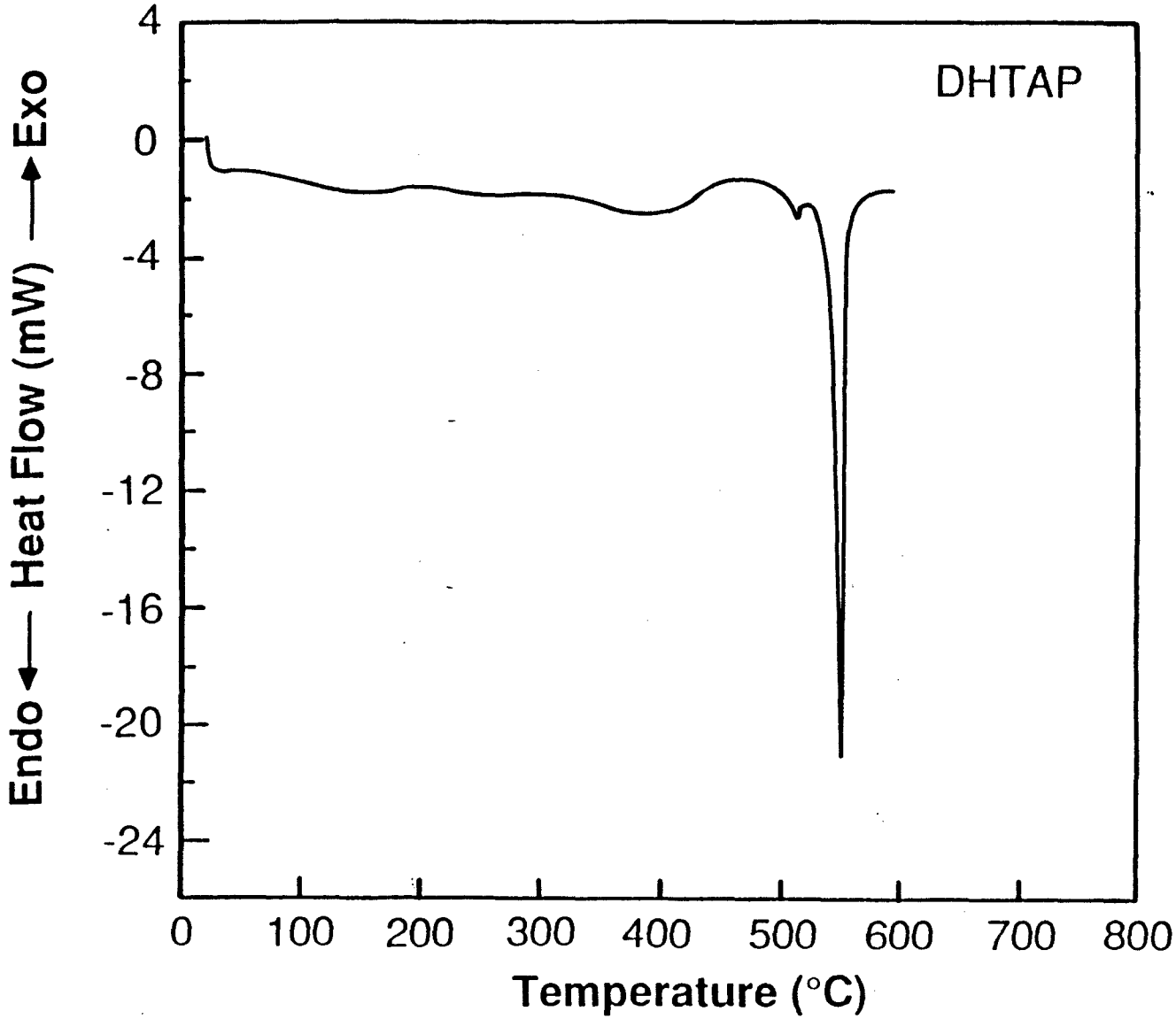

Figure 6: DSC thermogram of DHTAP obtained at heating rate of 7.5°C/min. 71072

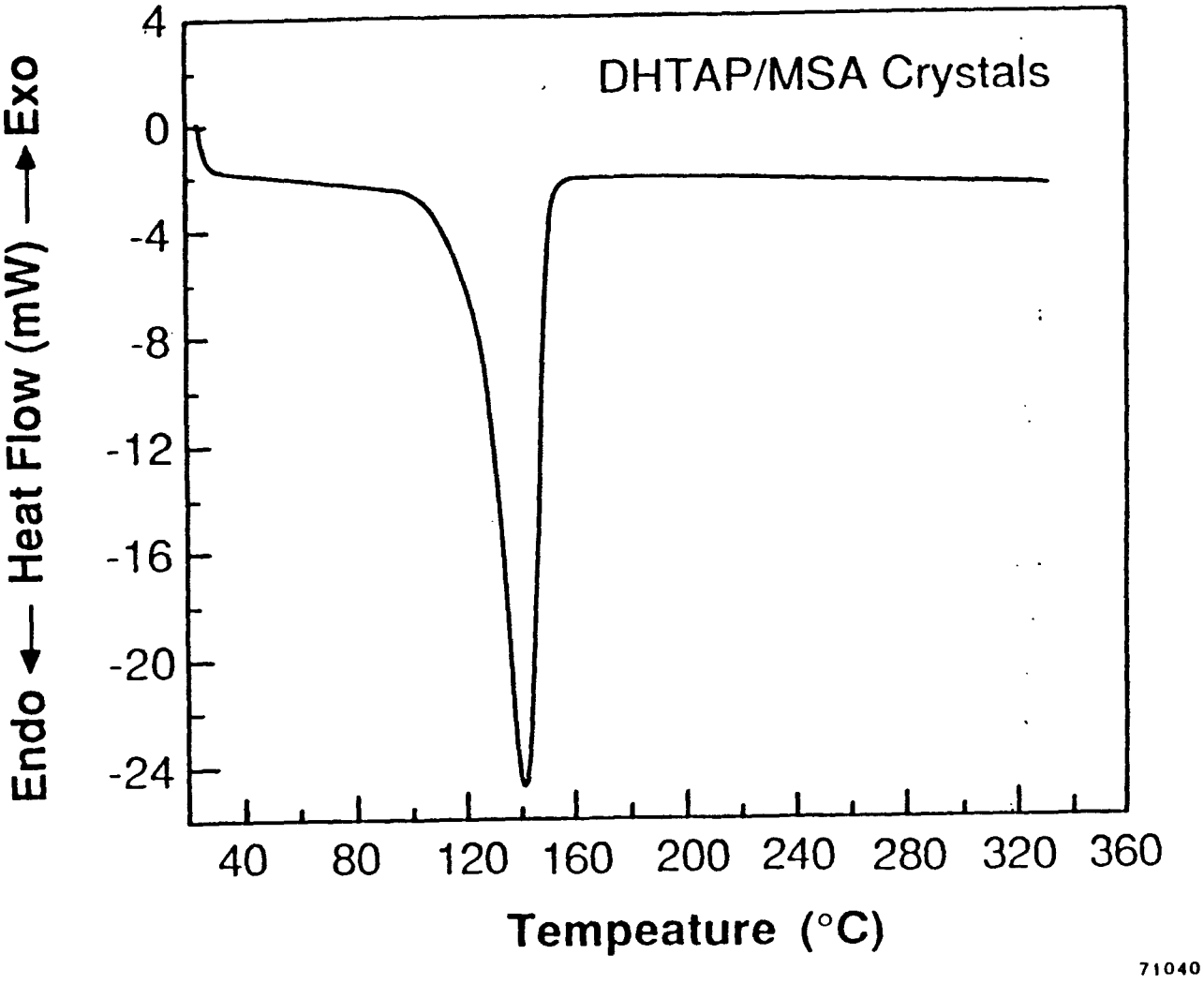

Figure 7: DSC thermogram of DHTAP/MSA complex obtained at a heating rate of 7.5°C/min.

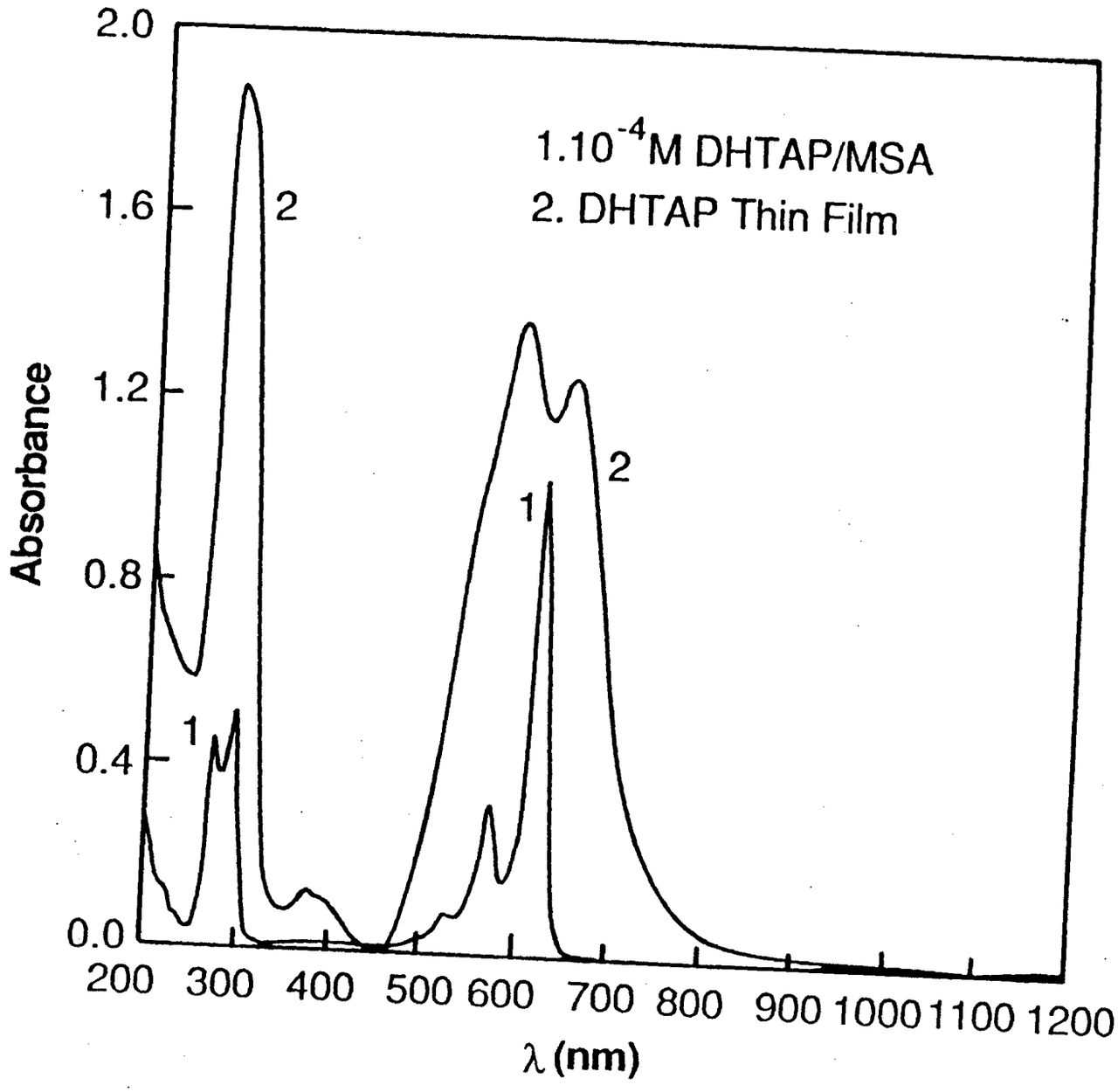

Figure 8: Electronic absorption spectra of: 1)10^{-4}M solution of DHTAP in MSA and 2) DHTAP thin film cast from MSA solution.

71129

nature of the observed electronic transitions, the two distinct absorption bands are most likely due to π-π^* excitations.

Figure 8 also shows the electronic absorption spectrum of DHTAP thin film in the solid state. The characteristic two absorption bands near 300 nm and 600 nm observed in solution are preserved in the thin film spectrum. However, in the solid-state spectrum, these two bands are broadened and the absorption maximum (λ_{max}) of the "600-nm band" is red shifted to 648 nm (1.91 eV) and 593 nm from 622 nm and 571 nm in solution. The observed high degree of π-electron delocalization in DHTAP is what might be expected for the essentially substituted planar tetraazapentacene. This is to be compared to a bandgap of 2.20 $\pm$ 0.3 eV reported for pentacene[28].

Figure 9 shows the solution electronic absorption spectra of DHTAP/MSA complex in methanol and pyridine. Clearly, the spectra have the same structure as those of the pure DHTAP as one would expect since essentially the same chromophone is present in both. However, we see differences between these solution spectra of DHTAP/MSA complex from both the corresponding solution and solid state spectra of pure DHTAP. First, the absorption maximum of the "300-nm band" in DHTAP/MSA complex at 284 nm (ϵ = 3.87 x 10^5) has no splitting and is more intense and broader, compared to DHTAP in solution. Secondly, although the "600-nm band" of pure DHTAP in Figure 8 is at the same position in the methanol solution of the complex (λ_{max} = 626 nm, 576 nm), it is considerably broader. The complex in pyridine exhibits a broader "600-nm band" which is blue shifted to λ_{max} = 549 nm (ϵ = 2.0 x 10^4) and 516 nm (ϵ = 2.1 x 10^4). Unfortunately, because of the absorption of pyridine below 300 nm, the "300-nm band" of the complex in pyridine could not be observed.

The absorption spectrum of a thin film of DHTAP/MSA complex in the solid state is shown in Figure 10. The characteristic two absorption bands near 300 nm and 600 nm are also observed; the "300 nm band" is located at 294 nm. However, the "600-nm band" actually consists of two peaks at 663 nm and 590 nm merged into a very broad single band (450-800 nm) with the center at 616 nm. Comparison of all the absorption spectra of DHTAP and DHTAP/MSA complex in solutionn and solid state (Figures 8 through 10) shows that broadening of the absorption bands is the primary effect of increasing solution concentration ultimately to the solid state. This is to be contrasted with emission properties which depend strongly on concentration and solvent.

The red fluorescence of concentrated sulfuric acid solutions of DHTAP was already visually observed and mentioned by Badger and Pettit[30]. The deep

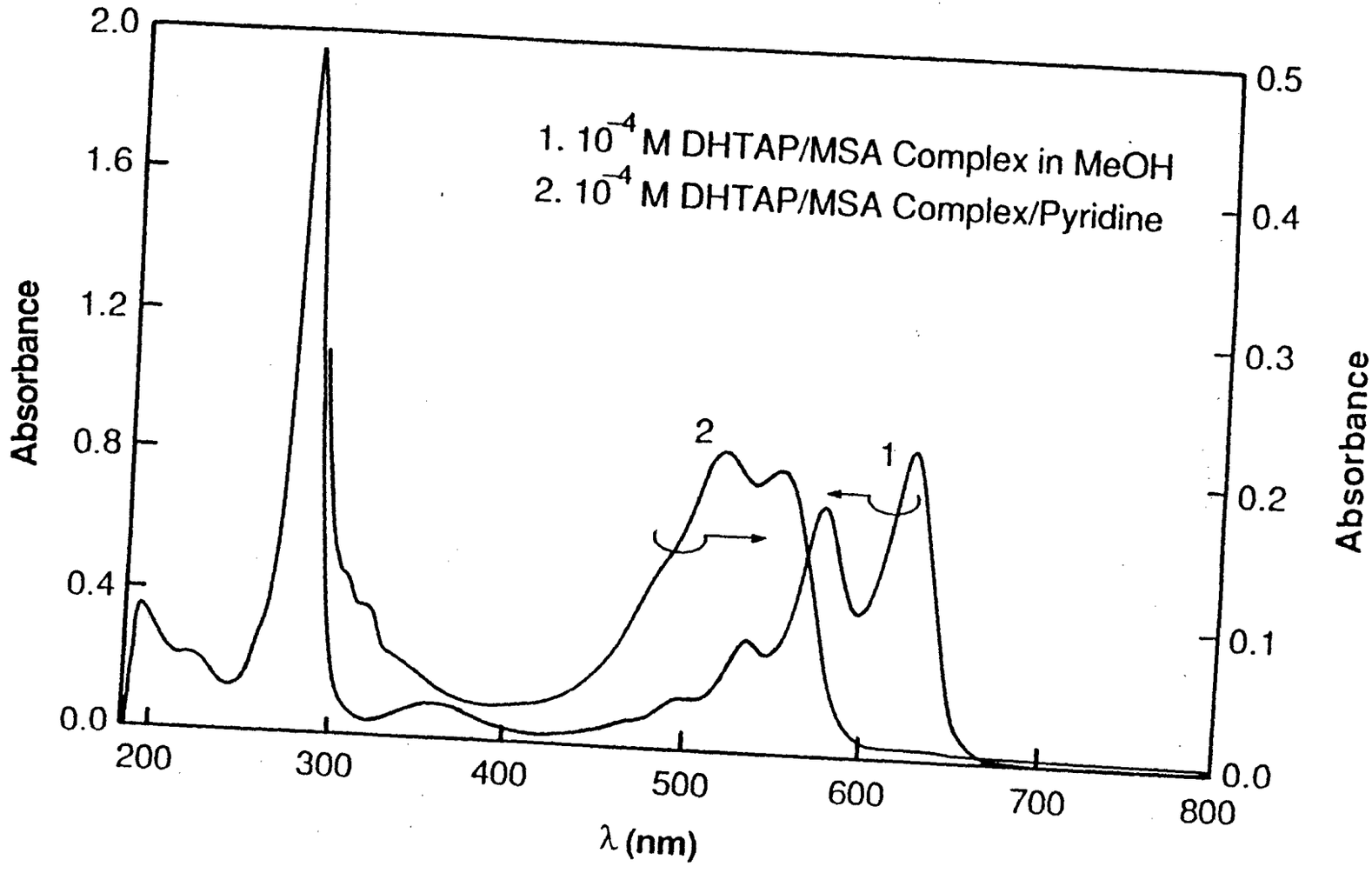

Figure 9: Electronic absorption spectra of DHTAP/MSA complex in solution: 1) 10^{-4}M methanol solution and 2) 10^{-4}M pyridine solution.

71130

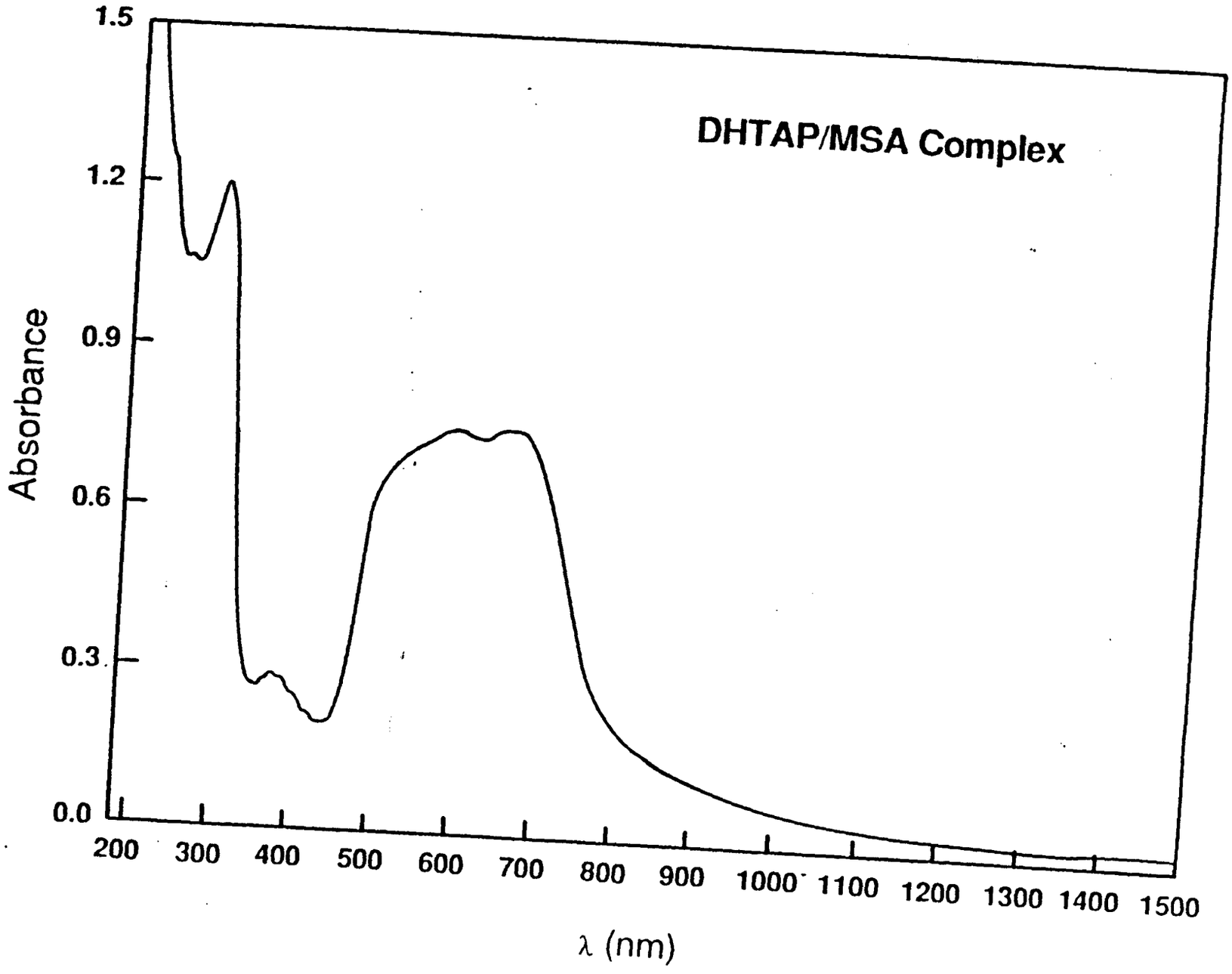

Figure 10: Electronic absorption spectrum of a thin film of DHTAP/MSA complex.

71189

blue acid (H_2SO_4, MSA) solutions of DHTAP exhibit visually observable red fluorescence as well as films cast on substrates from these solutions. Transparent blue films of DHTAP/polystyrene blends cast from conc. H_2SO_4 also show red fluorescence.

The typical fluorescence emission spectra of solutions of DHTAP or its methanesulfonate complex (DHTAP/MSA) are shown in Figures 11, 12, and 13. Emission from concentrated H_2SO_4 solutions of the pristine DHTAP excited at 566 nm is shown in Figure 11. Emission spectra of the DHTAP/MSA complex in methanol and DMF solutions are shown in Figures 12 and 13, respectively. One characteristic feature of the emission spectra is that a more symmetric and relatively sharp spectrum is generally obtained at the very low concentrations than at high concentration. In the case of DHTAP/MSA solution in MeOH, two fluorescence peaks are observed at the high concentration (1.38×10^{-4}M) compared with one peak at the low concentration (1.2×10^{-5}M). The observed fluorescence emission maximum (λ^e_{max}) in solutions of DHTAP and its complex are shown in Table 2. In general, the emission properties, and especially λ^e_{max}, strongly depend on the concentration of the solution and the solvent. Fluorescence intensity generally increased with increasing concentration at a fixed excitation wavelength, as would be expected.

Figure 14 shows the concentration dependence of λ^e_{max} for solutions of DHTAP in concentrated H_2SO_4. At concentrations of ~2.0×10^{-5}M or less, λ^e_{max} has a value of 622 nm, whereas at ~5.0×10^{-5}M or more λ^e_{max} has a value of 640 nm. Thus, a sharp transition in the nature of the excited state occurs in the narrow concentration range between 2-5 $\times 10^{-5}$M. Very similar concentration-dependent emission properties of DHTAP solution were observed at different excitation wavelengths. The concentration effects on the solution emission properties of the DHTAP/MSA complex in methanol are very similar to those of the pristine DHTAP, as indicated in Table 2. An even wider difference between the λ^e_{max} values at the low and high concentrations is observed compared to pristine DHTAP. However, emission maximum of the DHTAP/MSA complex in DMF is 580 $\pm$ 2 nm and is independent of concentration up to 1.65×10^{-4}M.

Concentration and solvent dependence of the emission properties of DHTAP and its methanesulfonate complex, and particularly λ^e_{max}, is the principal feature of the data that must be elucidated. We attribute the observed concentration dependence of the emission spectra to *aggregation phenomena* in solution at high concentrations. It is thus assumed that at sufficiently low concentrations the dicationic species of doubly protonated

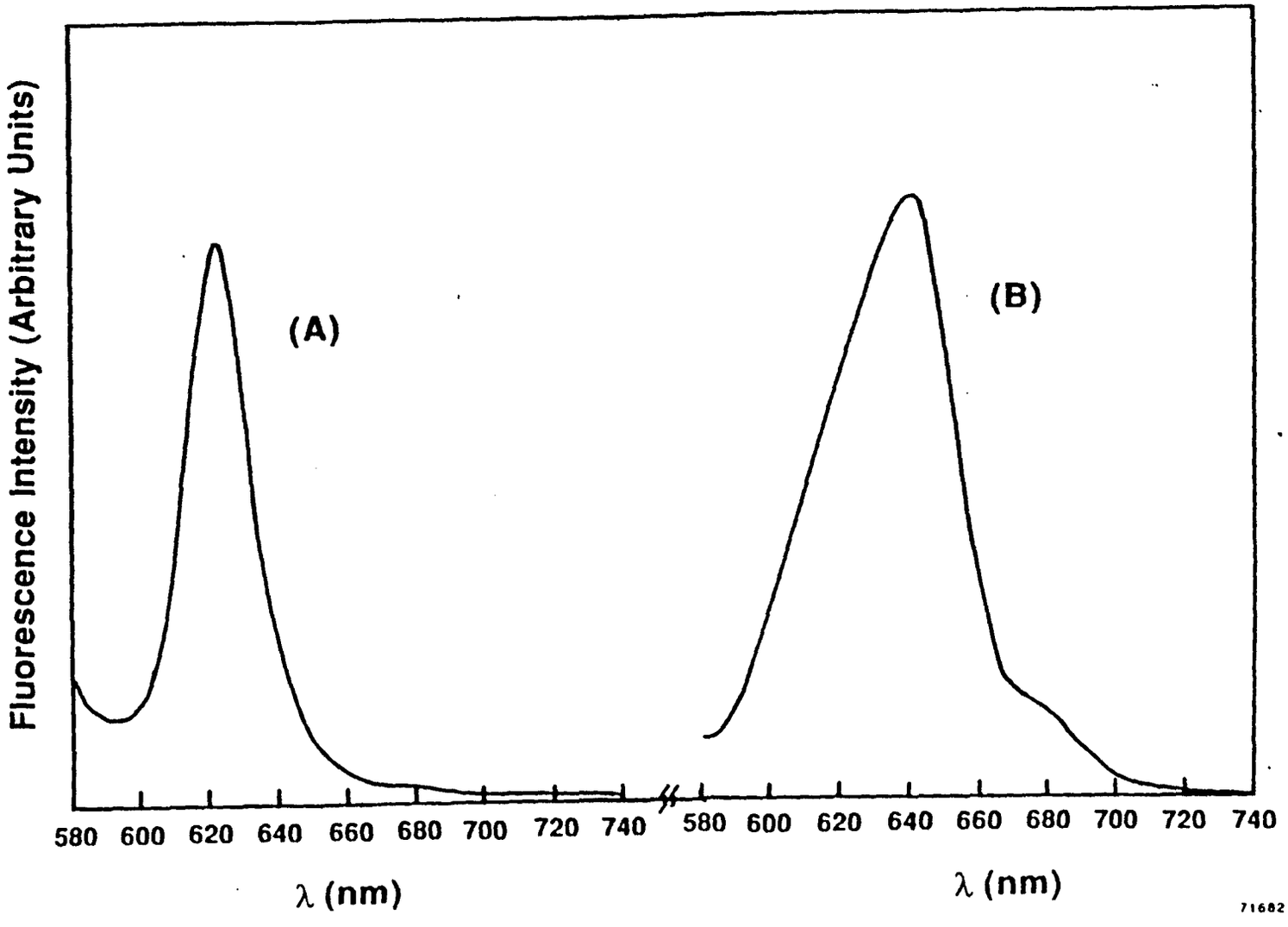

Figure 11: Fluorescence emission spectra of DHTAP solutions in conc. H_2SO_4, excited at 566 nm: A) 1.9×10^{-6}M; B) 1.9×10^{-4}M.

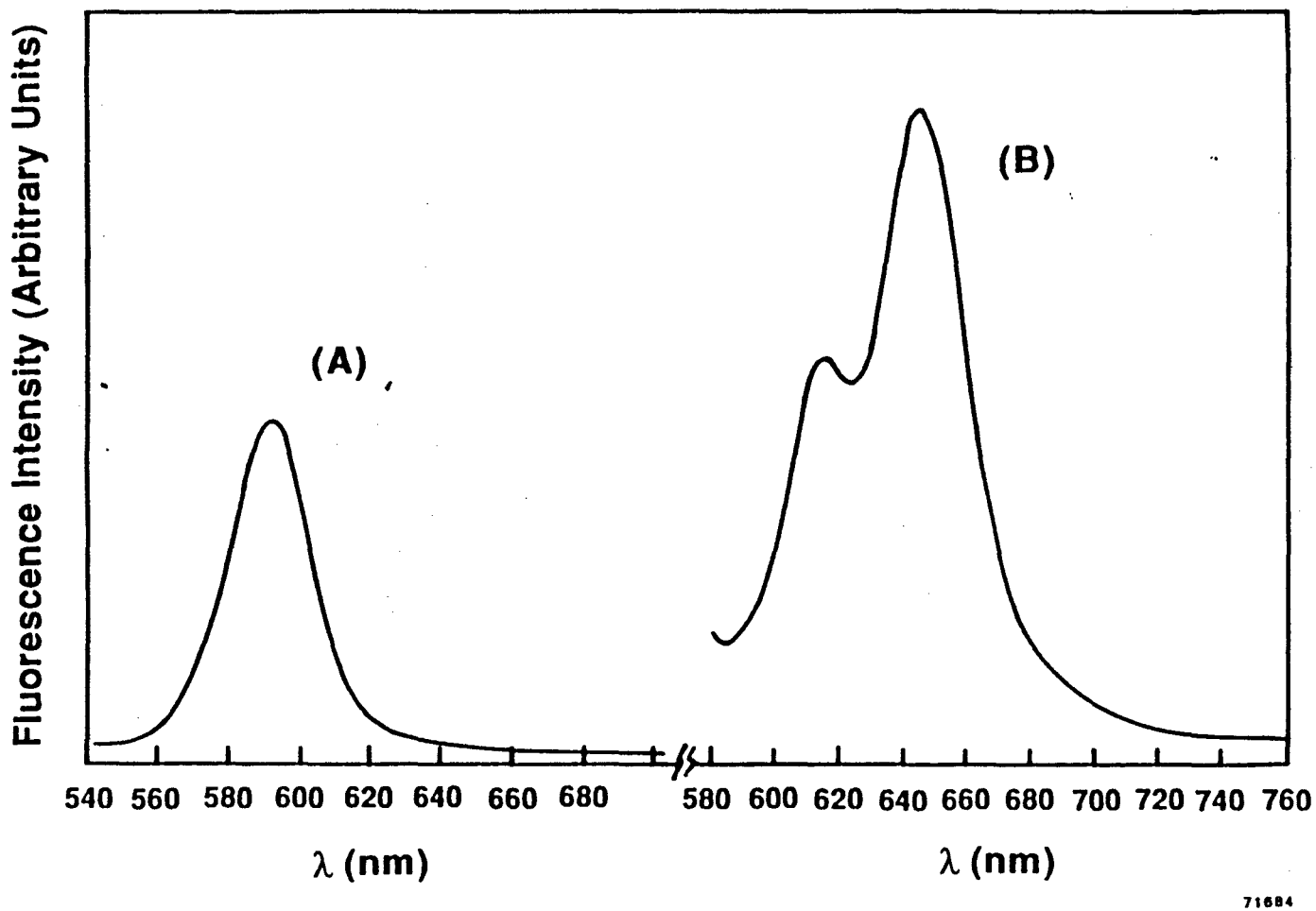

Figure 12: Fluorescence emission spectra of DHTAP/MSA complex solutions in MeOH, excited at 566 nm: A) 1.2 x 10^{-5}M; B) 1.38 x 10^{-4}M.

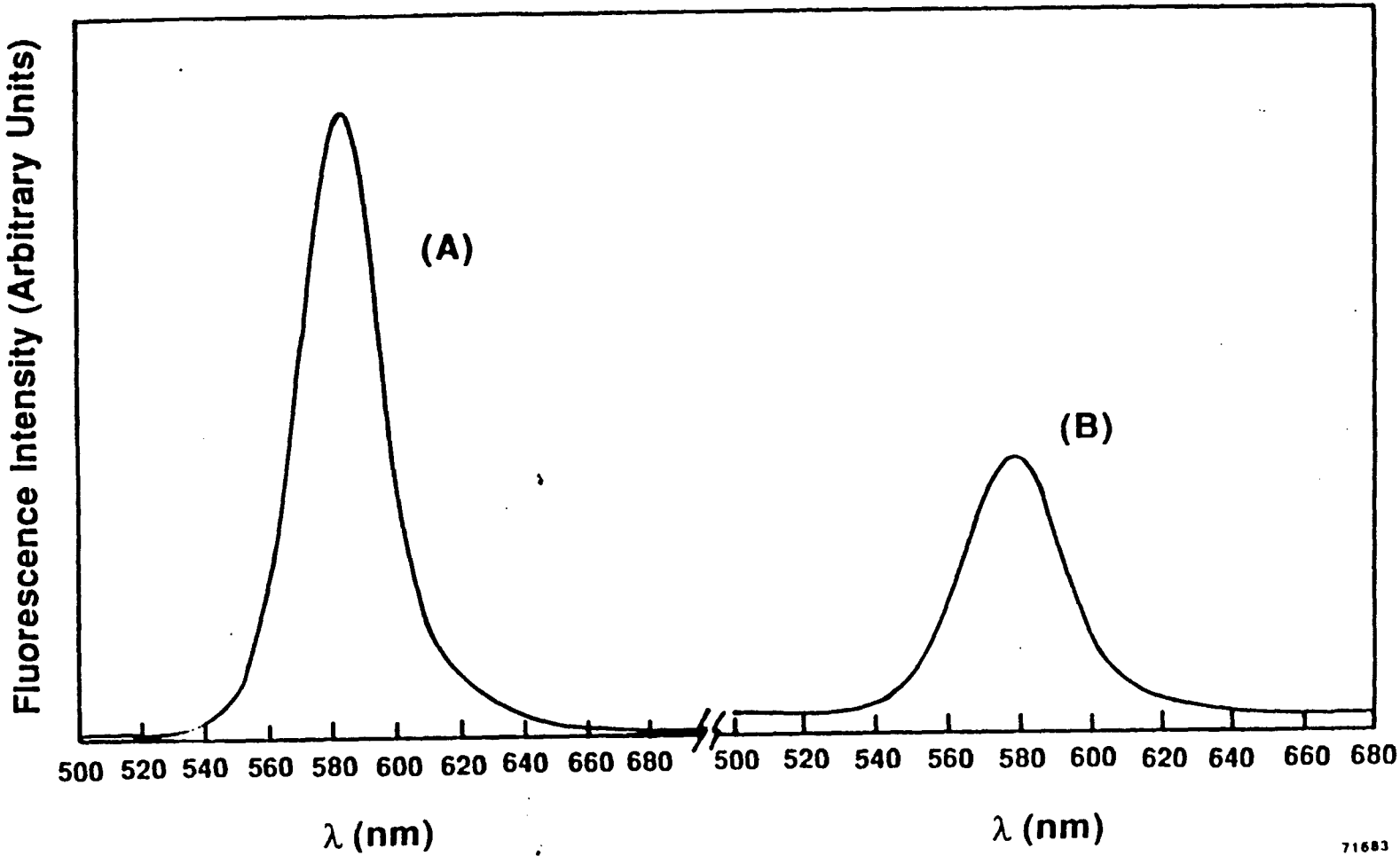

FIgure 13: Fluorescence emission spectra of DHTAP/MSA complex solutions in DMF, excited at 470 nm: A) 1.36 x 10^{-6}M; B) 1.65 x 10^{-4}M.

TABLE 2. FLUORESCENCE EMISSION PROPERTIES OF DHTAP AND ITS COMPLEXES IN SOLUTION IN DIFFERENT SOLVENTS AT 566 nm EXCITATION WAVELENGTH

DHTAP in H_2SO_4		DHTAP/MSA in MeOH		DHTAP/MSA in DMF	
Conc. (M)	λ^e_{max}(nm)	Conc. (M)	λ^e_{max}(nm)	Conc. (M)	λ^e_{max}(nm)
1.9×10^{-6}	622	1.2×10^{-5}	591	1.36×10^{-6}	580**
3.3×10^{-6}	622	1.2×10^{-5}	592*	1.45×10^{-5}	578**
8.6×10^{-6}	622	1.38×10^{-4}	645 (615)	1.65×10^{-4}	582**
1.6×10^{-5}	622				
2.5×10^{-5}	626				
3.5×10^{-5}	635				
4.0×10^{-5}	637.5				
6.0×10^{-5}	640				
8.0×10^{-5}	641 (615)				
9.5×10^{-5}	640				
1.9×10^{-4}	640				

* - Excitation Wavelength at 530 nm

** - Excitation Wavelength at 470 nm

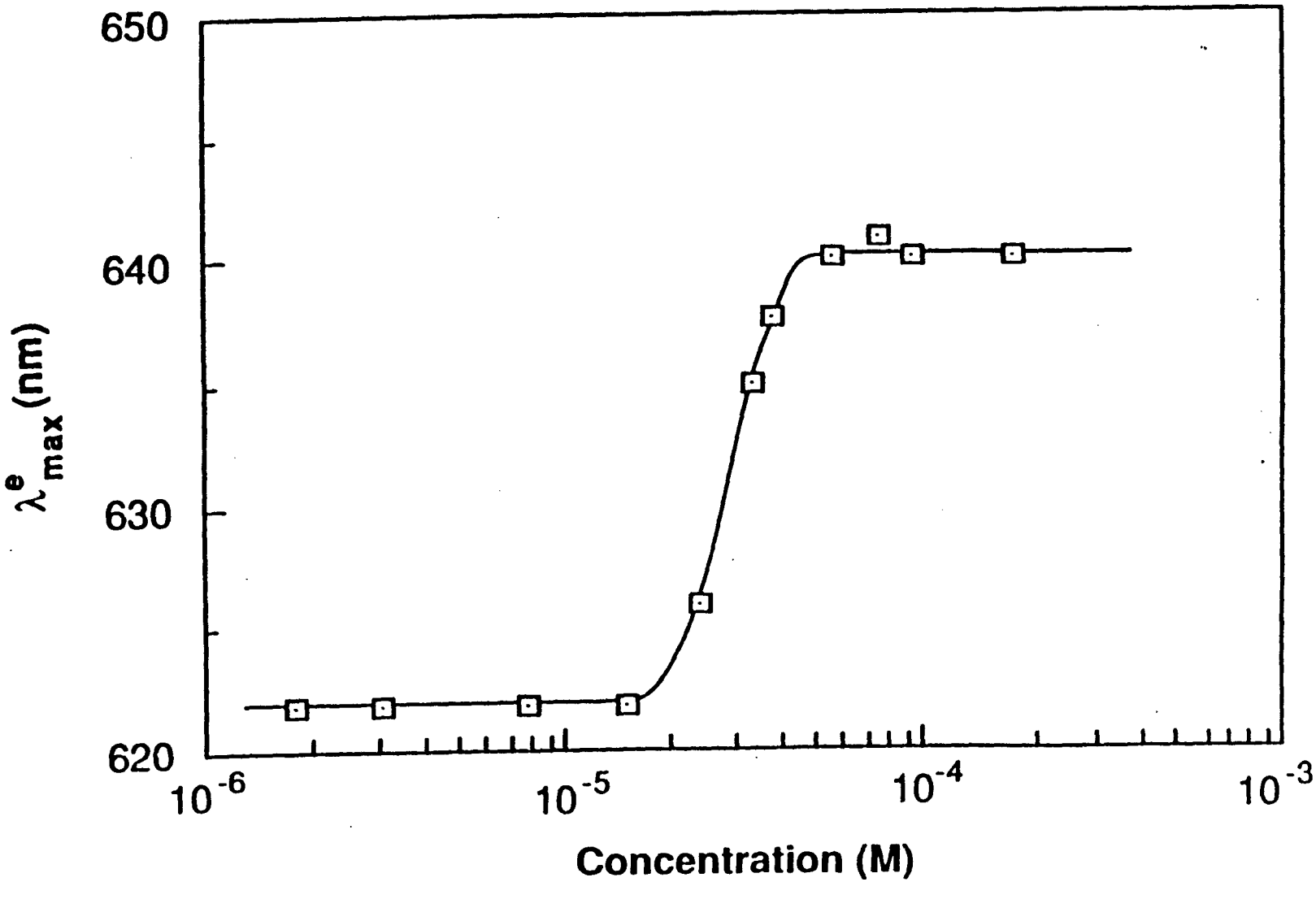

Figure 14: The concentration dependence of the emission maximum (λ^e_{max}) in DHTAP solutions in conc. H_2SO_4.

DHTAP (i.e., $DHTAPH_2^{2+}$) are fully ionized and dissociated, whereas at sufficiently high concentrations, dimeric or higher molecular weight aggregates of $DHTAPH_2^{2+}$ are formed. If such aggregates are formed in solution, it can be expected that due to the different effects of the aggregation and solvation on the excited states of the aggregated molecular system compared to the unaggregated molecular species, the observed results can be accounted for. Precedence for the effects of aggregation phenomena on the emission properties of organic molecules in solution exists[29,35], for example, cationic polymethine cyanine dyes. An alternative explanation based on complex formation between DHTAP species and solvent molecules was ruled out, since similar concentration effects were observed in sulfuric acid where complex formation in solution exists and in methanol where $DHTAPH_2^{2+}$ $(CH_3SO_3^-)_2$ is fully ionized in solution and is not expected to form a complex with MeOH.

Electrochemistry

There are many interesting aspects, as well as possible complications, in the electrochemistry of DHTAP and its derivatives because of the many possible electron and proton transfer processes, as shown in Figure 15. One question is the feasibility of electrochemical oxidation of the quiniodal DHTAP to the aromatic 5,7,12,14-tetraazapentacene (TAP). However, Badger and Pettit[30] have reported unsuccessful attempts to chemically oxidize DHTAP to TAP and consequently, suggested that the quinoid system of DHTAP seems to be more stable than the aromatic system of TAP. These authors have also reported successful chemical reduction of DHTAP in solution to the colorless 5,7,12,14-tetrahydro-5,7,12,14-tetraazapentacene (THTAP), which rapidly oxidized in air back to DHTAP. One difficulty in trying to understand the redox properties of DHTAP is that it is only soluble in strong acids and the fact that the electro-chemistry of imine (=N-) systems in acid solutions can be greatly complicated by accompanying protonation/deprotonation processes as is known in polyani-lines[36-37] and benzimidazolebenzophenanthroline-type ladder polymer (BBL)[19-20]. Badger and Pettit's results must be understood in this light, since their chemical redox reactions were performed in acid solutions. Our experiments and results on the electrochemistry of DHTAP and its derivatives are thus only a preliminary study of a complicated electrochemical system.

Figure 16 shows a cyclic voltammogram (CV) of the DHTAP/MSA complex, i.e., $DHTAPH_2^{2+}(CH_3SO_3^-)_2$, in solution (0.1M TEAP/DMSO). All the redox peaks are due to the complex, since a blank 0.1M TEAP/DMSO showed no peaks in the

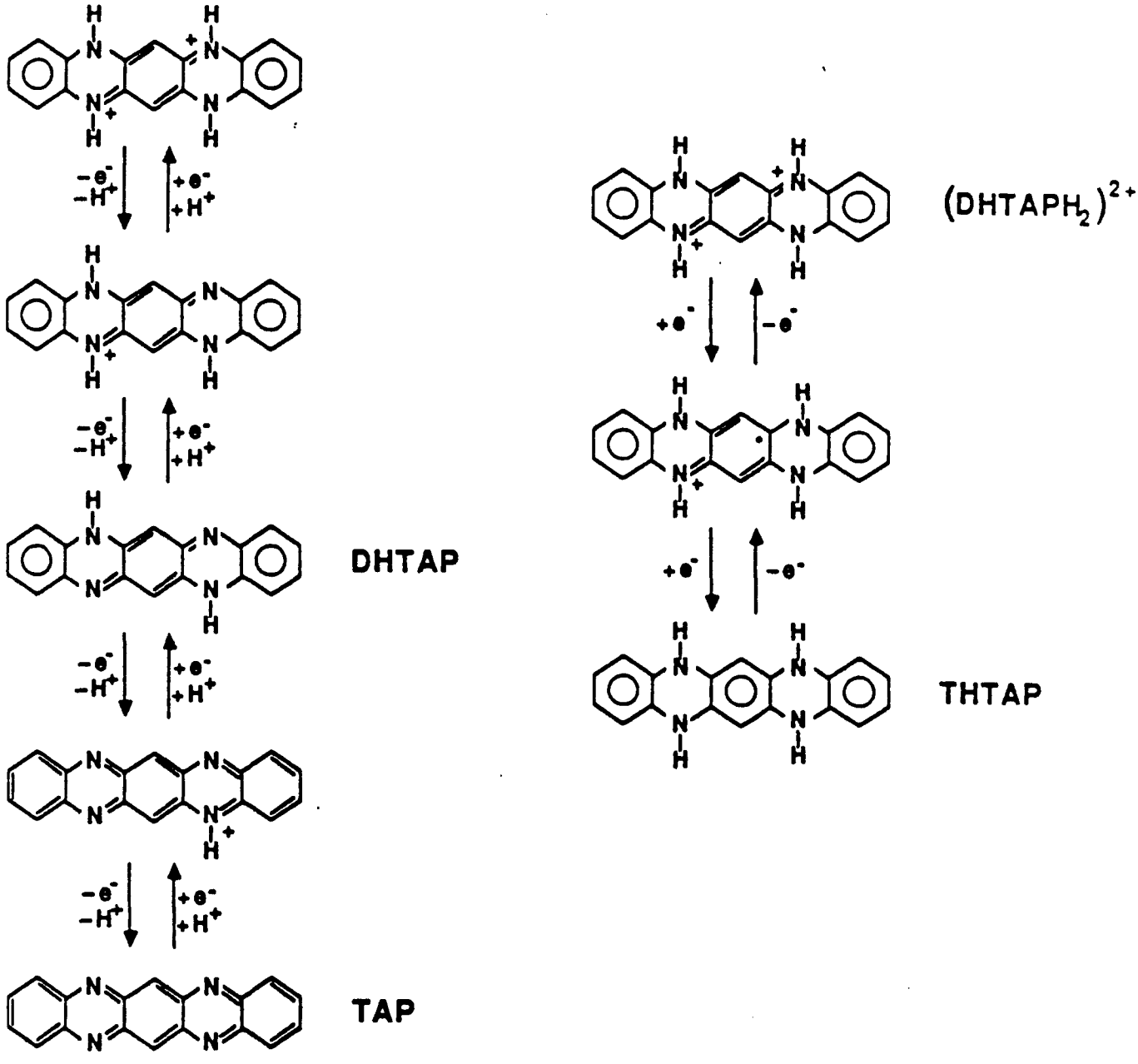

Figure 15: Some of the possible electron and proton transfer processes in DHTAP.

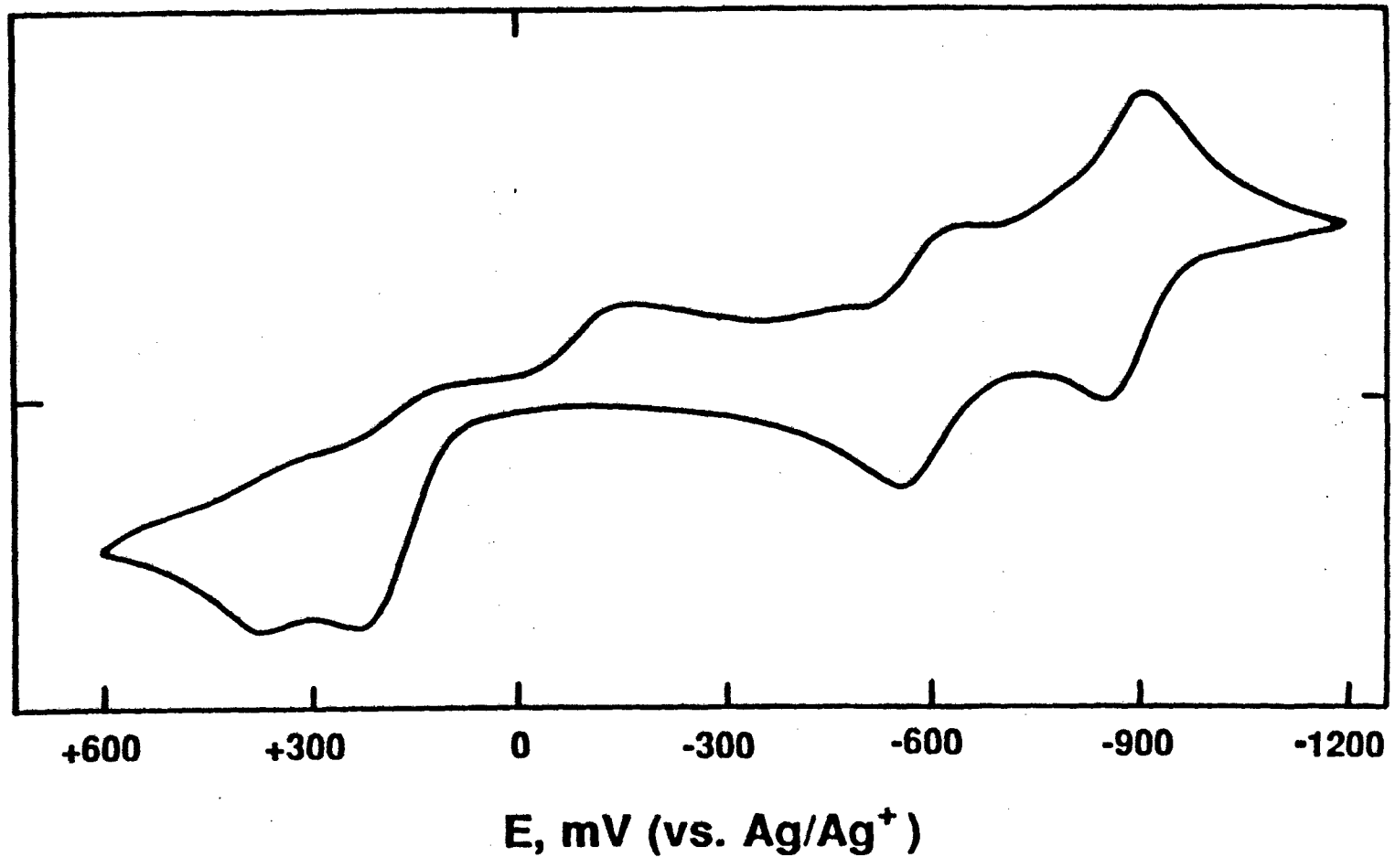

Figure 16: Cyclic voltammogram of 10^{-3}M DHTAP/MSA complex in DMSO/0.1M TEAP at 50 mV/s scanning rate.

potential range +600 mV to -1200 mV (vs Ag/Ag^+). The CV exhibits two reversible redox couples from which the first and second $E^{\bullet\prime}$ values, each calculated as $(E_p^{ox} + E_p^{red})/2$, are obtained at -0.57 V and -0.88 V (vs Ag/Ag^+). These $E^{\bullet\prime}$ values are tentatively interpreted as the first and second reduction potentials of $DHTAPH_2^{2+}$ in solution. In addition, two irreversible oxidation peaks are observed at +0.23 V and +0.37 V in the CV. These oxidation peak potentials cannot yet be assigned. Attempts to obtain a CV of pristine DHTAP in aqueous sulfuric acid solution were not successful; about four redox couples, all at potentials greater than OV (vs Ag/Ag^+), were always obtained, but could not be reproduced.

Electrochemical behavior of polycrystalline thin films of DHTAP on Pt flag (cast from MSA or H_2SO_4 solutions) was also investigated by cyclic voltammetry at a scan rate of 100 mV/s. A large irreversible redox couple, with peak reduction and oxidation potentials at -955 mV and -626 mV (vs Ag/Ag^+) respectively, as well as electrochromism, were observed by cycling between +100 mV and -1900 mV. Both the redox couple and the electrochromism were stable to repeated cycling. The as-deposited thin film on Pt electrode was gold-yellow in color, turning red (with patches of blue) after reduction at -955 mV and returning to gold-yellow upon oxidation at -626 mV. A detailed elucidation and delineation of the electron and proton transfer processes of DHTAP (see Figure 15) will require further studies of solution electrochemistry of DHTAP in conjunction with electronic absorption spectroscopy of the same species.

Electrical Conductivity

Compressed pellets of DHTAP had insulating electrical properties, the room temperature d.c. conductivity being less than could be measured on our instruments ($\sigma_{RT} < 10^{-12}$ S/cm). Compressed pellets of DHTAP/MSA crystals had a σ_{RT} value of $\sim 4 \times 10^{-2}$ S/cm. Higher values of the conductivity were observed in a humid atmosphere, indicating moisture sensitivity of the samples. TGA studies showed that unbaked DHTAP/MSA complex can pick up to 3-8% wt moisture from the air. The conductivity also decreased on cooling to dry ice temperature, which suggests that the methanesulfonate salt of DHTAP is a semiconductor and not a metal.

Even if the single crystal room temperature conductivity of DHTAP/MSA salt is two orders of magnitude higher than the compressed pellet value of σ_{RT}, as commonly observed, it is still quite small when compared to such

charge-transfer salts as N-methylphenazinium (NMP)/TCNQ or TTF/TCNQ which have single crystal σ_{RT} values in the range of 100-1000 S/cm. The two possible primary factors that might explain the small conductivity value for the salt $(DHTAPH_2)^{2+}(CH_3SO_3^-)_2$ are (1) the complete charge-transfer unlike partial charge-transfer obtained in TTF/TCNQ and related salts, and (2) mixed stack crystals versus segregated stack crystals observed in TTF/TCNQ and related metallic complexes. However, it is not yet clear from our X-ray powder diffraction results if the crystal structure of DHTAP/MSA complex is indeed of the mixed stack type. The role of first factor will be further evaluated when results on other DHTAP complexes, such as those of TCNQ, become available.

A very preliminary measurement of the room temperature d.c. conductivity of compressed powdered samples of $DHTAP^+ \cdot X^-$ ($X = BF_4$, HSO_4) showed values of $\sim 10^{-4}$ S/cm, which is orders of magnitude less than the conductivity of DHTAP/MSA complex. However, the purity and quality of the powdered $DHTAP^+ \cdot X^-$ samples were much poorer than the DHTAP methanesulfonate crystals.

Implications for High Molecular Weight Ladder Polyquinoxalines

The high molecular weight ladder polyhydroquinoxaline with identical molecular structure to DHTAP can be synthesized by a similar scheme except that the diamine is replaced by 1,2,4,5-tetraaminobenzene or its tetrahydrochloride[9,38]. Assuming a truly perfect ladder structure and a significantly higher degree of polymerization, the mechanical properties, melting, thermal stability, and solubility in solvents are obviously expected to be different from the model compound DHTAP. The electrochemistry of the high polymer is expected to be similar to the model compound. The optical properties, particularly the energy gap, are expected to improve with the degree of polymerization. Preliminary indications indeed show that the polymer (which is black in color) may have a much smaller bandgap[38]. It is not clear if *crystalline* charge-transfer complexes similar to DHTAP/MSA can be achieved in the polymer; however, similar charge-transfer or redox reactions are expected to produce electrically conducting polymers. Overall, it is anticipated that the structural and physicochemical properties of the high molecular weight ladder polyquinoxalines would be similar enough to the model compound DHTAP that the present results would provide insights into the more complex high polymers.

Conclusions

The structural and physico-chemical properties of a model compound of ladder polyquinoxalines, 5,12-dihydro-5,7,12,14-tetraazapentacene (DHTAP), have been investigated, including crystallization and melting, thermal stability, morphology, solubility, electronic absorption and emission, electrochemistry, charge-transfer complex formation, and electrical conductivity. DHTAP melts at 545°C, close to its decomposition. The electronic absorption spectra of DHTAP in solution and in the solid state each exhibits two characteristic intense bands -- near 300 nm and 600 nm -- interpreted as π-π^* transitions.

DHTAP and its charge-transfer complexes exhibit strong fluorescence in solution and the emission properties depend on concentration and solvent. The fluorescence emission maximum (λ^e_{max}) of DHTAP in concentrated H_2SO_4 in the concentration range 10^{-6} to 10^{-3}M, for example, exhibits a sharp transition from 622 nm to 640 nm at 2-5 x 10^{-5}M. The observed dependence of the fluorescence emission properties on concentration and solvent is attributed to aggregation phenomena in solution at the high concentrations.

It is shown that DHTAP forms a conductive crystalline charge-transfer complex with methanesulfonic acid (MSA) resulting in a methanesulfonate salt of the 7,14-protonated DHTAP: $(C_{18}H_{14}N_4)^{2+}(CH_3SO_3^-)_2$. Unlike the pristine DHTAP, the DHTAP/MSA complex is soluble in many polar solvents and it has a room temperature compressed pellet dc conductivity of about 10^{-2} S/cm. The highly anisotropic needlelike crystals of DHTAP/MSA complex exhibit a melting point at 138° and decompose at about 300°C. Other conductive charge-transfer complexes of DHTAP were prepared, demonstrating that DHTAP is an excellent new donor for the preparation of many conducting charge-transfer complexes.

The present results on the structural and physical properties of the model compound DHTAP and its charge-transfer complexes have direct implications for the high molecular weight ladder polyquinoxalines and will serve as a useful basis for comparison in subsequent studies of the related high polymers.

2.1.4 REFERENCES FOR SECTION 2.1

1. Van Deusen, R.L. *J. Polym. Sci.: Polym. Lett.*, **1966**, B14, 211-214.
2. Arnold, F.E.; Van Deusen, R.L. *Macromolecules*, **1969**, 2, 497-503.
3. Arnold, F.E.; Van Deusen, R.L. *J. Appl. Polym. Sci.*, **1971**, 15, 2035-2047.
4. Arnold, F.E. *J. Polym. Sci. Part A-1*, **1970**, 8, 2079-2089.
5. Bailey, W.J., In: "Encyclopedia of Polymer Science and Technology", Wiley: New York, Vol. 8, pp. 97-120.
6. Sicree, A.J.; Arnold, F.E.; Van Deusen, R.L. *J. Polym. Sci.: Polym. Chem. Ed.*, **1974**, 12, 265-272.
7. (a) Stille, J.K.; Mainen, E. *J. Polym. Sci.: Polym. Lett. Ed.*, **1966**, 4,39-41;
   (b) *ibid*, **1966**, 665-667.
8. Stille, J.K.; Freeburger, M.E. *J. Polym. Sci.: Polym. Lett. Ed.*, **1967**, 5, 989-992.
9. Stille, J.K.; Mainen, E.L. *Macromolecules*, **1968**, 1, 36-42.
10. Imai, K.; Kurihara, M.; Mathias, L.; Wittman, J.; Alston, W.B.; Stille, J.K. *Macromolecules*, **1973**, 6, 158-162.
11. Higgins, J.; Janovic, Z. *J. Polym. Sci.: Polym. Lett. Ed.*, **1972**, 10, 301-303.
12. Janovic, Z.; Higgins, J. *J. Polym. Sci. Part A-1*, **1972**, 10, 1609-1615.
13. De Schryver, F.; Marvel, C.S. *J. Polym. Sci. Part A-1*, **1967**, 5, 545-552.
14. Kellman, R; Marvel, C.S. *J. Polym. Sci.: Polym. Chem. Ed.*, **1975**, 13, 2125.
15. Lee, B.H.; Marvel, C.S. *J. Polym. Sci.: Polym. Chem. Ed.*, **1983**, 21, 83-87.
16. Overberger, C.G.; Moore, J.A. *Adv. Polymer Sci.*, **1970**, 7, 113-150.
17. (a) Ruan, J.Z.; Litt, M.H. *J. Polym. Sci.: Polym. Chem. Ed.*, **1987**, 25, 285-297;
   (b) *ibid*, **1987**, 299-309.
18. (a) Kim, O.K. *J. Polym. Sci.: Polym. Lett.*, **1982**, 20, 662;
   (b) Kim, O.K. *Mol. Cryst. Liq. Cryst.*, **1984**, 105, 161;
   (c) Kim, O.K. *J. Polym. Sci.: Polym. Lett.*, **1985**, 23, 137-139.
19. Jenekhe, S.A.; Tibbetts, S.J. *J. Polym. Sci.: Polym. Phys. Ed.*, in press.

REFERENCES (Continued)

20. Jenekhe, S.A.; Peterson, J.R. Manuscript in preparation.
21. (a) Perkins, P.G. *Revue Roumaine de Chemie*, **1973**, 18, 931-943;
(b) *ibid*, **1973**, 18, 1111-1119.
22. Wangbo, M.H.; Hoffmann, R.; Woodward, R.B. *Proc. Royal Soc. Lond.*, **1979**, A366, 23-46.
23. Kertesz, M.; Hoffmann, R. *Solid State Commun.*, **1983**, 47, 97-102.
24. Bredas, J.L.; Themans, B.; Andre, J.M. *J. Chem. Phys.*, **1983**, 78, 6137-6148.
25. Kivelson, S.; Chapman, O. *Phys. Rev. B.*, **1983**, 28, 7236-7243.
26. (a) Yamabe, T.; Tanaka, K.; Ohzeki, K.; Yata, S. *Solid State Commun.*, **1982**, 44, 823-825;
(b) Tanaka, K.; Ohzeki, K.; Nankai, S.; Yamabe, T.; Shirakawa, H. *J. Phys. Chem. Solids*, **1983**, 44, 1069-1075.
27. (a) Robertson, J.M.; Sinclair, V.C.; Trotter, J. *Acta Crystallogr.*, **1961**, 14, 697-704;
(b) Campbell, R.B.; Robertson, J.M.; Trotter, J. *Jcta Crystallogr.*, **1961**, 14, 705-711;
(c) Campbell, R.B.; Robertson, J.M.; Trotter, J. *Acta Crystallogr.*, **1962**, 15, 289-290.
28. Silinsh, E.A. *Organic Molecular Crystals: Their Electronic States*; Springer-Verlag: New York, **1980**.
29. Simon, J.; Andre, J.J. *Molecular Semiconductors*; Springer-Verlag: Berlin and New York, **1985**, pp. 201 ff.
30. Badger, G.M.; Pettit, R. *J. Chem. Soc.*, **1951**, 3211-3215.
31. (a) Wheland, R.C. *J. Am. Chem. Soc.*, **1976**, 98, 3926;
(b) Wheland, R.C.; Gillson, J.L. *J. Am. Chem. Soc.*, **1976**, 98, 3916.
32. Bryce, M.R.; Murphy, L.C. *Nature*, **1984**, 309, 119-126.
33. Ferraris, J.P.; Cowan, D.O.; Walatka, V.; Perlstein, J. *J. Am. Chem. Soc.*, **1973**, 95, 948.
34. Melby, L.R. *Can. J. Chem.*, **1965**, 43, 1448.
35. (a) Jelley, E.E. *Nature*, **1937**, 139, 631;
(b) Hofer, L.J.E.; Grabenstetter, R.J.; Wiig, E.O. *J. Am. Chem. Soc.*, **1950**, 72, 203;
(c) Czikkely, V.; Forsterling, H.D.; Kuhn, H. *Chem. Phys. Lett.*, **1970**, 6, 11;

REFERENCES (Concluded)

(d) Daltrozzo, E.; Scheibe, G.; Gschwind, K.; Haimerl, F. *Photog. Sci. Eng.*, **1974**, 18, 441;

(e) Kopainsky, B.; Hallermeier, J. K. ; Kaiser, W. *Chem. Phys. Lett.*, **1982**, 7, 87;

(f) Mizutani, F.; Iijima, S.-I.; Tsuda, K. *Bull. Chem. Soc. Jpn.*, **1982**, 55, 1295.

36. Michealis, L.; Hill, E.S. *J. Am. Chem. Soc.*, **1933**, 55, 1488.

37. (a) Diaz, A.F.; Logan, J.A. *J. Electroanal. Chem.*, **1980**, 111, 111;

(b) Wnek, G.E. *Polym. Preprints*, **1986**, 27(1), 277.

38. Jenekhe, S.A.; Peterson, J.R. Unpublished results.

2.2 Simultaneous Polymerization and Crystallization

Simultaneous polymerization and crystallization, especially from the liquid phase, is very rare in polymer systems[1-5]. Here, we report on observations of simultaneous polymerization and crystallization of 1,2,4,5-tetraaminobenzene tetrahydrochloride (I or TABH) in aqueous solution at room temperature (23°C) to give macroscopic needle-like crystals. Although it would seem that an appropriate polycondensation of the monomer I could afford an aromatic ladder polyquinoxaline or a related non-aromatic ladder derivative[6], the present results may initially be surprising. We had previously tried to synthesize a ladder polymer by electrochemical polymerization of I[7]. It has also been reported that 2,3,7,8-teraaminophenazine tetrahydrochloride (II or TAPH) was obtained by air oxidation of I in water[8,9]. However, consideration of the relative reactivity of I and II under the reaction conditions suggested to us that over a long time II should be just as susceptible to self-condensation as I. Preliminary results on the effects of the growth conditions on the product and characterization of the product, including morphology of the as-synthesized fibrous or needle-like crystals are reported.

Crystal growth during polycondensation of the monomer was explored under three slightly different conditions as follows: (a) air was bubbled continuously through a solution of 2_g of highly-purified TABH in 20 ml of deionized water for 2 hours. The originally pink solution turned deep blue after 0.5 hr. of air bubbling. The solution was capped, to prevent evaporation, and left to stand, without stirring, for 15 hours. A uniformly green product, consisting of very thin and long rods or needles, was recovered by vacuum filtration through a Buchner fritted glass funnel and Whatman filter paper (#41). The product formed a flexible film which was readily peeled off from the filter paper. The samples whose morphologies are reported here have intrinsic viscosity of 0.14 dL/g in dimethylsulfoxide (DMSO) at 23°C. The above growth experiment was repeated exactly, except: (b) stirring of the monomer solution with a magnetic stirring bar; and (c) no air bubbling through the solution and no stirring. The product recovered from growth "c" was identical in all manner to that in "a." However, the product from growth "b" was a rust/brown crystalline powder with some bluish crystals distributed uniformly throughout the product. Only the highly anisotropic fibrous crystals obtained from either growth "a" or "c" are described subsequently.

Thermal analysis of the products was done using a DuPont Model 1090 B thermal analyzer/1091 disk memory with a differential scanning calorimeter (DSC) and a 951 thermogravimetric analyzer (TGA) operated at 10°C/min.

Scanning electron microscope (SEM) observations of morphology were made using a JOEL Model 840 A II instrument. X-ray diffraction (XRD) patterns of the samples were obtained using a Rigaku powder diffractometer and a sealed tube CuK_α radiation (λ = 1.540562 Å). The 2θ scan was from 3° to 93°; the 2θ step size was 0.02° with 1 sec. counting time per point. As-synthesized products from growths "a" and "c" were examined as free-standing films.

Fourier transform infrared (FTIR) spectra of thin films cast on silicon wafers from methanol and DMSO solutions and films of as-synthesized crystals were obtained using a Digilab model FTS-14 spectrometer. The solution electronic absorption spectra of 10^{-3}M solutions in DMSO and methanol (MeOH) were obtained using a 1mm cell and a Perkin-Elmer model Lamda 9 UV-Vis-NIR spectrophotometer in the wavelength range 185-3200 nm.

Figure 17 shows the typical morphology of the product of simultaneous polycondensation and crystallization of TABH as revealed by a SEM micrograph. The needle-like or fibrous crystals are macroscopic, with diameters in the range of 0.2-5.0μm and lengths up to 0.5-2.0cm. The large anisotropy of the crystals is evident by their aspect ratio (L/d) of 10^3 to 10^5. Figure 18 shows the X-ray diffraction patterns of a free-standing film of the same product, revealing a purely crystalline sample. The melting behavior of the as-synthesized crystals was shown in a DSC thermogram which revealed a sharp peak melting point (T_m) of 327°C. This melting point is to be contrasted with the literature value of 176-177°C for phenazine.

Formation of flexible free-standing films by filtration of the needle-like crystals suggests that they are polymeric in nature. In contrast, a related quinoxaline ladder oligomer, 5,12-dihydro-5,7,12,14-tetraazapentacene (DHTAP), prepared by condensation of *o*-phenylenediamine with 2,5-dihydroxy-*p*-benzoquinone does not form films[10]. However, the needle-like crystals have intrinsic viscosity of 0.14 dL/g in dimethylsulfoxide (DMSO) at 23°C, which suggests that the polymer molecular weight is probably not very high. A related high molecular weight ladder polyquinoxaline prepared by condensation of TABH with 2,5-dihydroxy-*p*-benzoquinone, PHQXL, has intrinsic viscosity of 0.65-0.75 dL/g in methane sulfonic acid[11].

Upon dissolution in polar organic solvents (DMSO, MeOH), the highly anisotropic crystalline morphology could not be regenerated by recrystallization, precipitation, or solution casting. This inability to regenerate

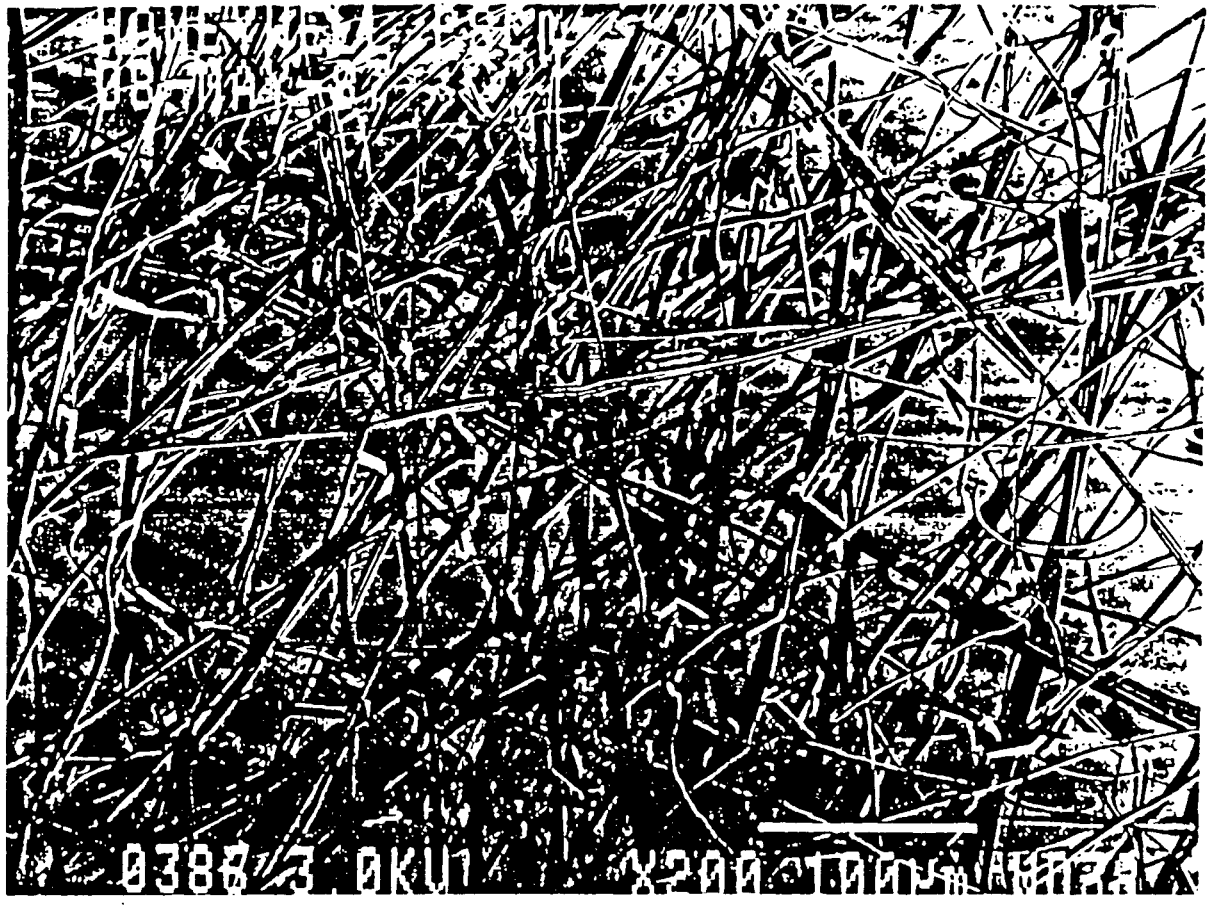

FIGURE 17 The morphology of as-synthesized needle-like crystals.

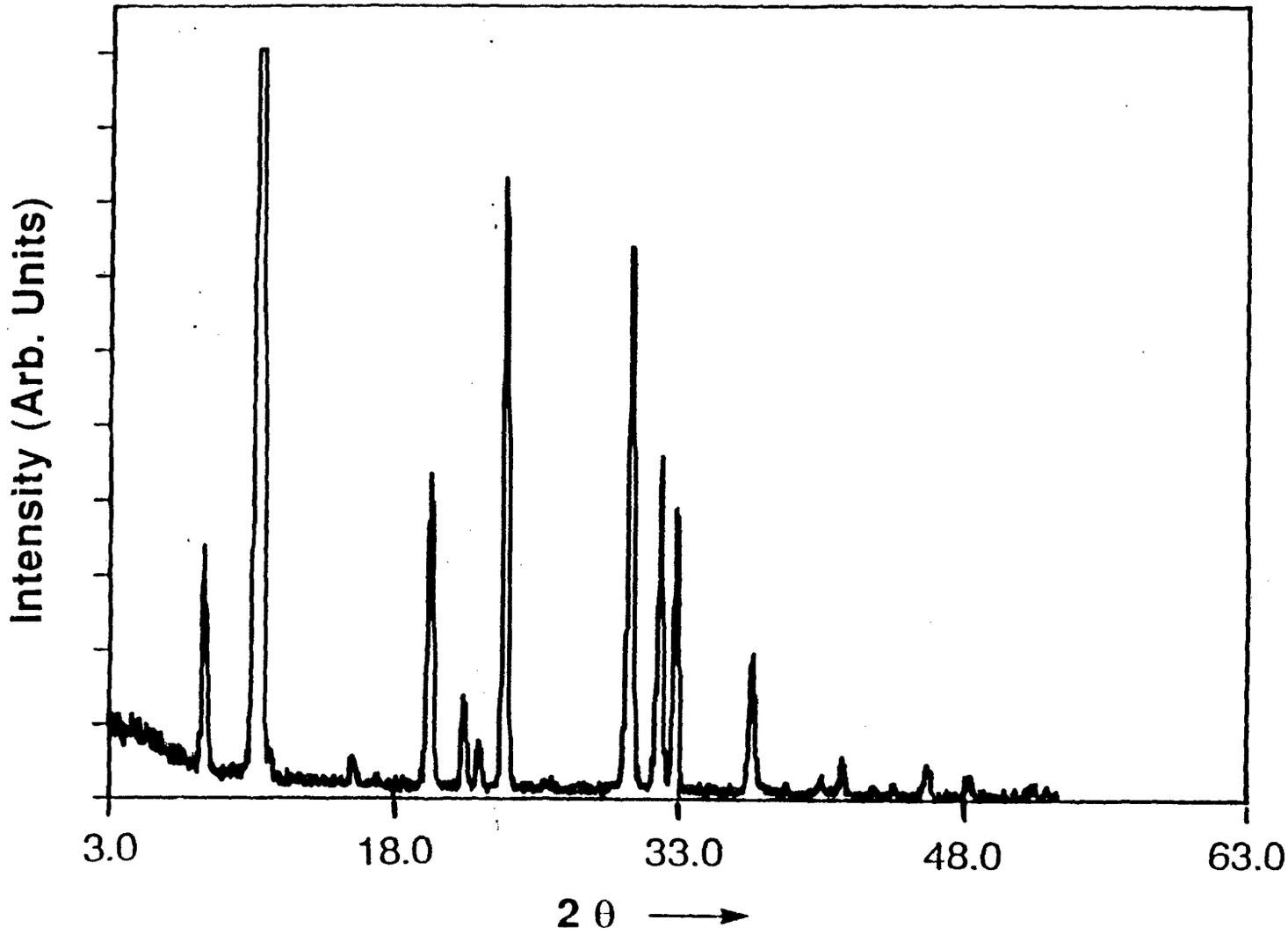

FIGURE 18 X-ray diffraction patterns of a film of as-synthesized crystals.

the needle-like crystals suggests that crystallization during polycondensation is crucial for achieving the macroscopic crystals.

The solution electronic absorption spectra of the product III in methanol and DMSO are shown in Figure 19. An intense absorption maximum in the visible is observed at 549 nm (ϵ = 24,800) with a very low intensity shoulder at ~ 621 nm in DMSO. However, in methanol, two intense visible absorption bands at 541 nm (ϵ = 18,000) and 621 nm (ϵ = 14,000) are observed. The important suggestion from these solution electronic spectra results, together with the green color of the as-synthesized crystals, is that the fibrous crystals contain fused rings longer than tetraazapentacene[10] and perhaps also the aza analog of heptacene[12].

The simplest possible scheme for the self-condensation of TABH to a polymer involves II as an intermediate as shown below:

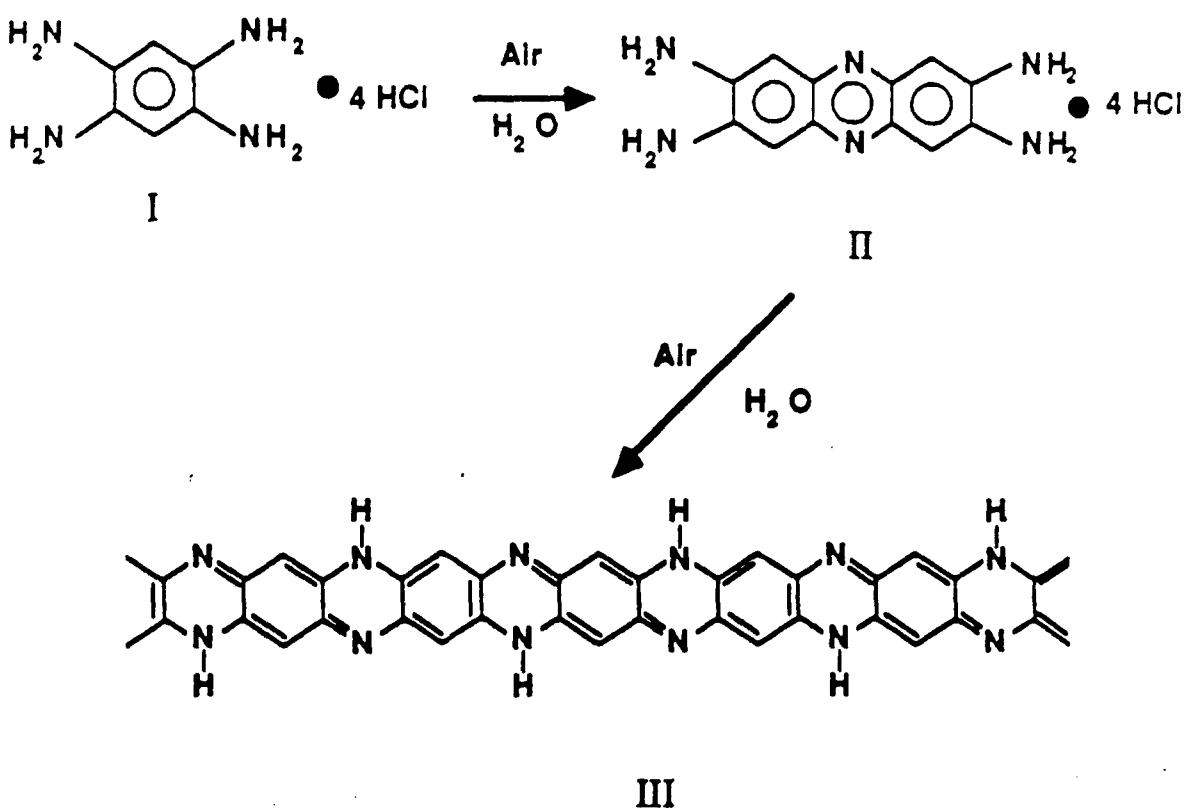

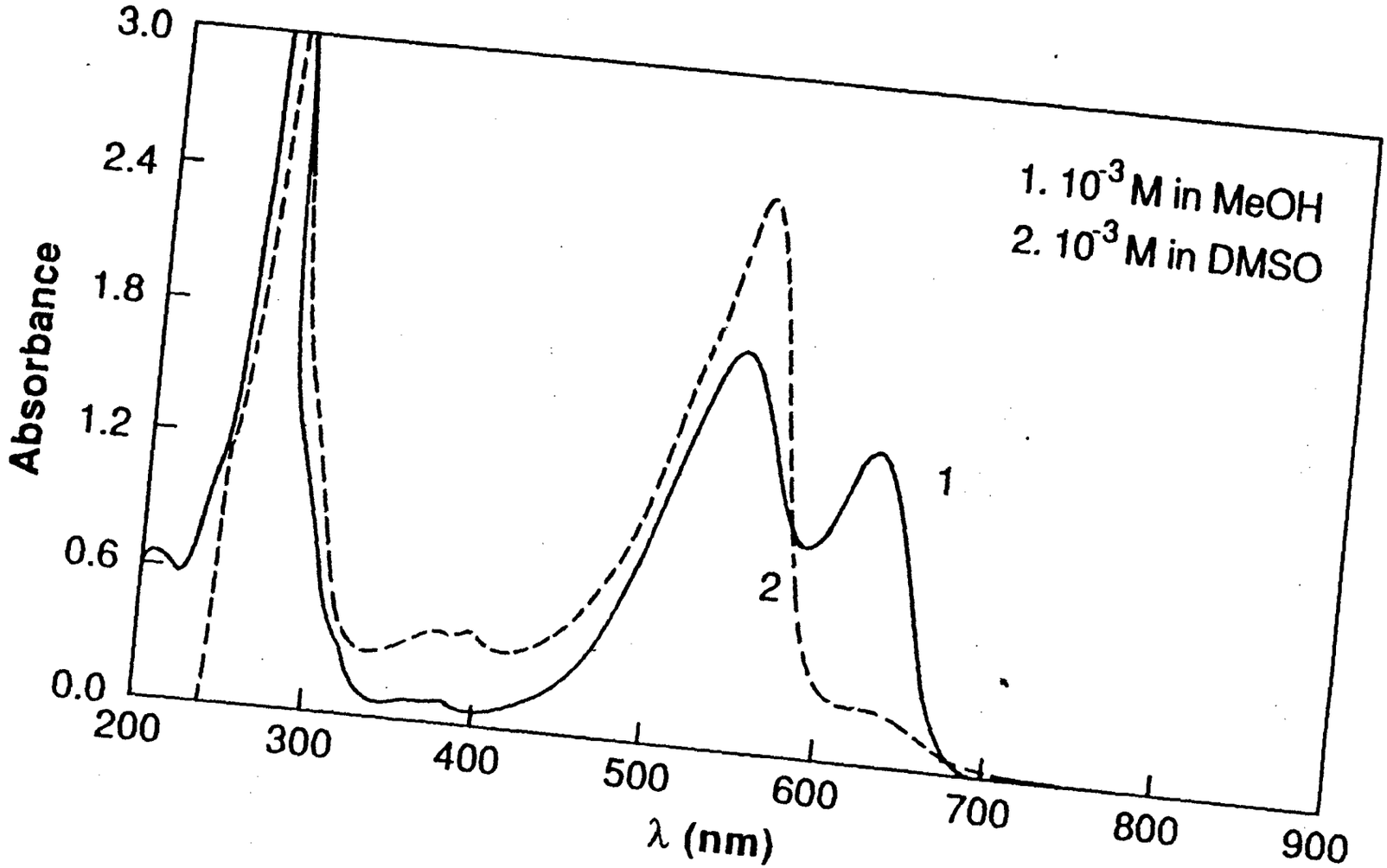

FIGURE 19 Electronic absorption spectra of the needle-like crystals of Figures 1-2 in methanol and DMSO solutions.

71394

This scheme is consistent with the fact that the intermediate II has previously been so prepared[8-9]. The proposed quinodal ladder polyquinoxaline structure III (or PHQXL) is consistent with the IR spectrum[13], which is similar to that of the authentic high molecular weight PHQXL[14]. However, the elemental analysis[15] does not agree with the structure III, but suggests its hydrate and hydrochloride. Also, authentic high molecular weight III is black[14]; however, when vacuum baked at 200°C, the green needle-like crystals turn black and then gradually revert back to green after standing in air. This suggests that the vacuum-baked black product is most likely the aromatic derivative of III and the green product a non-aromatic oxidation product of III. In fact, it is known that 5,7,12,14-tetraazapentacene is less stable than its non-aromatic dihydro derivative, DHTAP[9,12]. The TGA weight loss curve of the vacuum-baked product was identical to that of authentic PHQXL.

In summary, macroscopic needle-like crystals of a ladder polyquinoxaline are obtained by simultaneous polymerization and crystallization of TABH in aqueous solution at 23°C. Evidence that the fibrous crystals are polymeric includes: the film-forming properties; the solution electronic absorption spectra and color of the as-synthesized crystals; intrinsic viscosity; and the reasonable reaction scheme. Flexible films of the fibrous crystals were obtained by vacuum filtration of as-synthesized crystalline fibers. Upon dissolution in organic solvents, the highly anisotropic crystalline morphology cannot be regenerated by recrystallization or solution casting, suggesting that crystallization **during** polycondensation is crucial to the formation of the macroscopic fibrous crystals. Further studies of the structural and physical properties of the needle-like crystals and the growth process are in progress.

---

13. IR: 3380(s), 3335(s), 3290(s), 3160(vs), 1675(s), 1620(s), 1505(vs), 1350(s), 1200, 848(s), 735(s), 665, 547(s), 427 cm^{-1}.

14. Authentic III (PHQXL) prepared by condensation of I with 2,5-dihydroxy-*p*-benzoquinone in polyphosphoric acid was black and had intrinsic viscosity of 0.65-0.75 dL/g.

15. Elemental analysis, found: %C = 40.45, %H = 5.30, %N = 23.48, %Cl = 21.64, %O = 9.07.

REFERENCES FOR SECTION 2.2

1. Wunderlich, B. *Adv. Polym. Sci.*, 1968, 5, 568-619.
2. Wunderlich, *Macromolecular Physics,* Vol. 1, *Crystal Structure, Morphology, Defects,* Academic Press: New York, 1973.
3. Wegner, G.; Fischer, E. W.; Munoz-Escalona, A. *Makromol. Chem. Suppl.*, 1975, 1, 521-558.
4. Shu, H. C.; Wunderlich, B. *J. Polym. Sci.: Phys. Ed.*, 1977, 15, 355; *J. Polym. Sci.: Polym. Phys. Ed.*, 1980, 18, 443-447.
5. Bloor, D. *Developments in Crystalline Polymers 1* (D. C. Basset, ed.) Applied Science: Barking, 1982, pp. 151-193.
6. De Schryver, F; Marvel, C. S. *J. Polym. Sci.:* Part A-1, 1967, 5, 545-552.
7. Jenekhe, S. A.; Peterson, J. R. Unpublished results.
8. Sicree, A. J.; Arnold, F. E.; Van Deusen, R. L. *J. Polym. Sci.: Polym. Chem. Ed.*, 1974, 12, 265-272.
9. Nietzki, E.; Muller, H. *Ber.*, 1889, 22, 440.
10. Jenekhe, S. A. *Macromolecules*, submitted (companion paper).
11. Jenekhe, S. A.; Peterson, J. R. Manuscript in preparation.
12. Badger, G. M.; Pettit, R. *J. Chem. Soc.*, 1951, 3211-3215.

2.3 Mediated Solubilization and Processing of Ladder Polymers in Organic Solvents

2.1.1 Introduction

The heteroaromatic rigid chain and ladder polymers, exemplified by poly(p-phenylene-2,6-benzoxazole) (PBO), poly(p-phenylene-2,6-benzothiazole) (PBT), poly(p-phenylene-2,6-benzimidazole) (PBI), and benzimidazobenzophenanthroline-type ladder polymer (BBL) and derivatives, whose structures are shown in Figure 20, have been of considerable interest since the 1960's because of their exceptionally high temperature stability, very high mechanical strength, and unusual resistance to solvents[1-12]. More recently, these polymers are attracting scientific and technological interest because of their equally unusual electronic and nonlinear optical properties[13-19]. However, these rigid chain polymers and even those modified with pendant groups[11], have never shown solubility in aprotic organic solvents; only strong and corrosive concentrated acids, such as methane solfonic acid (MSA), sulfuric acid, and triflic acid (CF_3SO_3H), are solvents in which to both characterize their properties and process them into films or fibers[1-11]. The general insolubility of these types of polymers in organic solvents has been attributed to two main factors[9]: (1) intramolecular or conformational effects, particular the rigidity of the chains; and (2) intermolecular effects, especially interchain interactions which are largely van der Waals in orgin. The observed solubility of these rigid chain polymers in strong acids is generally thought to originate from protonation of the polymer chains forming polyelectrolytes, such as shown below for protonated BBL, with

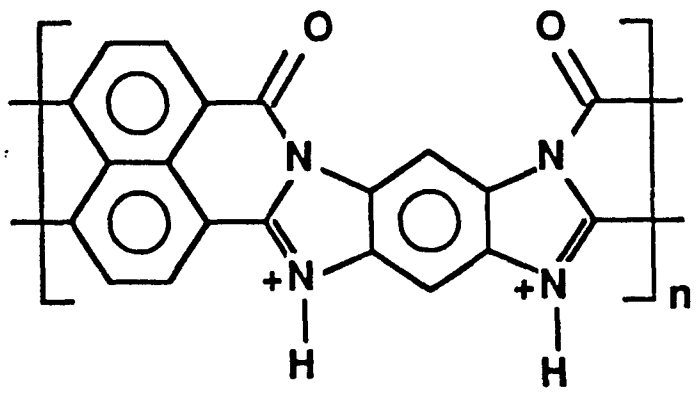

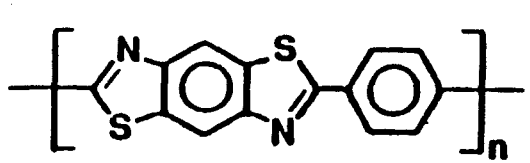

PBT

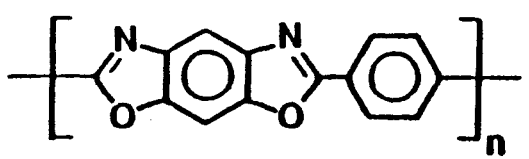

PBO

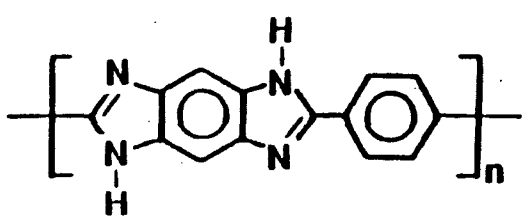

PBI

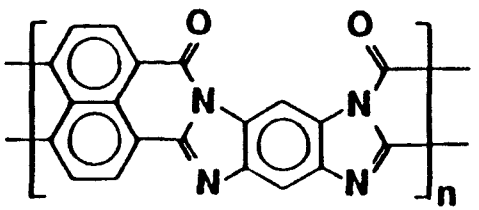

I (BBL)

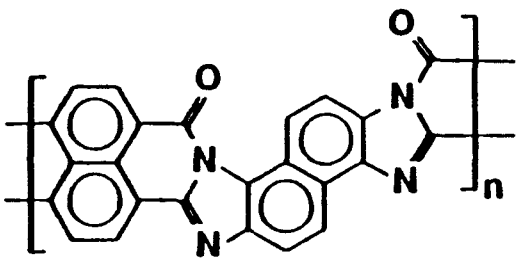

II (BBL-N)

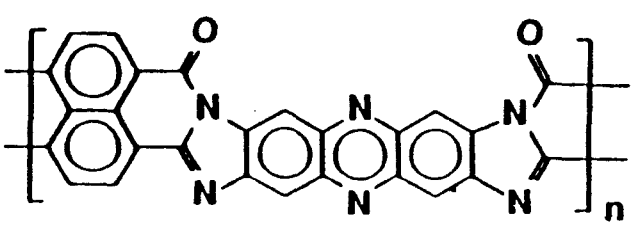

III (BBL-P)

FIGURE 20 Molecular structures of typical heterocyclic aromatic rigid rod and ladder polymers.

consequent significant reduction of the intermolecular attractions and the rigidity of the chains. Thus, in order to be able to dissolve the polymers in aprotic organic solvents other mechanisms of solubilization must be explored.

We recently initiated investigation of a new approach to the solubilization and processing of rigid chain and ladder polymers in aprotic organic solvents. It is known that certain rigid chain polymers such poly(1,4-benzamide) (PBA), poly(1,4-phenyleneterephthalamide) (PPTA or Kevlar) and related para-linked aromatic polyamides can be dissolved in organic solvents, such as N,N-dimethylformamide (DMF), N,N-dimethylacetamide (DMAc), and N-methylpyrrolidone (NMP), containing about 3-20% wt LiCl, $CaCl_2$ or other salts[20-23]. At sufficiently high PBA or PPTA concentrations in such salt/-organic solvent systems, liquid-crystalline solutions are obtained and used to prepare high-strength, high-modulus oriented fibers[20]. However, these salt/amide solvent systems do not dissolve the heteroaromatic rigid chain and ladder polymers exemplified in Figure 20. We have previously reported the solubilization of conjugated heteroaromatic polycarbazoles in liquid Lewis acids (Br_2 and I_2), resulting in conducting polymer solutions from which doped conducting films of polycarbazoles can be obtained[24-25]. The solubilization of poly(p-phenylene sulfide) (PPS) in liquid AsF_3/AsF_5 to produce conducting solutions from which conducting films of PPS can be obtained has also been reported[26]. The rigid chain polymer polybisbenzimidazobenzophenathroline-dione (BBB), the non-ladder analog of BBL, has also been solubilized in molten antimony trichloride ($SbCl_3$)(mp=73°C)[27]. In recent studies in our laboratory we have found that many rigid chain and ladder polymers, including those in Figure 20, dissolve in liquid or molten pure Lewis acids such as bromine, $SbCl_3$ and AsF_3. However, these pure liquid or molten Lewis acids are not practical solvents for potential large-scale processing of the rigid chain and ladder polymers to films or fibers for obvious technical, environmental, and economic reasons.

The basic premise of our approach is that solubilization of the rigid chain polymers in aprotic organic solvents could be achieved via in situ or nonin situ chemical reactions, forming soluble polymer complexes. In view of the fact that some of the pristine rigid chain polymers are conjugated and some contain carbonyl or other oxygen, one may envision two possible mechanisms of solubilization: (1) formation of a soluble charge transfer complex between the pristine polymer (P) and a mediating agent such as Lewis acids (MX_n),

$$P + MX_n \underset{\text{aprotic organic solvents}}{\rightleftharpoons} P^{+y}(MX_{n+1}^-)_y \qquad (1)$$

and (2) in the case of oxygen-containing polymers (P), formation of a soluble complex between P and MX_n at oxygen sites on P analogous to intermediates of Friedel-Crafts acylation reactions,

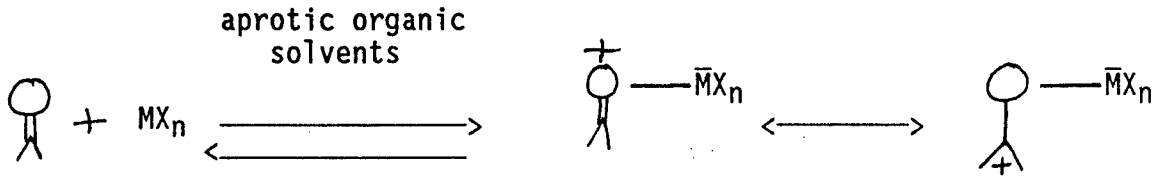

(2)

Either possibility is of theoretical and practical interest. We have found that the rigid chain polymers, exemplified by BBL and PBO, dissolve in aprotic organic solvents, such as nitroalkanes and nitroarenes, containing Lewis acids. This paper presents the preliminary results of our investigation of the mediated solubilization of these rigid chain and ladder polymers in aprotic organic solvents/Lewis acids systems and solution polymer processing to films and coatings.

2.3.2 Experimental Section

Polymers and Model Compounds

The BBL samples were synthesized following the original synthesis of Arnold and Van Duesen[1,2], but modified by carrying out polymerizations in the liquid crystalline phase as described for ordered rigid rod (PBT, PBO, etc.) polymers[12]. The BBL samples used have intrinsic viscosity of 7.91 dL/g in pure MSA at 25°C and infrared spectra identical to the published one[2]. A sample of PBO was provided as fibers by F.E. Arnold's group at the Air Force Materials Laboratory/Polymer Branch; the detailed molecular and physical properties are not known.

The synthesis and characterization of the model compound 5,7-dihydro-5,7,12,14-tetraazapentacene (DHTAP) are described in a previous paper[28]. The high molecular weight polyhydroquinoxaline (PHQXL) of which DHTAP is a model

compound was synthesized following the scheme of Stille et al[29]; studies of its electrical, electrochemical, and physical properties will be reported on separately[30]. A sample of polyimide film (DuPont's Kapton) was used as received by cutting the film into small pieces.

Organic Solvents and Lewis Acids

All organic solvents and Lewis acids were used without further purification, including: Nitromethane (Aldrich); Nitroethane (Aldrich); 2-Nitropropane (Aldrich); nitrobenzene (J.T. Barker); acetonitrile (Aldrich); N,N-dimethylformamide (DMF); Dimethylsulfoxide (DMSO); acetic acid; pyridine; Dimethylacetamide (DMAc); N-methylpyrrolidone (NMP); methanol; ethanol; tetrahydrofuran (THF); methylene chloride; $AlCl_3$ (Alfa); $FeCl_3$ (Aldrich); $SbCl_3$ (Alfa); $SbCl_5$ (Alfa); $InCl_3$ (Alfa).

Procedures - Solution Preparation and Solubilization

Except otherwise stated, all solution preparations were performed in a Vacuum Atmosphere's dry box filled with nitrogen. Once prepared, most solutions were stored in the dry box and only brought into air when needed. However, some solutions were stored in air to observe their stability in air over time. Initial screening of the solubility of a polymer or model compound sample in a Lewis acid/organic solvent system was done by adding about 1-5 mg each of the sample to several 10 mL solutions of the Lewis acid in an organic solvent in which the Lewis acid concentration was varied from 0 to 1.0 M or saturation.

2.3.3 Results and Discussion

The rigid rod, polymers of Figure 20 do not dissolve or swell in aprotic solvents, including CH_3NO_2, Ph-NO_2, $C_2H_5NO_2$, and MeCN. However, BBL dissolves readily in solutions of $FeCl_3$, $AlCl_3$, $SbCl_3$, and $SbCl_5$ in CH_3NO_2, $C_2H_5NO_2$, and Ph-NO_2 and with difficulty in $SbCl_5$/MeCN; the minimum concentration of the Lewis acid in solution when polymer dissolution commences is about 0.01-0.05M, the polymer solubility increasing with the Lewis acid concentration. All the BBL solutions were red; characteristic of oxidized polymer, and similar to the solutions of the polymer in MSA[16]. Addition of excess solvent or non-solvent to a solution precipitates small blue sheets of the polymer, again similar to what is observed when excess non-solvent is added to an MSA solution of the polymer.

Figure 21 shows the electronic absorption spectra of a BBL solution in 0.05M $FeCl_3/CH_3NO_2$ at different times or concentrations after adding a solid sample of the polymer into a neat $FeCl_3/CH_3NO_2$ solution. A λ_{max} at 546 nm, and a shoulder at 516 nm, which increases in intensity as the polymer concentration increases, is observed. The dissolution kinetics was conveniently followed by monitoring the intensity of the optical absorption maximum (λ_{max}); however, after 30 minutes the absorbance of the 546-nm peak exceeded the limit of the instrument and went off-scale in Figure 21. The results of Figure 21 are to be compared to the electronic absorption spectra of BBL solution in pure MSA and in the solid state shown in Figure 22. Clearly, identical polymer electronic spectra are observed in MSA and in $FeCl_3/CH_3NO_2$ solutions and indeed in all the solvents examined so far. The λ_{max} value of 544 nm in 100% MSA is to be compared to its value in other solvents and the solid state, all shown in Table 3. The maximum blue shift from the solid state λ_{max} is seen in the acid solution. A major difference between all the solution electronic absorption spectra and the solid state spectrum is that the latter one is significantly broader and results in about 120 nm difference in the long wavelength absorption edges of the solution and solid state spectra. This suggests that there is a reduction in the degree of π-electron delocalization upon solubilization.

The pure rigid rod polymer is readily regenerated from these solutions by precipitation with excess solvents or any non-solvent or by casting films from the solution followed by washing in a non-solvent. Figure 23b shows the FTIR spectrum of a BBL film case from a 0.1M $FeCl_3/CH_3NO_2$ solution, washed first in methanol and then acetone; Figure 23a is the FTIR spectrum of a BBL obtained from a uniaxially rolled film of as-synthesized BBL/polyphosphoric aced (PPA) sample extracted with boiling water and dried in vacuum. The two FTIR spectra are identical, suggesting that the pure polymer has indeed been regenerated. In fact, other properties of the <u>regenerated</u> and <u>pristine</u> polymer, such as redox properties, electronic absorption spectra, color (gold-yellow) and visual appearance, are identical.

Conclusions

In conclusion, rigid rod and ladder polymers, exemplified by BBL, have been solubilized in aprotic organic solvents for the first time by using Lewis acid charge-transfer complex forming agents. It is suggested from the present results that the principal reason for the general insolubility of rigid rod and ladder polymers is interchain interactions which are largely van der Waals

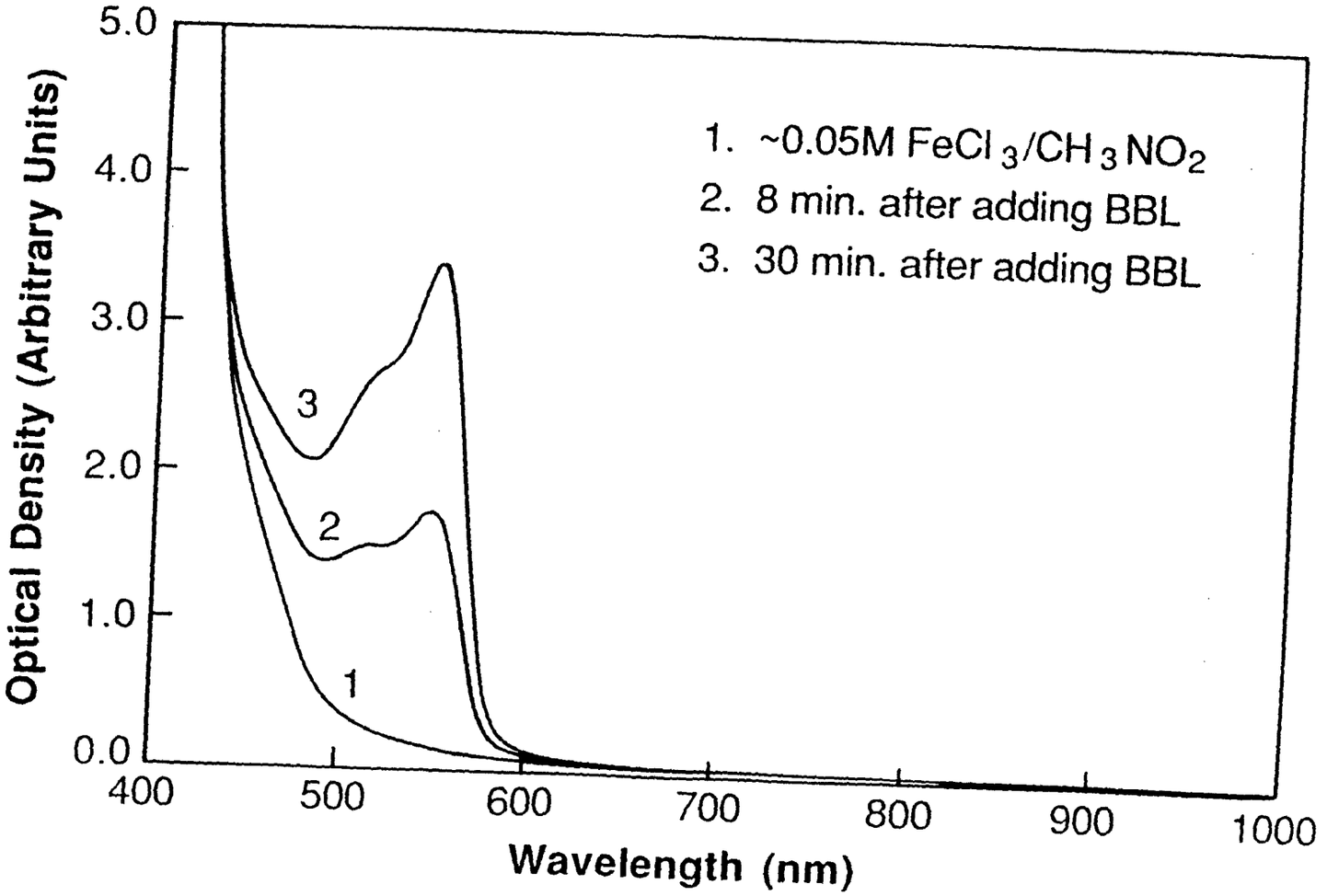

FIGURE 21 Electronic absorption aspects of BBL in 0.05M $FeCl_3/CH_3NO_2$.

70290

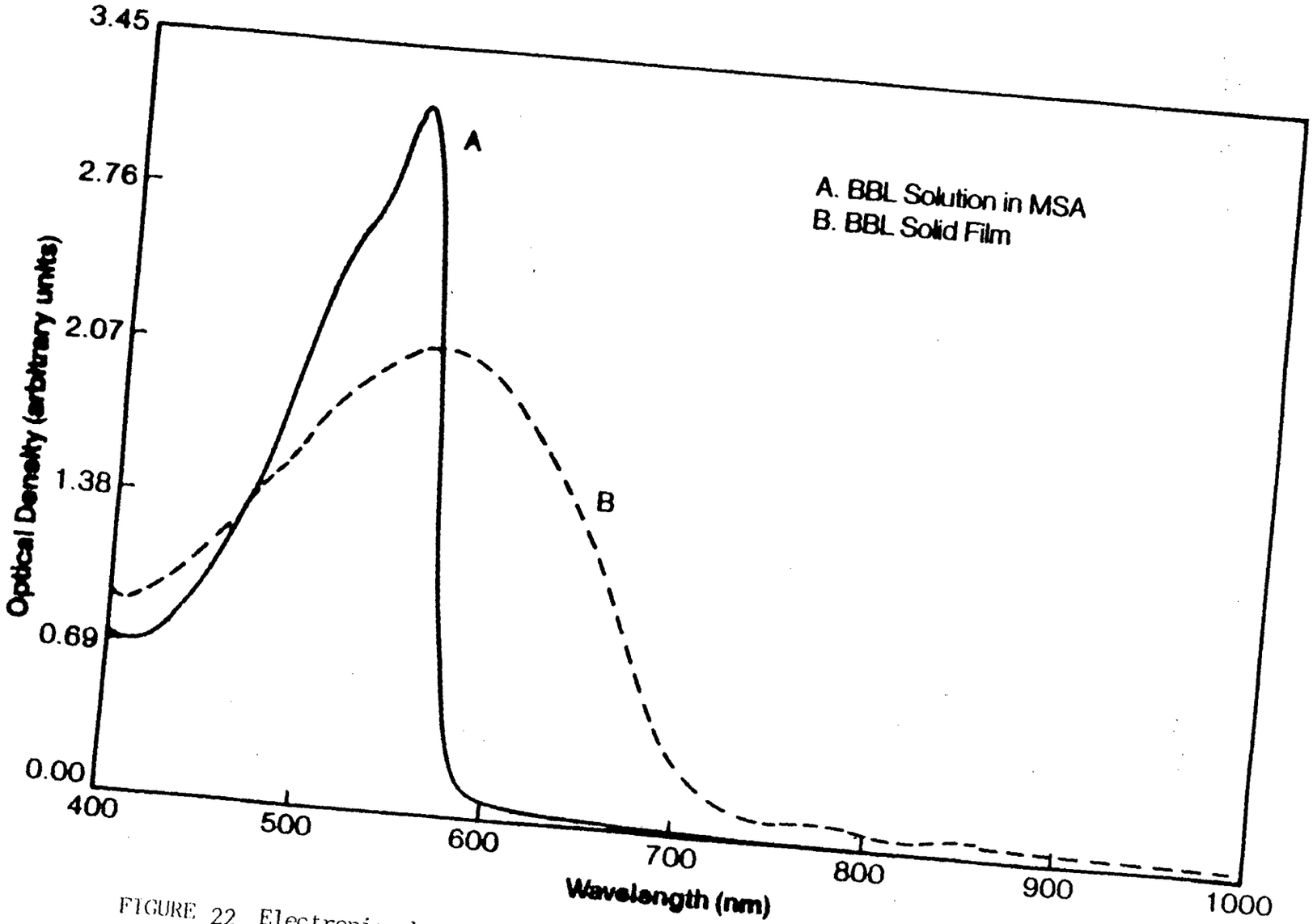

FIGURE 22 Electronic absorption spectra of BBL in 100% MSA and BBL thin solid film.

Table 3 Optical absorption maximum of BBL in various solvents and in the solid state.

Solvent	λ_{max}(nm)	λ_{max}-560(nm)
100% MSA	544	16
$FeCl_3/CH_3NO_2$	546	14
$AlCl_3/CH_3NO_2$	546	14
$SbCl_3/CH_3NO_2$	550	10
$AlCl_3$/Ph-NO_2	557	3
$SbCl_5$/Ph-NO_2	557	3
BBL thin solid film	560	0

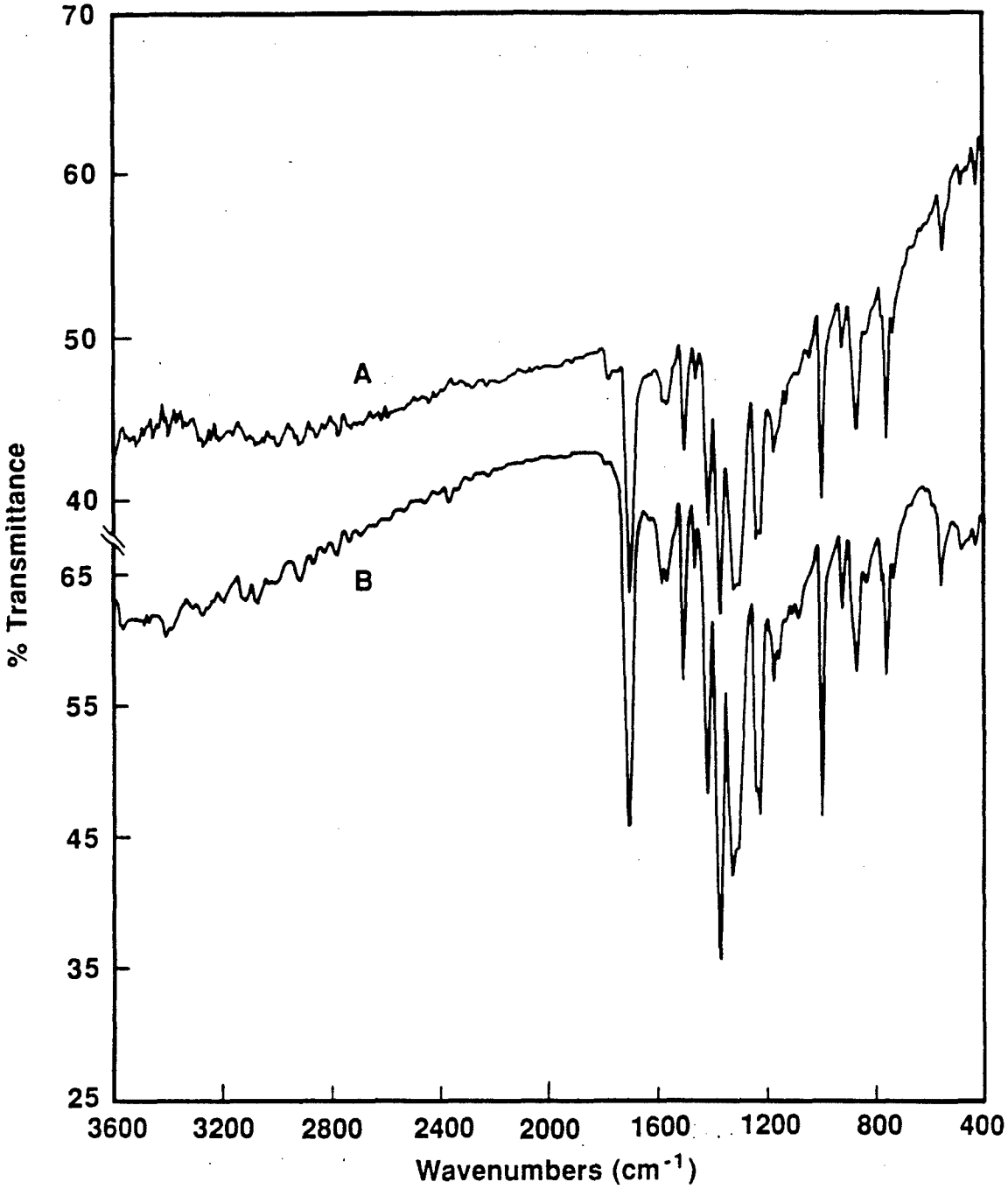

FIGURE 23 FTIR spectra of BBL thin films: A -- pristine polymer; B -- polymer regenerated from a $FeCl_3/CH_3NO_2$ solution.

in origin; thus, charge-transfer complex formation significantly reduces these intermolecular attractive forces and allows solubilization of the highly-rigid macromolecules. Facile regeneration of pure polymer from solutions is suggested to originate from instability of the complexes or decomplexation in the solid state or in the presence of excess non-solvents. The mediated solubilization process together with facile regeneration of the polymers from their complexes in solution is suggested to hold promise for easier processing of rigid rod and ladder polymers to films, fibers and other useful forms.

2.3.4 References for Section 2.3

1. Van Deusen, R.L. *J. Polym. Sci.: Polym. Lett.*, 1966, B14, 211-214.

2. Arnold, F.E.; Van Deusen, R.L. *Macromolecules*, 1969, 2, 497-503.

3. Arnold, F.E.; Van Deusen, R.L. *J. Appl. Poly. Sci.*, 1971, 15, 2035-2047.

4. Arnold, F.E.; *J. Polym. Sci. Part A-1*, 1970, 8, 2079-2089.

5. Bailey, W.J. In: "Encyclopedia of Polymer Science and Technology," vol. 8, 1968; pp. 97-120.

6. (a) Wolfe, J.F.; Arnold, F.E. *Macromolecules*, 1981, 14, 909-915.
(b) Wolfe, J.F.; Loo, B.H.; Arnold, F.E., *Macromolecules*, 1981, 14, 915-920.

7. Choe, E.W.; Kim, S.N. *Macromolecules*, 1981, 14, 920-924.

8. Evers, R.C.; Arnold, F.E.; Helminiak, T.E. *Macromolecules*, 1981, 14, 925-930.

9. Bhaumik, D.; Welsh, W.J.; Jaffe, H.H.; Mark, J.E. *Macromolecules*, 1981, 14, 951-953.

10. Sicree, A.J.; Arnold, F.E.; Van Deusen, R.F. *J. Polym. Sci: Polym. Chem. Ed.*, 1974, 12, 265-272.

11. Tsai, T.-T.; Arnold, F.E. *Polym. Preprints (ACS Div. Polym. Chem)*, 1986, 27(2), 221-222.

12. Wolfe, J.F. *Polym. Mat. Sci. Eng. (ACS Div. Polym. Mat. Sci. Eng.)*, 1985, 57, 99-101.

13. Jenekhe, S.A.; Tibbetts, S.J. *J. Polym. Sci.: Polym. Lett. Ed.*, 1988, 26, 201-209.

14. (a) Kim, O.K. *J. Polym. Sci: Polym. Lett. Ed.*, 1982, 20, 662;
(b) Kim, O.K. *Mol. Cryst. Liq. Cryst.*, 1984, 105, 161.

15. Marks, T.J. *Science*, 1985, 227, 881-889.

16. Jenekhe, S.A.; Peterson, J.R. Manuscript in preparation.

17. Garito, A.F. Paper presented at the 193rd Am. Chem. Soc. National Mtg., Denver, Div. Phys. Chem., Abstract #11, April 5-10, 1987.

18. Bitler, S.P.; Wolfe, F.F. Paper presented at the 193rd Av. Chem. Soc. National Mtg., Denver, Div. Phys. Chem., Abstract #167, April 5-10, 1987.

19. Depra, P.; Gaudiello, J.G.; Giesler, J.; Li, D.; Carr, S.H.; Ratner, M.A.; Marks, T.J. Paper presented at the 193rd Ave. Chem. Soc. National Mtg., Denver, Div. Phys. Chem., Abstract #181, April 5-10, 1987.

20. Kwolek, S.L.; Morgan, P.W.; Schaefgen, J.R.; Gulrich, L.W. Macromolecules, 1977, 10, 1390-1396.

REFERENCE (Concluded)

21. Planar, M.; Beste, L.F. Macromolecules., 1977, 10, 1401-1406.,

22. Morgan, P.W. Macromolecules, 1977, 10, 1381-1390.

23. Blair, T.I.; Morgan, P.W.; Killian, F.L. Macromolecules, 1977, 10, 1396-1400.

24. Jenekhe, S.A.; Wellinghoff, S.T.; Reed, J.F. Mol. Cryst. Liq. Cryst., 1984, 105, 175.

25. Jenekhe, S.A.; Fure, B.J. U.S. Patent 4,568,482 (February 4, 1986 to Honeywell, Inc.)

26. Frommer, J.E. Acc. Chem. Res., 1986, 19, 2-9.

27. Berry, G.C.; Liwak, S.M. J. Polym. Sci: Poly. Phys. Ed., 1976, 14, 1717-1720.

28. Jenekhe, S.A. Macromolecules, submitted.

29. Stille, J.K.; Mainen, E.L. Macromolecules, 1968, 1, 36-42.

30. Jenekhe, S.A.; Peterson, J.R. Manuscript in preparation.

2.4 Ion Implantation Doped Ladder Polymers

2.4.1 Introduction

Ion implantation is a well-established technique in the electronic industry for introducing controlled amounts of impurities into semiconductors to modify their electronic properties and for integrated circuit (IC) and other microelectronics device fabrication.[1] This technique has recently been used to enhance the electrical conductivity of several conjugated polymers, including polyacetylene[2], polysulfur nitride[2], poly p-phenylene sulfide[3] and polyquinoline[4], to semiconducting levels (~10^{-5} to 1S/cm). Though the achieved conductivity enhancement by ion implantation has been generally less than by the standard conducting polymer chemical and electrochemical doping techniques, the technique of ion implantation is ideal for the potential fabrication of microelectronic devices with thin films of conductive polymers. Most importantly in this regard, it is very difficult to obtain spatially selective or localized conductivity enhancement of polymer thin films by chemical and electrochemical doping which rely on diffusion from the vapor or liquid phase.

Our studies reported here were motivated by the need to explore spatially localized conductivity enhancements in conjugated polymer thin films and their possible device applications. Our choice of high temperature ladder polymers stems from our ongoing studies of the electronic, electrochemical, and physico-chemical properties of this class of polymers[5]. Advantages of ladder polymers for ion implantation studies include (1) their high temperature stability could withstand inevitable sample heating during ion bombardment; (2) since the main result of ion-beam damage induced structural changes in ion-implanted polymers is carbonization, this should lead to highly fused graphite-like sheet structures in ion-implanted ladder polymers; (3) the chances of retaining their pristine structure and mechanical properties are much higher in implanted ladder polymers than non-ladder ones. The first ladder polymer we have investigated is the benzimidazobenzophenanthroline-type, BBL, whose structure is shown below:

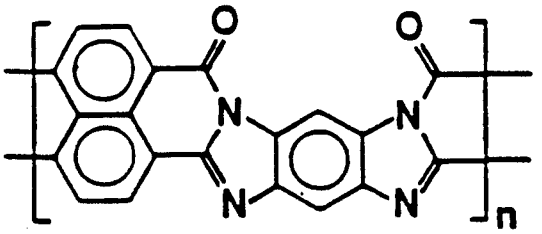

BBL

BBL has excellent thermal stability as shown in the thermogram of Figure 24, withstanding temperatures in excess of 600°C in air and 700°C in inert atmosphere or vacuum. Films of BBL prepared by various methods have a tensile strength of 9600-16,000 psi[6]. Films of BBL can be chemically[7-8] and electrochemically[8] doped to both n-type and p-type materials with conductivity as high as 2 S/cm.

2.4.2 Experimental

The BBL samples were synthesized using the general method of Arnold and Van Deusen[9]. However, our polymerizations were carried out in the liquid crystalline phase according to Wolfe's recent method for ordered polymers[10]. The BBL samples employed here have intrinsic viscosity of 7.9 dL/g in pure methanesulfonic acid (MSA) at 25°C and infrared spectra identical to the published one[9]. Free-standing films were prepared by precipitation of MSA solutions into water, filtration through a fritted glass funnel[6] and vacuum drying at 200°C for 16 hours. The resulting gold-yellow films were insulators ($\sigma < 10^{-12}$ S/cm). Films supported on substrates can be readily produced by solution casting, for example by spin coating deposition. A typical X-ray diffraction pattern of such films is shown in Figure 25, revealing two main Bragg d-spacings at 7.5 and 3.3 Å attributable to a high degree of ordered parking of the polymer chains.

The free-standing polymer films with thicknesses in the range 25-100μ and areas of 2.5 x 2.5 cm^2 to 5 x 5 cm^2 were mounted on a copper block from two sides with strips of metal and screws. Contacts to the films for insitu measurements of conductivity were made with small drops of high purity silver paint (Structure Probe, Inc.). For these insitu measurements, a two-point probe resistance measurement technique was used. Two-point probe and four-point probe techniques were used to measure the sheet resistance outside the implanter. In all cases the contacts were found to be ohmic. To convert all sheet resistance (ohm/) values to conductivity, we assumed that the thickness of the implanted layer is identical to the projected range R_p. The R_p values used are shown in Table 4. The projected range for boron in BBL film was estimated from available experimental data for boron implant in polymers[11-12]. It has been suggested that the projected range of boron in polymers, at a given energy, is nearly identical for all polymers ranging from photoresists to polyimides[11]. No experimental projected range data for argon and krypton in polymers were available for a similar estimate of the range of these ions

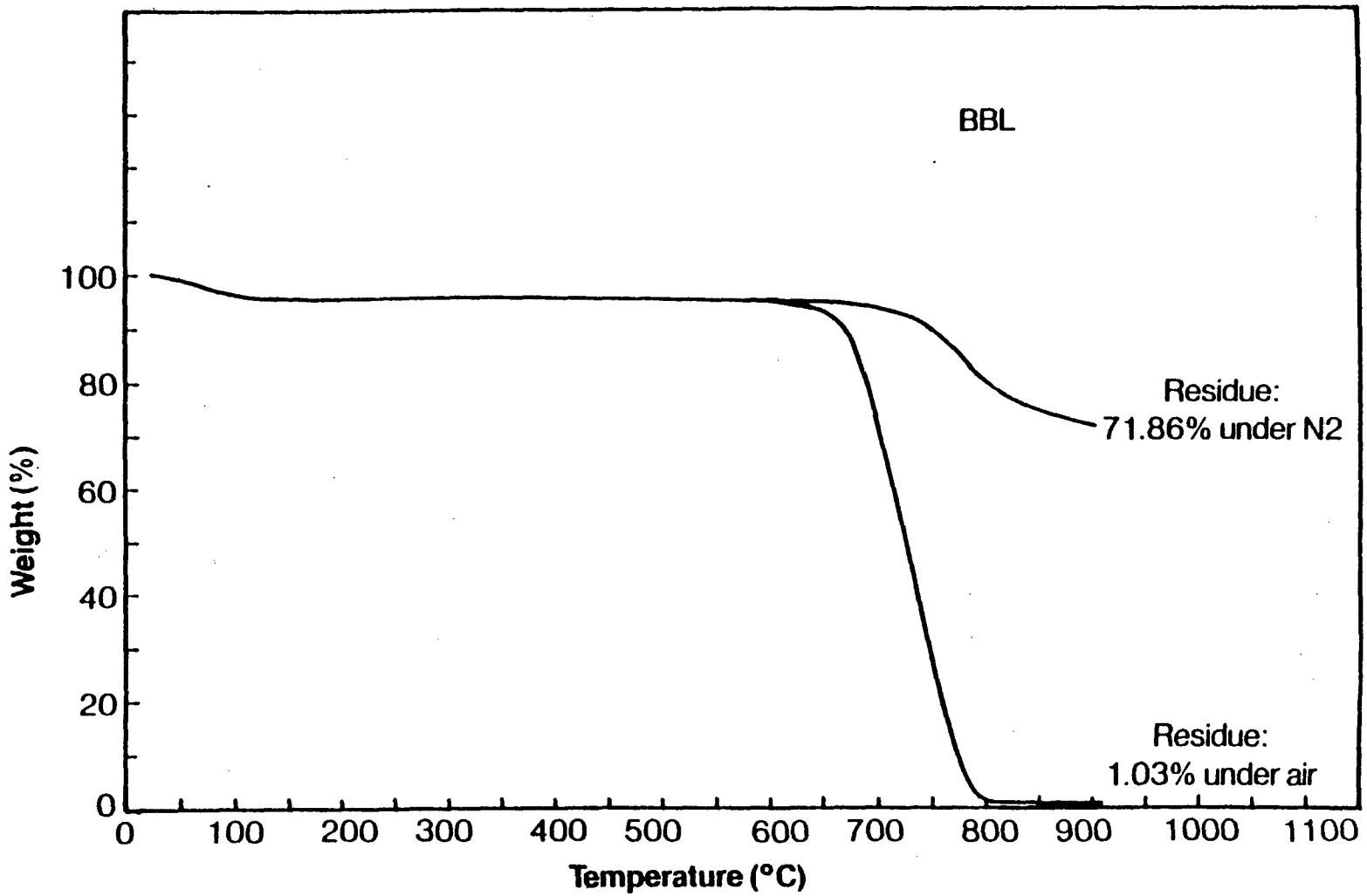

Figure 24 A thermogram of BBL obtained at a heating rate of 10^{o}C/min.

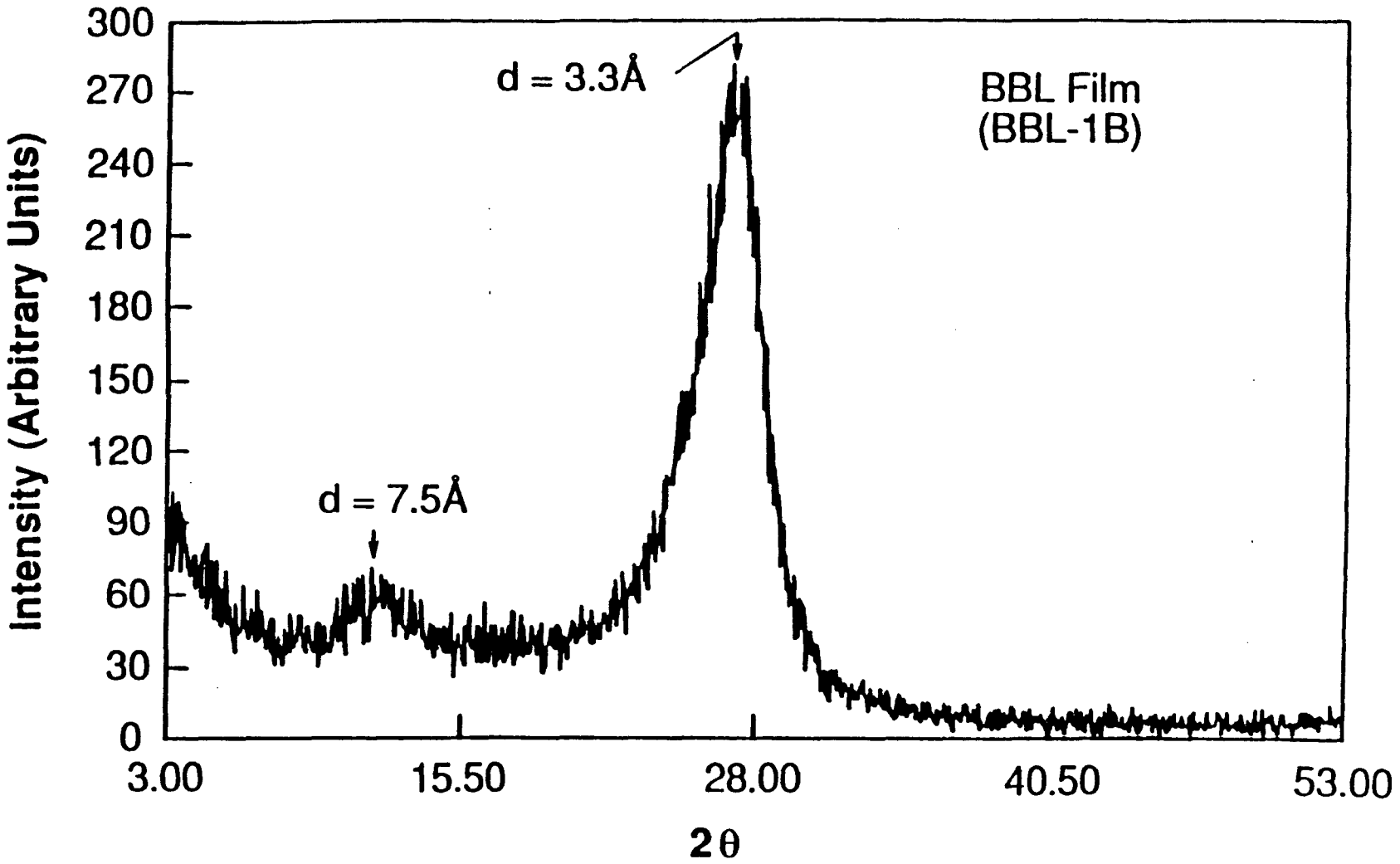

Figure 25 Typical X-ray diffraction patterns of a free-standing BBL film.

TABLE 4 PROJECTED RANGE VALUES

E (keV)	Ion	R_p (μm)	ΔR_p (μm)
200	B^+	0.70 (1.8445)*	0.11 (0.1518)*
200	Ar^+	0.36 (0.7225)*	0.058 (0.1157)*
200	Kr^+	0.21 (0.4206)*	0.034 (0.0678)*

* calculated values for AZ 111 photoresist[13]

in ladder polymers. The theoretical estimates of R_p for various ions in photoresists[13] are unfortunately generally 2-3 times higher than experimental values[11-12]. The projected range values shown in Table 4 for Ar^+ and Kr^+ are therefore half of the calculated values[13] also shown in the table. It must be noted that BBL has atomic composition, $(C_{20}H_6N_4O_2)n$, which is certainly different from most photoresists but closer to the polyimides. Hence the true experimental projected range data for ions in BBL and other ladder polymers, yet to be determined, may be quite different from those in Table 4. Nevertheless, the errors in R_p values should have little effect on the order of magnitude values of the conductivity.

Ion implantation was done using a Varian Model 400-AR ion implanter which has a maximum ion energy of 400 keV and a vacuum of 10^{-6} torr. For the data reported here the beam current density (J_b) was maintained at 1.0 or 2.0 $\mu A/cm^2$ while the corresponding power density was 0.2 or 0.4 W/cm^2. The substrate temperature was monitored with a thermocouple and found to be at or near room temperature (25-29°C) during implantation. Spatially selective implantation was achieved using a metal mask held in contact with the sample. Some gas evolution from the samples evidenced by pressure changes was observed during ion implantation, but no analysis of the residual gas was done.

2.4.3 Results and Discussion

Figure 26 shows the current-voltage characteristics of the electrical contacts made to Ar^+ implanted BBL (200 keV, $\Phi = 4.0 \times 10^{16}/cm^2$) with high purity silver paint. Clearly, ohmic behavior is observed over the temperature range -69°C to 146°C. Ohmic behavior was also observed at even higher currents and voltages than shown in Figure 26. Ohmic behavior was similarly observed when the polarity of the current was reversed.

Figures 27 through 29 show the dependence of the conductivity of ion implanted BBL films on dose (ions/cm^2) at a given ion energy. A relatively steep rise in conductivity from the pristine film value of less than 10^{-12} S/cm to values in excess of 1 S/cm at a dose of $10^{16}/cm^2$ is observed. Further increase of the dose results in conductivity increase to a saturation value of about 26-74 S/cm at about 2.0-3.5 x $10^{16}/cm^2$. Effect of beam current density (J_b) on the saturation conductivity is shown in Table 5. Note that the saturation or near-saturation conductivity value has been increased by a factor of 2.2-3.0 times simply by doubling the current beam density. The final conductivity values at 4.0 x $10^{16}/cm^2$ are 56, 224, and 136 S/cm respec-

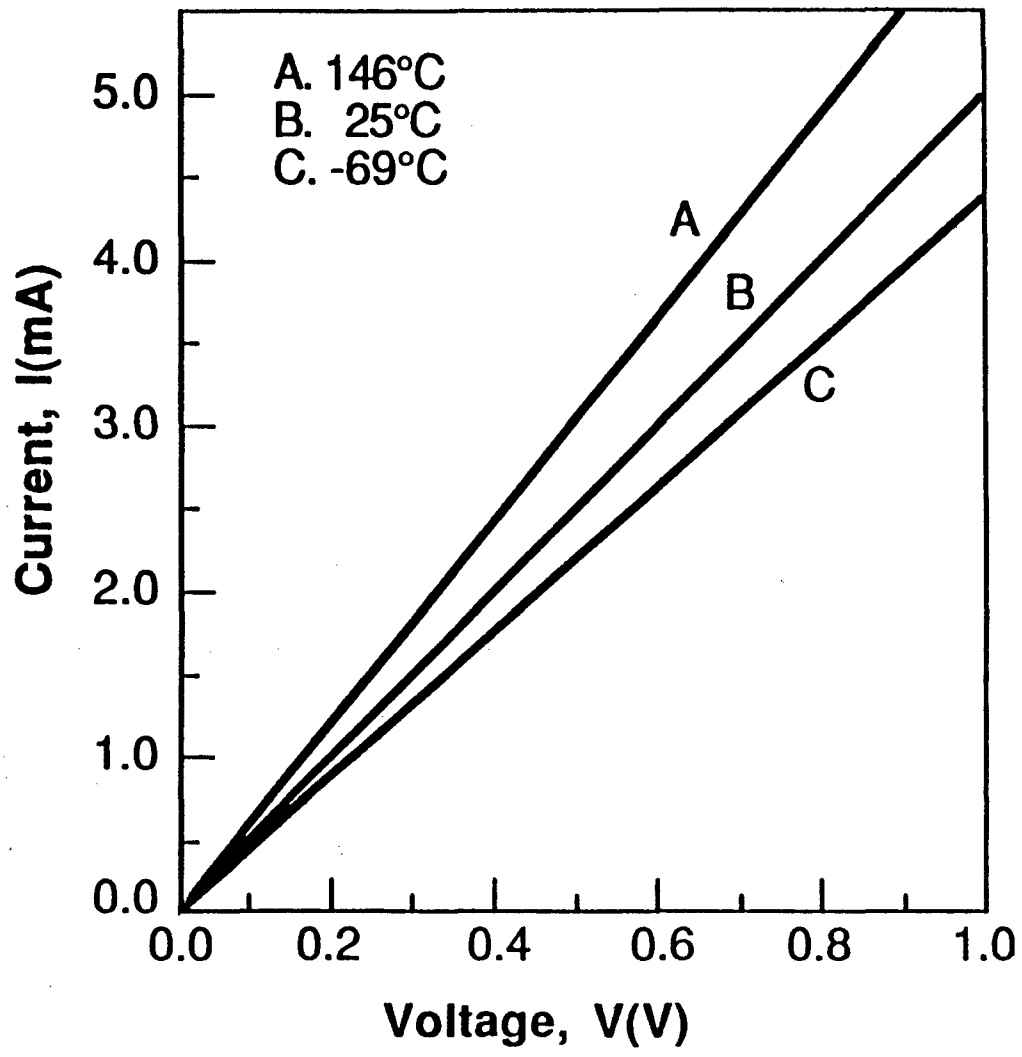

70235

Figure 26 The current-voltage characteristics of electrical contacts to argon-implanted BBL film at different temperatures.

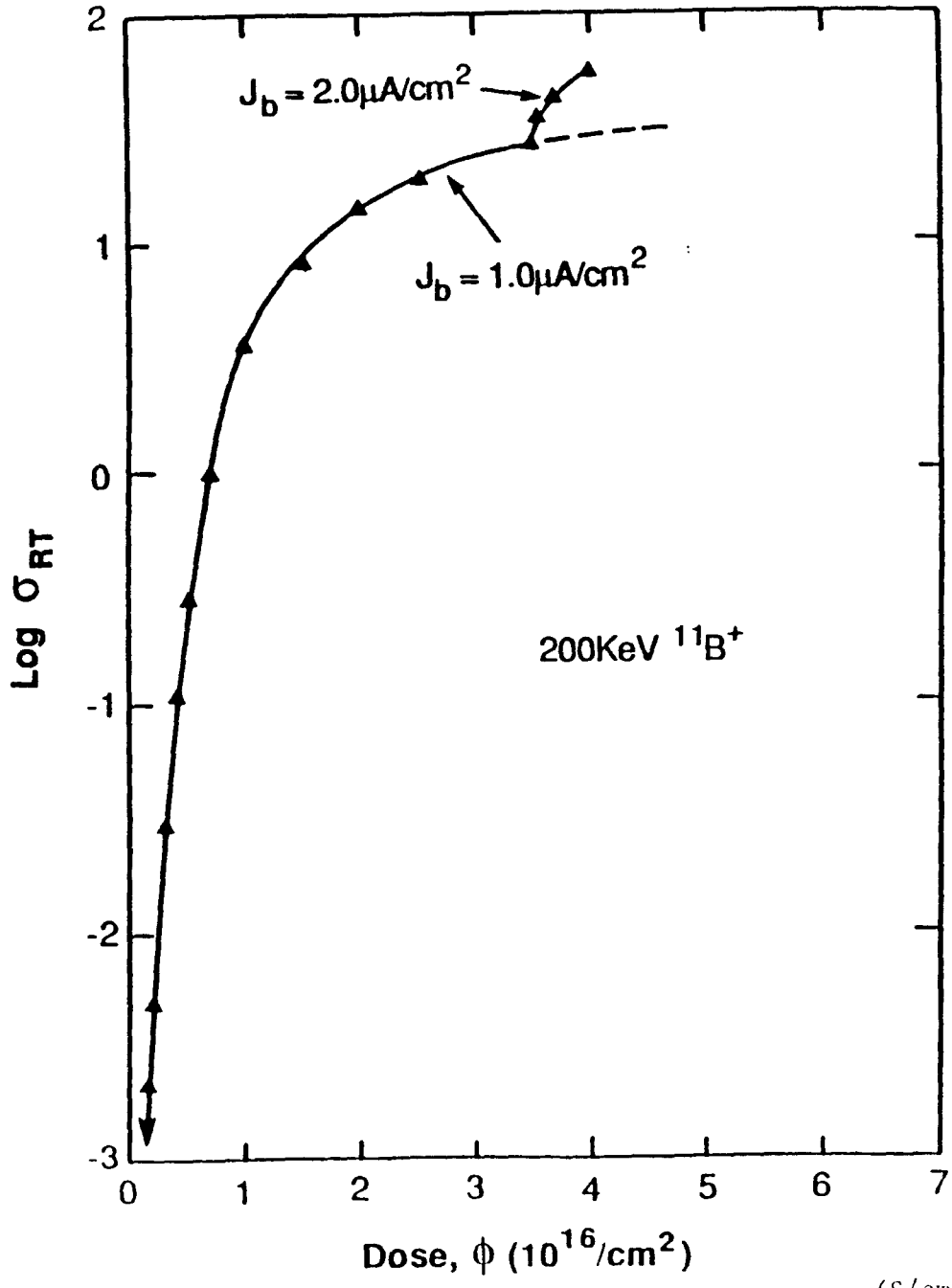

70286

Figure 27 A semi-log plot of room temperature conductivity (S/cm) versus dose for a BBL film implanted with 200 keV $^{11}B^+$.

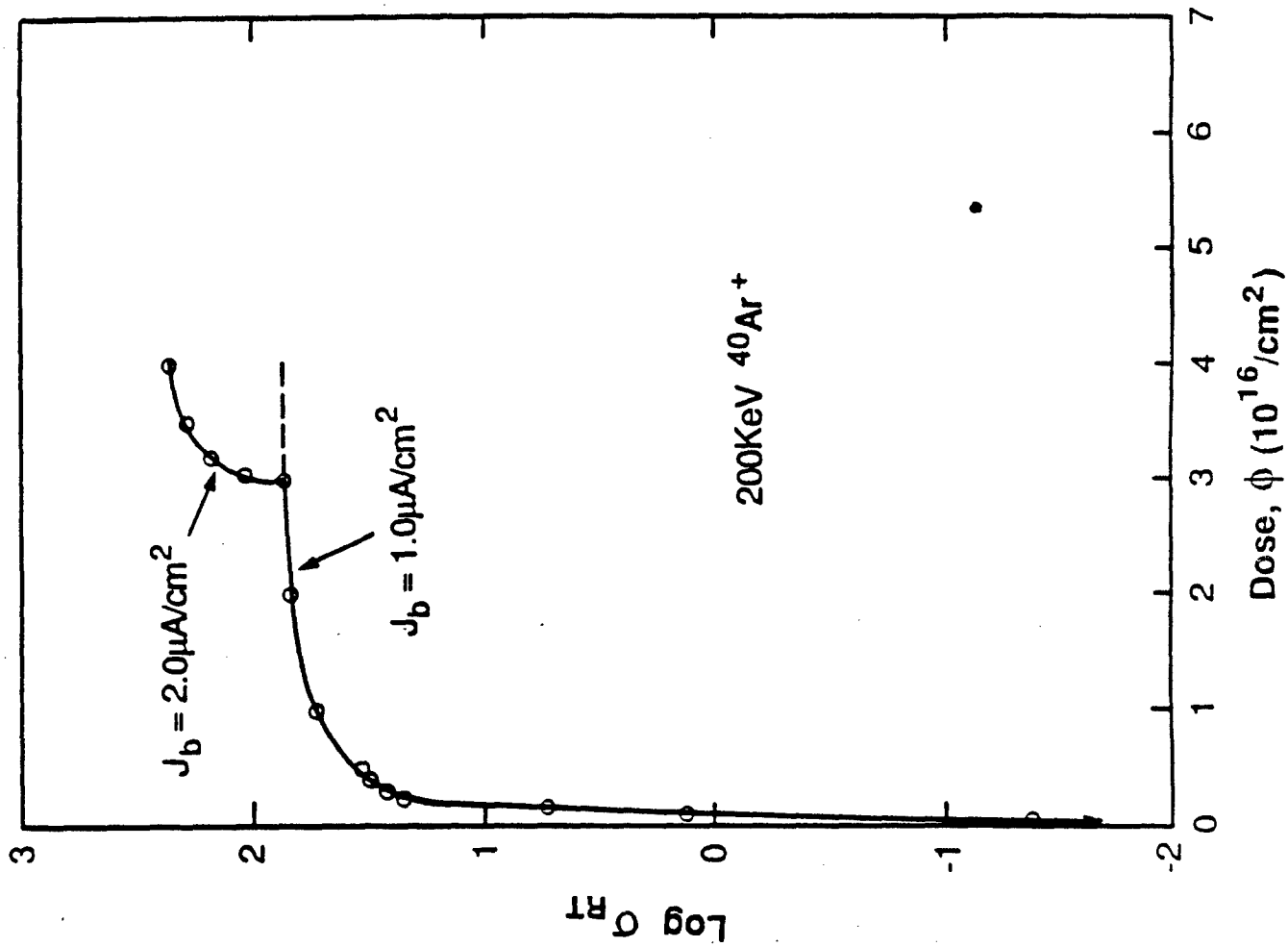

Figure 28 A semi-log plot of room temperature conductivity (S/cm) versus dose for a BBL film implanted with 200 keV $^{40}Ar^+$.

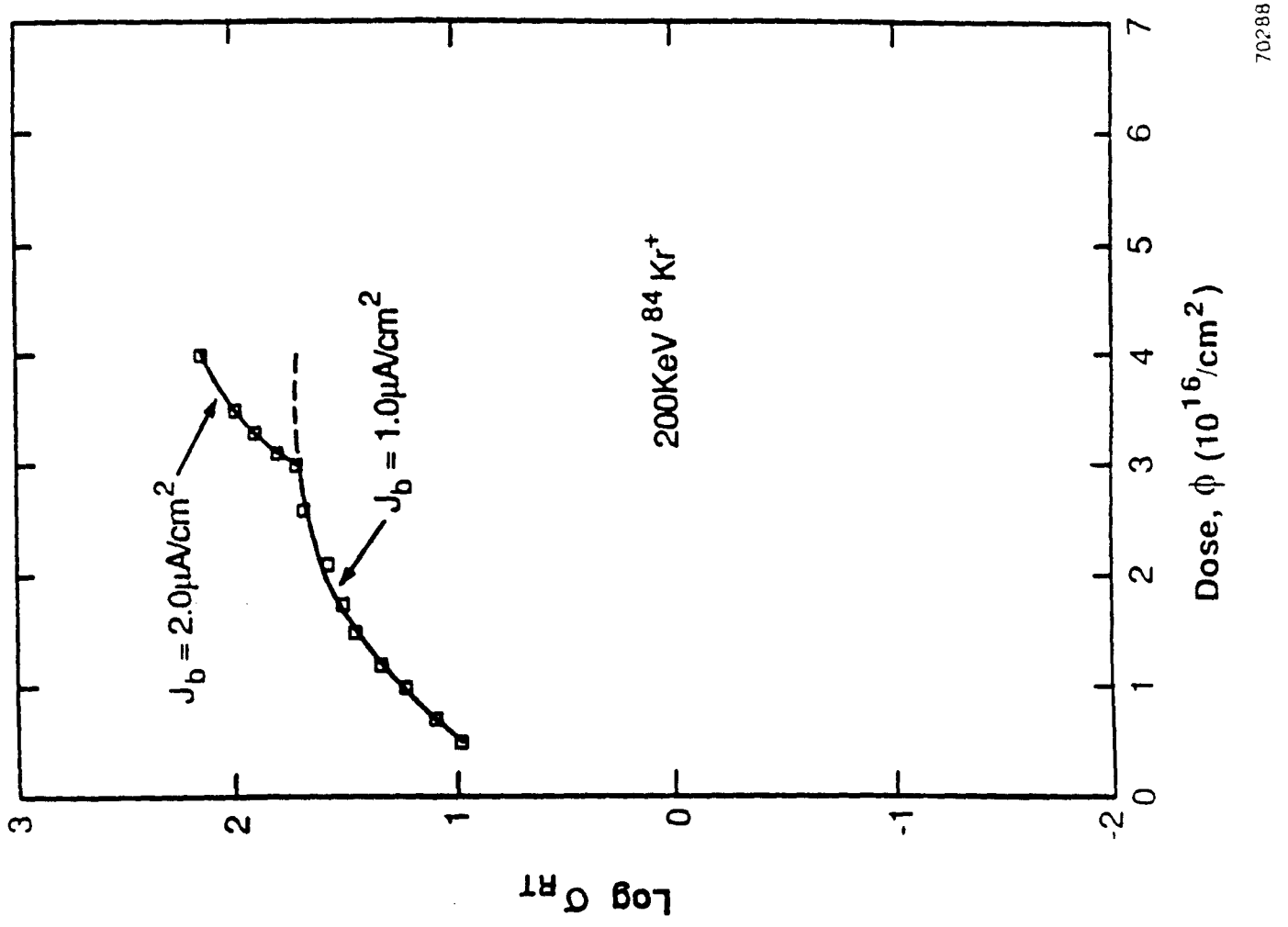

Figure 29 A semi-log plot of room temperature conductivity (S/cm) versus dose for a BBL film implanted with 200 keV $^{84}Kr^+$.

TABLE 5 EFFECT OF BEAM CURRENT DENSITY (J_b) ON SATURATION CONDUCTIVITY OF IMPLANTED BBL FILMS

Implant	σ^* (S/cm) J_b = 1.0 $\mu A/cm^2$	J_b = 2.0 $\mu A/cm^2$	σ_2^*/σ_1^*
200 keV $^{11}B^+$	26 (31)**	56 (92)**	2.2 (3.0)**
200 keV $^{40}Ar^+$	74 (74)**	224 (235)**	3.0 (3.2)**
200 keV $^{84}Kr^+$	50 (50)**	136 (175)**	2.7 (3.5)**

σ^* = saturation conductivity

** = extrapolated true saturation values

σ_2/σ_1 = ratio of saturation conductivities at the two J_b values

tively for the 200 keV boron, argon and krypton implanted films. It is noteworthy that the room temperature saturation conductivity of ion implanted BBL films is one to two orders of magnitude higher than that achieved in chemically or electrochemically doped samples. Even higher saturation conductivities in ion implanted BBL and ladder polymer films can be expected via (1) higher beam current density (> 2.0 $\mu A/cm^2$; (2) higher dose (> 4.0 x $10^{16}/cm^2$); or (3) higher ion energy. A reasonable upper limit on the saturation conductivity in BBL films is probably of the order 10^3 to 10^4 S/cm. In fact, studies of non-conjugated (pristine) polymers and carbon films with ion energies of 200 keV to 25 MeV suggest that the saturation conductivity obtained with high energy ions ($\geq$ 400 keV) is about four to six orders of magnitude higher than with low energy ions[14].

The temperature dependent conductivity $\sigma(T)$ exhibits a linear fall with decreasing temperature (K) on a semi-log plot shown in Figure 30. Clearly, this indicates that the material is a semiconductor. However, the nature of the conduction mechanism is as yet unclear. Attempts to fit $\ln\sigma(T)$ versus T^{-1} or $T^{-1/2}$ failed to give a straight line in the range of 77-298K and 77-419K. The best fit to the data of Figure 30 is of the form $\sigma = \sigma_0 \exp(T/T_0)$, where σ_0 is the conductivity at T = 0K. Best fit values of σ_0 and T_0 are: boron -- (8.2 S/cm; 208.8K); argon -- (65 S/cm; 643.9 K; krypton -- (90 S/cm; 753.3 K).

The gold-yellow pristine BBL films gradually turned black and then silver-gray with metallic luster as the concentration of implanted impurities increased. Correspondingly, the optical reflectivity increased with dose. The excellent mechanical properties of the films, including flexibility, were retained after implantation to doses of 4.0 x $10^{16}/cm^2$ or higher. In contrast carbon films are usually very brittle materials. This suggests that a significant portion of the original BBL sheet structure is retained after implantation. A possible intermediate structure resulting from partial carbonization by implantation consists of BBL structure with the oxygen eliminated:

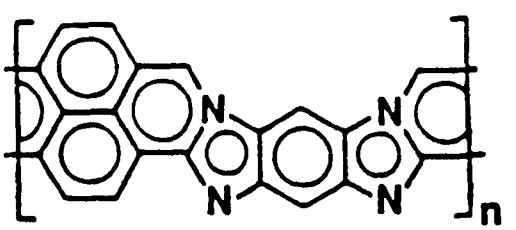

I

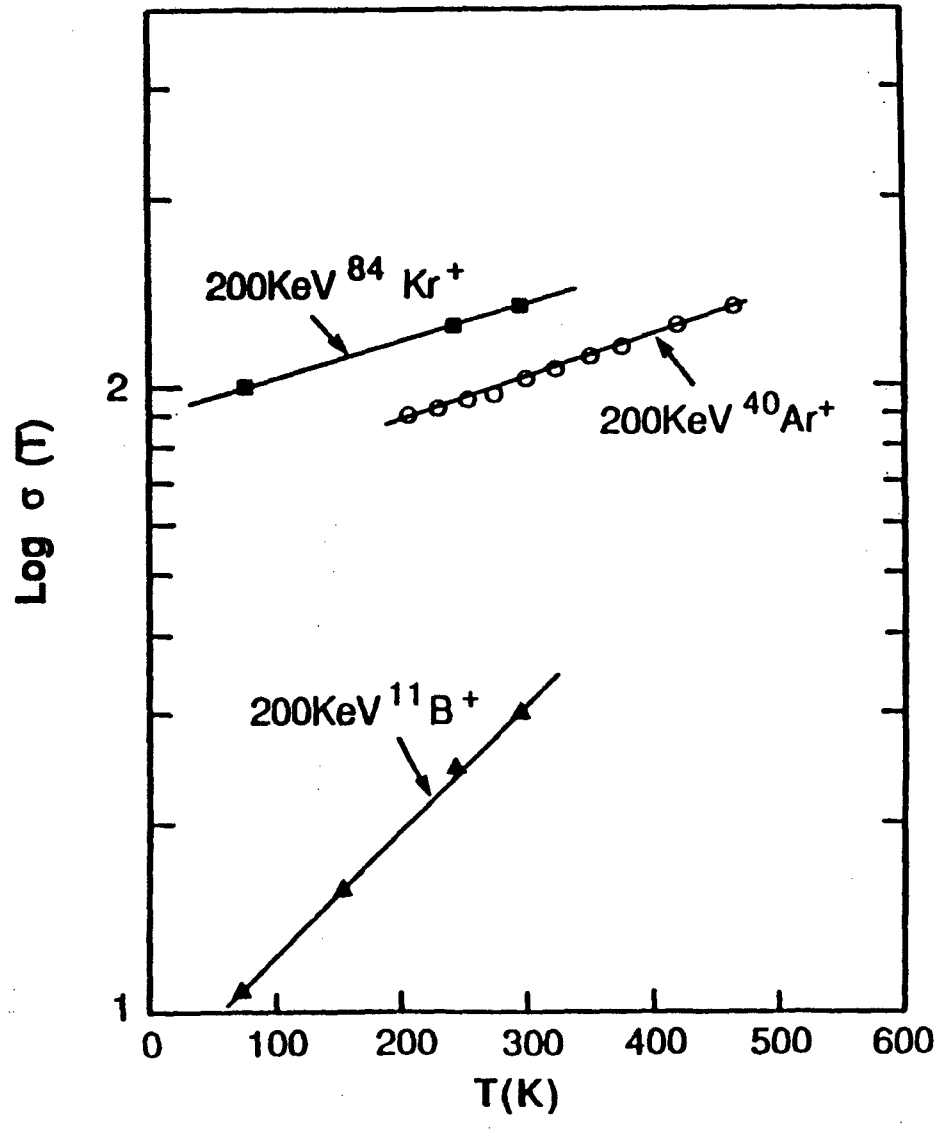

Figure 30 Temperature dependent conductivity of ion implanted BBL films.

Figure 31 shows a schematic illustration of spatially selective enhancement of the conductivity of an otherwise insulating BBL film achieved by ion implantation. A metal masking technique was used to produce linewidths (w) of about 25μm to 3mm. However, smaller linewidths down to the 1-micron range can be obtained using photolithographic pattern definition techniques together with metal or polymeric masks. Two-point probe measurements of the conductivity of the implanted regions gave values close to those reported above. Unimplanted regions of the film remained insulating. The high conductivity of patterned conducting lines within an insulating polymer film matrix and ohmic behavior of contacts made to such conducting regions suggest the potential application of the high temperature ladder polymers in microelectronic devices and packaging, for example in high density interconnection.

Ongoing effort is directed at spectroscopic characterization of ion implanted BBL and other ladder polymer films, elucidation of the mechanism of conduction, and exploration of device applications of selective enhancement of the conductivity of high temperature ladder polymer films.

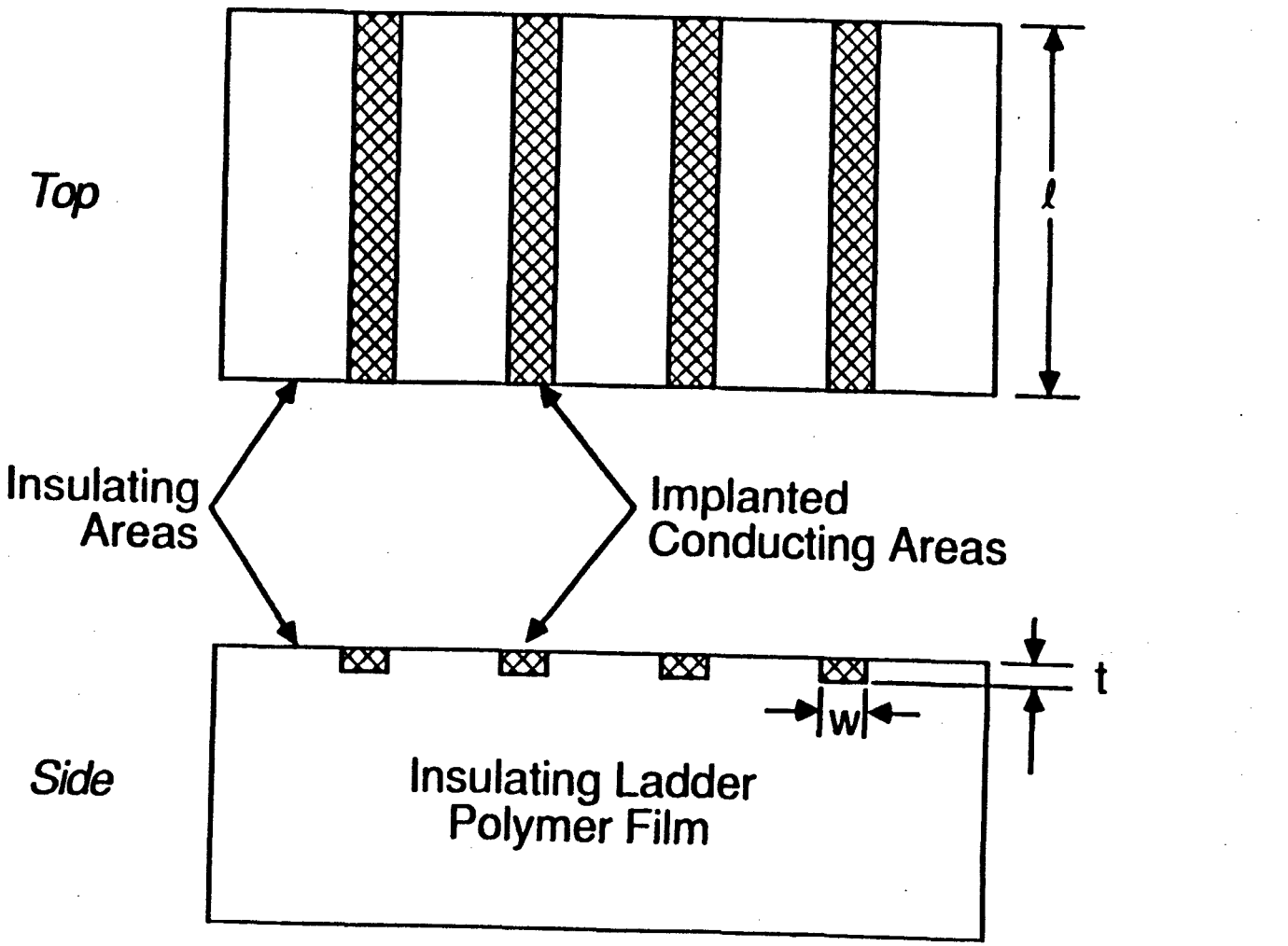

Figure 31 A schematic illustration of spatially selective enhancement of the conductivity of insulating BBL films by ion implantation. No to scale.

2.4.4 REFERENCES FOR SECTION 2.4

1. (a) J.W. Mayer, L. Eriksson, and J.A. Davies, Ion Implantation in Semiconductors. Academic Press: New York, 1970.(b) S. Namba (ed.), Ion Implantation in Semicondor: Science and Technology, Plenum Press: New York, 1975.

2. W.N. Allen, P. Grant, C.A. Carosella, J.J. DeCorpo, C.T. Ewing, F.E. Saalfeld, and D.C. Weber, Synthetic Metals, 1, 151 (1980).

3. H. Mazurek, D.R. Day, E.W. Maby, J.S. Abel, S.D. Senturia, M.S. Dresselhaus, and G. Dresselhaus, J. Polym. Sci: Polym. Phys. Ed., 21, 537 (1983).

4. G.E. Wnek, B. Wasserman, M.S.Dresselhaus, S.E. Tunney, and J.K. Stille, J. Polym. Sci: Polym. Lett. Ed., 23, 609 (1985).

5. (a) S.A. Jenekhe, unpublished results.
(b) S.A. Jenekhe, J. Am. Chem. Soc., submitted.

6. F.E. Arnold and R.L. Van Deusen, J. Appl. Polym. Sci., 15, 2035 (1971).

7. O.-K. Kim, J. Polym. Sci: Polym. Lett. Ed., 20, 663 (1982); Mol. Cryst. Liq. Cryst., 105, 161 (1984).

8. S.A. Jenekhe and J.R. Peterson, manuscript in preparation.

9. F.E. Arnold and R.L. Van Deusen, Macromolecules, 2, 497 (1969).

10. J.F. Wolfe, Polym. Mat. Sci. Eng. (Proc. ACS Div. Polym. Mat. Sci. and Eng.), 57, 99 (1985).

11. D.M. Tennant, A.H. Dayem, R.E. Howard, and E.H. Westerwick, J. Vac. Sci. Technol., B3, 458 (1985).

12. I. Adesida and L. Karapiperis, J. Appl. Phys., 56, 1801 (1984).

13. J.F. Gibbons, W.S. Johnson, and S.W. Mylroie, Projected Range Statistics of Semiconductors and Related Materials, 2nd ed., Dowden, Hutchinson, and Ross: Stroudsburg, PA, 1975.

14. T. Venkatesan, R. Levi, T.C. Banwell, T. Tombrello, M. Nicolet, R. Hamm, and A.E. Meixner, in: "Ion Beam Processes in Advanced Electronic Materials and Device Technology" B.R. Appleton, F.H. Eisen, and T.W. Sigmon (eds.), Materials Research Soc. Symp. Proc. Vol. 45, Pittsburg, PA, 1985; pp. 189-196.

SECTION 3
CONCLUSIONS AND RECOMENDATIONS

3.1 Conclusions

The electronic and electrical properties of ordered ladder polymers, exemplified by benzimidazobenzophenanthroline-type ladder polymer (BBL) and ladder polyhydroquinoxaline (PHQXL), were investigated. High molecular weight thermally stable BBL polymer with intrinsic viscosity, $[\eta]$, in the range 4.78-7.91 dL/g in methane sulfonic acid (MSA) was prepared by polymerization in the liquid crystalline phase in polyphosphoric acid (PPA). Moderate molecular weight ($[\eta]$=0.65 to 0.80 dL/g in MSA) ladder polyhydroquinoxaline (PHQXL) was prepared by polymerization in isotropic PPA solutions. The two types of ladder polymers studied, BBL and PHQXL, were found to be insulators ($\sigma_{RT} < 10^{-12}$ ohm^{-1}cm^{-1}) in the pristine undoped state. However, upon chemical, electrochemical, or ion implantation doping the room temperature electrical conductivity of films of these ladder polymers was enhanced up to 2-220 ohm^{-1}cm^{-1}. The observed temperature dependent conductivity showed that the doped highly conducting ladder polymers were semiconductors. A composite metal (Ag) and Ag^+-doped BBL film produced by electrochemical methods had a room temperature conductivity of 324 ohm^{-1}cm^{-1} and a <u>metallic</u> temperature dependent conductivity. The present results (σ_{RT} < 220 ohm^{-1}cm^{-1}) on ion implantation doping of BBL and the observed effects of dose rate and ion energy suggest the possiblity of achieving metallic conductivities (10^3 to 10^5 ohm^{-1}cm^{-1}) in ion implanted ladder polymer films.

The hypothesis that a higher electronic charge mobility, and hence a high <u>intrinsic</u> electrical conductivity, might be obtained in conjugated ladder polymers has not been fully tested in the present study of BBL and PHQXL because even these double-stranded ladder polymers show only a <u>single-stranded conjugation path</u> like the non-ladder conjugated polymers. Ordered ladder polymers which exhibit <u>double-stranded conjugation paths</u>, such as ladder polyquinoxaline (PQXL) and Marvel's graphite-type ladder polymer, are expected to be better model systems to test the role of ladder structure on the intrinsic electrical conductivity of organic polymeric solids.

A novel mechanism of solubilization of rigid chain and ladder polymers which has allowed the solubilization of BBL, PBO and related polymers in

aprotic organic solvents for the first time was discovered in this study. This solubilization approach involves the reversible formation of complexes of the rigid chain polymers which are soluble in organic solvents using Lewis acids as the mediating agents. Isotropic and anisotropic (> 8% wt) BBL solutions were successfully prepared in organic solvents (nitroalkanes and nitrobenzene) and processed to films and coating. This new mediated solubilization process together with the facile regeneration of the pristine polymers after solution processing hold promise for easier processing to films, coatings, and fibers and commercial applications of the rigid chain and ladder polymers.

Solution processing of BBL to films and coatings was accomplished by both conventional processing from acid solutions and the new mediated solubilization and processing from aprotic organic solvents. Included among the previously known methods that we investigated are (1) precipitation of the polymer from acid solutions followed by filtration of the resulting fine dispersion (PPt/filtration method), (2) spray coating of BBL dispersion obtained by precipitation from acid solutions, (3) uniaxial orientation of BBL/PPA dope followed by aqueous extraction of the PPA, and (4) spin coating of acid solutions. Film and coating processing from BBL solutions in organic solvents prepared by mediated solubilization included (5) solvent casting of films, (6) spray coating of dilute solutions in organic solvents, (7) spin coating of dilute solutions, and (8) uniaxial orientation of concentrated (>6% wt) solutions. The latter four methods generally gave superior films or coatings in terms of smoothness, coherence, and film or coating strength. However, only the former four methods have been studied extensively in accessing the effects of processing on BBL film or cating morphology using visual and optical microscope observations, X-ray diffraction and scanning electron microscopy. Methods 3 and 8 gave uniaxially oriented microstructures. The two basic Bragg d-spacings of BBL film at 7.5 and 3.35 Å were found to vary from 6.3 to 8.4 Å and 3.3 to 4.0 Å respectively, depending on the processing conditions.

The possible applications of ladder polymers in electronics were explored in two types of experiments using BBL films. Four large-area (> 10 inches length) actual printed circuit (pc) boards with all the devices in place were successfully spray coated from solutions in organic solvents and doped to high conductivity for evaluation of electromagnetic interference

(EMI) applications at Honeywell's Signal Analysis Center. The second type of experiment evaluated the feasibility of spacially selective enhancement of conductivity, creating regions of conducting lines in an insulating matrix, using ion implantation. The experimental results demonstrated the feasibility of creating such conducting patterns in an otherwise insulating film and hence suggest the potential applications of the high temperature materials in microelectronic devices and electronic packaging, such as in high density electronic interconnection.

The electrochemical properties of BBL film were studied by cyclic voltammetry at neutral pH in non-aqueous electrolyte and as a funtion of pH in aqueous electrolyte. At neutral pH the redox potential (E°') of BBL, defined as $(E_p^{ox} + E_p^{red})/2$, was found to be -1.25V (vs. Ag/Ag^+); the redox potential increased linearly with decreasing pH to -0.39V (vs. Ag/Ag^+) at a pH of -0.24. The dependence of the redox properties of BBL underline the importnce of protonation/deprotonation phenomena in the electronic and physico-chemical properties of this ladder polymer. Thin films (~1 μm) of BBL coatings on platinum (Pt) electrodes were found to exhibit electrochromism in non-aqueous electrolytes (e.g. $Et_4N^+ClO_4^-$/MeCN). At a potential of ca. -1.6V (vs. Ag/Ag^+) or less the BBL film was blue/green due to reduction in $BBL^{y-}(Et_4N^+)_y$ whereas at ca. -1.0V (vs. Ag/Ag^+) or higher the color was switched to bright red due to oxidation to $BBL^{y+}(ClO_4^-)_y$. The red <-> blue/green switching was quite stable to indefinite cycling, suggesting its potential application in display devices.

The mechanical properties of undoped insulating and doped highly conducting (~1 $ohm^{-1}cm^{-1}$) BBL films were characterized by dynamic tensile moduli (E',E") measurements in the temperature range -150° to 350°C and frequency range 0.10 to 100 Hz. The dynamic storage modulus (E') of both the undoped and potassium doped BBL films was virtually constant at a value of ~1.8 GPa throughout the temperature range -150° to 350°C. All the other measured tensile properties were found to be virtually identical in the undoped and potassium-doped BBL films. These findings on the excellent mechanical properties of doped conducting ladder polymers contrast sharply with the generally poor mechanical properties of most of the other doped conjugated polymers.

Comparative studies of a model compund of ladder polyhydroquinoxaline (PHQXL), 5,12-dihydro-5,7,12,14-tetraazapentacene (DHTAP), and its complexes

were made as a basis for spectroscopic and structural understanding of the high molecular weight polymer and for understanding of the effects of polymer chain length on electronic and optical properties of ladder polymers. Undoped DHTAP, like PHQXL, is an insulator and is insoluble in most common organic solvents; its solution and solid-state electronic absorption spectra have two characteristic intense absorption maxima near 300 nm and 600 nm due to π–π^* transitions. Anisotropic crystalline complex of DHTAP with methane sulfonic acid (MSA) was found to exhibit a pressed dc conductivity of 10^{-2} ohm $^{-1}$cm^{-1} at room temperature and to be soluble in many polar organic solvents. DHTAP and its complexes exhibit strong flourescence in solution.

The feasibility of direct electrochemical synthesis of ladder polymer films was demonstrated by the successful preparation of uniform, coherent, and electroactive ladder polyquinoxaline films from 1,2-phenylenediamine or mixtures of 1,2-phenylenediamine and 1,2,4,5-tetraaminobenzene tetrahydrochloride in acidic aqueous solutions. Preliminary characterization of these films by spectroscopy and elemental analysis indicate the presence of quinoxaline rings and a structure close to PHQXL.

Overall, the present research program and its results have established thermally stable ordered ladder polymers as a promising new class of highly conducting polymers for potential applications in electronics and as conductive coatings in aerospace vehicles.

3.2 Recommendations

The technical results and conclusions of the preceding sections of this report show that this research program has made considerable progress in the understanding of the electronic and electrical properties of ordered ladder polymers and in developing new processing techniques for the rigid chain polymers. Some areas of the present research effort were of necessity exploratory in nature and would require further study to fully clarify and develop. The following specific areas are recommended for subsequent research effort:

(1) Undertake a detailed investigation of mediated solubilization and processing of rigid chain and ladder polymers in aprotic organic solvents.

This discovery of a novel mechanism of solubilization of BBL and related rigid chain polymers organic solvents is of utmost theoretical and practical importance. Such a study is expected to give rise to new fundamental results on the chemistry of polymer processing as well as immediate improvements in the processing and applications of BBL and related rigid chain polymers. The solubilization of these rigid chain polymers in organic solvents should produce both isotropic and liquid crystalline solutions which are important for future commercial processing of the materials but also for understanding of the molecular and physical properties of the polymers.

(2) Further studies of ion implantation of high-temperature ladder polymers are needed to answer the question whether room temperature conductivities in the 10^3 to 10^5 $ohm^{-1}cm^{-1}$ can be achieved while retaining the excellent mechanical properties of ordered ladder polymer films. If the answer to this question is affirmative, many immediate applications of the thermally stable materials in microelectronics, such as microelectronic interconnection and flexible circuits, are expected. The optical properties of such ion implanted ladder polymers are also of technological interest.

(3) Although the present study has demonstrated that ordered ladder polymers are a promising new class of conducting polymers, much remains unknown about the electronic and electrical properties of these polymers. The true mechanism of electronic conduction in chemically, electrochemically, and ion implantation doped conducting ladder polymers are still unsettled questions. A future study of electronic transport properties of conducting ladder polymers should include temperature dependent conductivity, thermopower, and charge mobility measurements along with electron spin resonance spectroscopy. The hypothesis that high electronic charge mobility, and hence a high intrinsic conductivity without doping, might be obtained in ladder polymers should be tested by choice of conjugated ladder polymers that exhibit <u>double-chain conjugation paths</u> unlike BBL and related polymers that are only conjugated along one of their double chains. Also, the electronic and electrical properties of model compounds of all the ladder polymers studied, including the non-ladder but molecularly similar high molecular weight polymers, should be investigated in order to determine effects of chain length and ladder structure on electronic properties.

(4) Ladder polymers which have good high temperature resistance in the 300-500°C range and solution processibility will eventually find wide applications

in electronics, such as insulating dielectrics, protective coatings and ion implant masks, even as insulators. High electrical conductivity in the ladder polymers will further expand their possible applications to include microelectronic devices, electronic packaging and conductive coatings. Knowledge of the insulating dielectric properties of the ladder polymers is also important in most of these electronic applications. Thus, it is recommended that the insulating dielectric properties of the most promising ladder polymers, such as BBL, should be determined.

☆U.S.Government Printing Office: 1989 — 648-056/04239